James H. Williams, Jr.
Principal Investigator

Thermal Nondestructive Testing of Fiberglass Using Liquid Crystals

A Two-Part Report

MASSACHUSETTS INSTITUTE OF TECHNOLOGY
Sea Grant Program

EDITORIAL NOTE

MITSG 81-16
Thermal Nondestructive Testing of Fiberglass
Using Liquid Crystals

Because of the exorbitant cost of color xeroxing, there are several
photographs in this two-part report that we have reproduced in black
and white, instead of color. Color copies are available on order for
$1 a page.

Part I: Page 107, 111, 115, 116

Part II: Page 23, 24, 25, 26

MIT Sea Grant Program
E38-368
Cambridge, MA 02139

Attn: Information Center

THERMAL NONDESTRUCTIVE TESTING

OF FIBERGLASS

USING LIQUID CRYSTALS

A Two-Part Report

James H. Williams, Jr.
Principal Investigator

ACKNOWLEDGMENTS

RESEARCH GROUP

James H. Williams, Jr. is a professor of mechanical engineering and head of the Composite Materials and Nondestructive Evaluation Laboratory in the MIT Department of Mechanical Engineering.

Samson S. Lee is a lecturer in the MIT Department of Mechanical Engineering.

S. Hossein Mansouri is a graduate student in the MIT Department of Mechanical Engineering.

MIT SEA GRANT REPORTS

This report, and all others in the Sea Grant Program technical and advisory service series, may be ordered through the:

> MIT Sea Grant Information Center
> 77 Massachusetts Avenue
> E38-302
> Cambridge, MA 02139

THERMAL NONDESTRUCTIVE TESTING

OF FIBERGLASS

USING LIQUID CRYSTALS

Part I

S. Hossein Mansouri
James H. Williams, Jr.
Samson S. Lee
July 1979

Part II

Samson S. Lee
James H. Williams, Jr.
July 1980

PREFACE

Thermal nondestructive testing is a technique for obtaining
surface temperature profiles on a structure and subsequently relating
this information to some imperfection within the structure. When
structure with no inherent heat source is heated externally, a flaw
in the structure will generally alter the heat flow because of differ-
ences in heat transfer properties. When the flow pattern is sufficiently
altered, significant variations in surface temperature profiles can be
detected.

This two-part report details research sponsored by the Sea Grant
Program at MIT to investigate cholesteric liquid crystals as the thermal
medium for identifying fiberglass flaws. Increasingly fiberglass, a
composite material, is replacing wood, steel and aluminum in boat
manufacture and an easy to use, inexpensive, but effective testing
method to detect manufacturing defects or accident damage.

Part I describes a one-dimensional heat transfer model through
a laminate with various kinds of interlaminar flaws. The effects of
flaw thickness, depths, and heat flow characteristics have been plotted
for a range of variables that model most practical situations.

Part II of the report focuses on studies of a fiberglass laminate
containing simulated flaws or orthogonal to the surface. Various plots
on the sensitivity and effectiveness of liquid crystal thermal testing
are put forth.

PART I

NONDESTRUCTION DETECTION OF DELAMINATIONS AND

INCLUSIONS IN FIBERGLASS LAMINATES USING LIQUID CRYSTALS

S. Hossein Mansouri

James H. Williams, Jr.

Samson S. Lee

ABSTRACT

Based upon this investigation, thermal testing with cholesteric liquid crystals provides a simple nondestructive evaluation technique for the detection of interlaminar flaws in fiberglass composite laminates. Virtually no training is required in order to recognize the presence of a flaw. Also, no complex electronic equipment is needed to record the data as any ordinary camera can be used to produce a permanent visual record of the results.

A one-dimensional model of the heat conduction through a laminate, containing an interlaminar flaw, with natural convection on both faces has been devised. An analytical solution of the surface temperatures above the flawed and unflawed regions of the laminate has been developed. Nondimensional groups have been identified which make it possible to define "optimal", "acceptable", "moderately acceptable", and "limiting" testing conditions in relation to the parameters of the flaw and the laminate being inspected. Comparisons between experiments and theory clearly show that interlaminar flaws can be distinctively seen under "optimal", "acceptable", or "moderately acceptable" testing conditions.

In general, the testing conditions may be chosen by satisfying the theoretical performance indices corresponding to either "optimal", "acceptable", or "moderately acceptable" conditions. In order to facilitate the conduct of future experiments, sets of data have been generated for most practical situations.

ACKNOWLEDGEMENTS

TABLE OF CONTENTS

NOMENCLATURE

Symbol	Description	Units
α_1	Thermal diffusivity	ft^2/hr
h	Heat transfer coefficient	Btu/hr sq ft F
k_1	Thermal conductivity	Btu/hr ft F
ℓ	Thickness of laminate	ft
ℓ_1	Depth of defect	ft
ℓ_2	Thickness of defect	ft
q''	Net radiant heat flux	Btu/hr sq ft
t	time	hr
T_∞	Ambient temperature	°F
T_{Is}	Surface temperature in region I	°F
T_{IIs}	Surface temperature in region II	°F
T^*_{Is}	Nondimensional surface temperature corresponding to T_{Is}	--
T^*_{IIs}	Nondimensional surface temperature corresponding to T_{IIs}	--
$T_{L.c.}$	Transition temperature of liquid crystal (that is, temperature at which liquid crystal starts changing color during heating)	°F
$\Delta T_{L.c.}$	Color-play range of liquid crystal	°F
ΔT	Temperature difference	°F
ΔT^*	Nondimensional temperature difference	--
Fo	Fourier number	--
Bi	Biot number	--

Symbol	Description	Units
RK	Thermal conductivity ratio	—
RA	Thermal diffusivity ratio	—
R1	Nondimensional defect depth	—
R2	Nondimensional defect thickness	—

LIST OF FIGURES

CHAPTER I

INTRODUCTION

1.1 BACKGROUND

Thermal testing is based on the detection of surface temperature gradients induced by variations in the properties of a test object which alter the object's normal heat flow pattern. For example, when thermal energy is applied or extracted uniformly on the surface of a uniform test material, the appearance of an uneven temperature pattern may be related to variations in the material properties or the integrity of the test material. Detection of an irregular temperature pattern containing a hot point is a major aspect of thermal testing techniques. In addition, many tests require simultaneous detection of rapidly changing temperature at a large number of points. This can be done with the infrared imaging technique or, more simply, by applying a thermally sensitive coating to the test surface and observing changes in the coating. In dynamic testing the latter approach has the advantage that the thermal patterns on the test material can be observed directly.

Recently, liquid crystals have been introduced into thermal testing. Liquid crystals are inexpensive temperature-indicating coatings that change color in response to changes in temperature. Thin films of these liquids can thus be used to depict isotherms as vivid color bands.

Temperature-sensitive cholesteric liquid crystals are the most widely

used liquid crystals to date. In the presence of white light, cholesteric liquid crystals selectively reflect one wavelength of light at each angle of reflection, and the reflected beam is circularly polarized. The reflected color is an accurate index of temperature, and temperature measurements are possible to within 0.1°C. Liquid crystals are colorless except in their color-play range. For example, a liquid crystal with a color-play range of 30°C to 31°C may appear dark red at 30°C; as the temperature rises to 31°C its color will successively pass through yellow, green, blue, and finally violet. By proper mixing of liquid crystals, the color-play range can be made as narrow as 1°C and as wide as 30°C within an overall range of -20°C to 250°C. Many of the cholesteric compounds and mixtures reflect light at different wavelengths only upon cooling through the color-play range, while others display the colors while passing through the color-play range during either heating or cooling. The response time is about 0.1 sec.

Thus liquid crystals have the ability to reflect colors dependent upon the temperature of their environment. They may be used to project a color picture of transient temperature anomalies or minute thermal gradients associated with material discontinuities. These discontinuities, which may be voids, delaminations, or other defects, may sufficiently impede a flow of heat to disturb the normal temperature patterns of a material being tested. Because of their different heat transfer characteristics, defects will then show up as distinct color patterns.

1.2 PURPOSES OF RESEARCH

The purposes of this investigation are (1) to examine the feasibility of using cholesteric liquid crystals for the detection of interlaminar defects in fiber reinforced laminates, and (2) to establish the requirements for determining the testing conditions and for choosing a liquid crystal system to define the quantitative features of a delamination flaw in fiber reinforced laminates.

The primary emphasis throughout this investigation will be on the quantitative determination of the effectiveness of cholesteric liquid crystals for the nondestructive evaluation of fiberglass reinforced laminates.

CHAPTER II

LITERATURE REVIEW OF THERMAL TESTING WITH LIQUID CRYSTALS

2.1 INTRODUCTION

In the comprehensive sense, thermal testing comprises all test methods which depend upon heat sensors. These techniques fall into two categories: (1) direct contact techniques, in which a thermally sensitive device or material is placed in physical and thermal contact with the specimen under examination, and (2) noncontact techniques, which depend upon thermally generated electromagnetic energy radiated from the test specimen [1]. (See Fig. 1.) At moderate temperatures, such energy is predominantly infrared; hence, infrared testing is the most important branch of noncontact thermal testing.

The present feasibility of thermography for nondestructive evaluation depends on advances in the precision of infrared radiometers and on improved contact thermographic coatings. Advances in radiometry have been paced principally by the introduction and improvement of solid-state infrared detectors, cryogenically cooled to reduce self-generated noise. Contact thermography has been revitalized by the introduction of liquid crystals and other thermochromic compounds for indicating small thermal gradients in convenient temperature ranges.

Infrared radiometers are presently being used for most thermal non-destructive testing studies because of the ability of these instruments

```
                        Thermal Methods
                              |
          ┌───────────────────┴───────────────────┐
     Thermographic                            Thermometric
          |                                        |
    ┌─────┴─────┐                            ┌──────┴──────┐
 Contact    Non-Contact                   Contact     Non-Contact
            (IR Imaging)
    |            |                            |            |
    |       ┌────┴────┐                       |            |
 Paints  IR Scanners  IR Film         Thermocouples   Radiometers
 Phosphors  Cameras                    Thermopiles     Pyrometers
 Coatings   Microscopes              Metal Bolometers
 Treated Paper                         Thermistors
 Liquid Crystals                     Meltable Materials
```
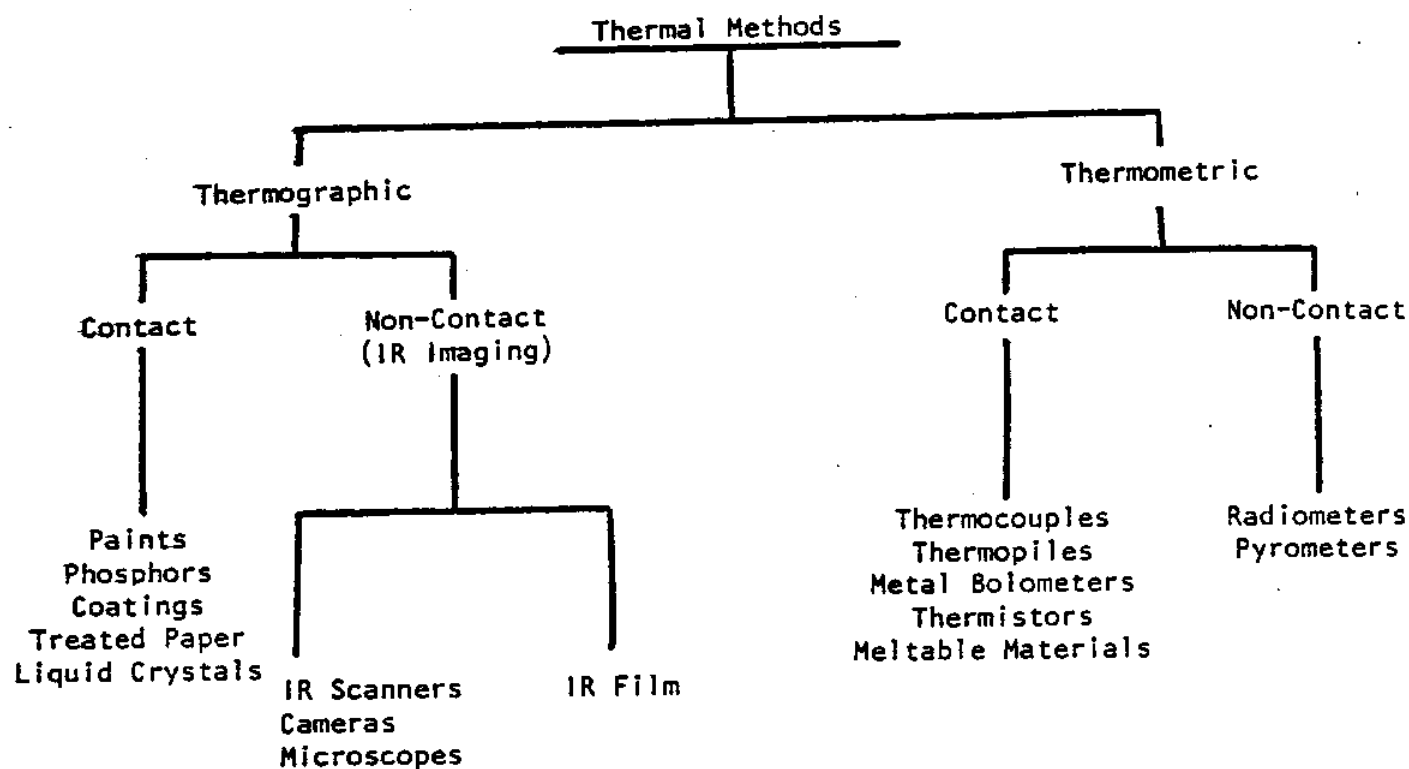
Fig. 1. Methods used in thermal nondestructive testing [1].

to measure, without surface contact, small, rapidly changing surface temperatures associated with material discontinuities. Most of these radiometric measurements have been made by monitoring a single point or line on the object being tested. This means that for full coverage of a substantial area, a scanning system must be devised which will systematically move the radiometer focal spot over the test object. These systems usually become complex, expensive, and difficult to use on irregularly shaped components [2].

In many cases, simultaneous detection of rapidly changing temperatures at a large number of points is required. This can be done with infrared imaging equipment or, more simply, by applying a thermally sensitive coating to the test surface and observing changes in the coating. The latter approach has some advantages, particularly in dynamic testing, since the thermal pattern can be observed directly, thus making it possible to determine if heat is injected too slowly or too rapidly, or whether heat is generated during mechanical or electrical tests [3].

Cholesteric liquid crystals can be used in contact thermography to visualize, directly on the surface under study, many of the transient temperature anomalies associated with material discontinuities [4]. The thermal sensitivity of cholesteric liquid crystals is such that it should be possible to employ these materials in many thermal tests formerly requiring the use of radiometers [5]. Liquid crystals are relatively inexpensive chemicals which may be reused if applied and removed from the test surface properly [1,6]. Further, no sophisticated electronic instrumentation is

needed to monitor the results.

2.2 LITERATURE REVIEW

2.2.1 Testing Metal to Metal Adhesive Bonds with Liquid Crystals

One of the first tests in which liquid crystals were used was the visualization of voids in adhesively bonded aluminum stiffener panels [4,7].

2.2.2 Inspection of Adhesively Bonded Structures with Liquid Crystals

The first use of liquid crystals for the contact thermography of bonded structures for aircraft was reported by Cohen [8]. A total of 290 square feet of bonded honeycomb and laminated metallic and nonmetallic structural panels were tested in an analysis of technique capability. Test specimens with built-in flaws were fabricated by NASA and represented 52 variations of materials and construction types used in aerospace structural composites. Cohen's report concluded that thermographic testing of bonded structures with liquid crystals is entirely feasible and could offer advantages over other thermographic testing techniques. The conclusion was also reached that the use of liquid crystals for testing and recording results is far less expensive than infrared systems.

Woodmansee successfully tested several honeycomb composite structures [3,4] using Teflon patches of 1 in. by 1 in., $\frac{1}{2}$ in. by $\frac{1}{2}$ in., and $\frac{1}{4}$ in. by $\frac{1}{4}$ in. to simulate voids in a panel with a 0.012 in. aluminum skin and

an aluminum honeycomb core. The larger two patches were detected while the ¼ in. by ¼ in. patch was not detected. Another test panel of 0.020 in. titanium with High Temperature Phenolic (HRP) honeycomb core was prepared by cutting out areas of adhesive between the skin and the core. The sizes of the areas that were cut out were 1 in. by 1 in., ½ in. by ½ in., and ¼ in. by ¼ in. All of these simulated voids were detectable.

Brown [9,10], used liquid crystals for finding voids in aluminum honeycomb composites with simulated debond areas. She simulated voids in three ways: Teflon inserts, crushed core, and cured adhesive. Teflon inserts were the most difficult to observe, while crushed core was sharply defined. Aluminum honeycomb composites with up to 0.190 in. skins were tested successfully. The minimum detectable defect was ¹⁄₁₆ in. by ¹⁄₁₆ in. for 0.060 in. skins and 1 in. by 1 in. for 0.190 in. skins. Types of structures tested with equal success were aluminum skins with HRP honeycomb core, glass cloth skins with glass fiber honeycomb core, titanium skins with aluminum honeycomb core, titanium skins with HRP core, and glass cloth laminates. The best results were obtained by heating the back side of the test panel and cooling the side being observed.

Southworth and Woodmansee [7,11] tested adhesively bonded composites with titanium skins and either titanium honeycomb core or HRP honeycomb core. Voids were simulated by removing the adhesive in areas of 1 in. by 1 in., ½ in. by ½ in., and ¼ in. by ¼ in. The skin thickness varied from 0.010 to 0.020 in. Detection depended upon the thickness of the metal between the surface painted with liquid crystal and the bondline

being tested. The thicker the metal, the more lateral heat transfer and so the fewer the flaws which could be detected. In other words, the thinner the skin, the smaller the void which could be detected.

2.2.3 Crack Detection and Leak Detection with Liquid Crystals

Cholesteric liquid crystals have been used for leak and crack detection [3,4,7]. For crack detection on a titanium marine propeller, for example, the detail of definition of the crack with the liquid crystal was comparable to that seen with a visible penetrant [3].

CHAPTER III

LITERATURE REVIEW OF LIQUID CRYSTALS

3.1 INTRODUCTION

The liquid crystalline or mesomorphic state is an intermediate state between solid and liquid. The molecules of a liquid crystal possess an order greater than that of a random liquid and less than that of a crystalline solid. These substances are named "liquid crystals" because they exhibit the optical properties of a crystal while possessing the fluid properties of a liquid. Liquid crystals may be visualized as multiple layers of two-dimensional crystals (which accounts for the optical properties) in which the layers are allowed to slide over one another (which accounts for the fluid properties).

Liquid crystals are by no means rare. It is estimated that one out of every 200 organic compounds is subject to liquid crystalline behavior. Most substances have only one solid-liquid transition temperature. Liquid crystals, on the other hand, have a solid-liquid transition temperature range. (See figs. 2 and 3.) Generally, liquid crystal substances are colorless on either side of the liquid crystal state, while in the liquid crystal state they resemble a highly viscous turbid fluid.

There are two main classes of liquid crystals -- lyotropic and thermotropic. Lyotropic liquid crystals are formed when certain compounds are treated with a controlled amount of water or other polar solvent. A

crystalline solid | liquid

temperature

crystalline solid | Liquid Crystal
or
Mesomorphic
State | liquid
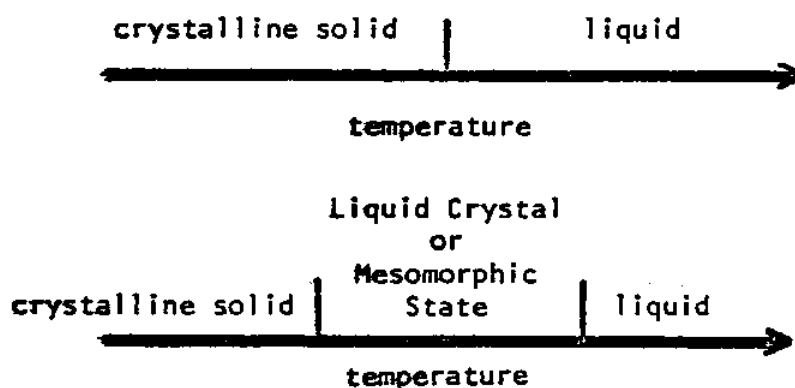
temperature

Fig. 2. Temperature dependence of liquid crystal state [18].

	liquefies
Heating Behavior	crystal	cholesteric	isotropic

77°C   92°C
ultraviolet scattering
66°C   74.6°C 77°C   92°C

| Cooling Behavior | crystal | smectic | cholesteric | isotropic |

Visible Color   Temperature
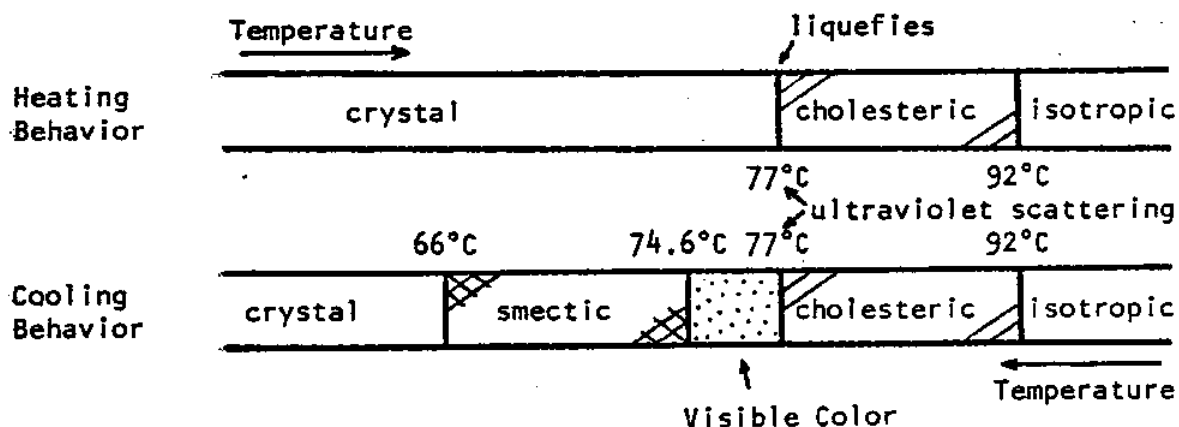
Fig. 3. PHASE CHANGES of cholesteryl nonanoate illustrate
liquid crystal phase relationships. All liquid-
crystal phenomena occur in the mesophase between
that of a crystalline solid and an isotropic, or
ordinary, liquid. When cholesteryl nonanoate crys-
tals are heated, they melt at 77°C and are choles-
teric to 92°C, where they become isotropic. Cool-
ing the liquid at any time after it reaches 77°C
causes it to pass through its color-play region,
77 to 74.6°C, and into the smectic phase. Finally,
at 66°C it begins recrystallizing. [24]

true solution is not formed, but additional solvent converts it to a true solution. Most soaps and detergents will form lyotropic liquid crystals when treated with the proper amount of water.

Thermotropic liquid crystals are formed by heating the crystal lattice above the temperature at which it is stable. There are two subclasses in this group. Enantiotropic types can be formed by heating the crystalline solid or by cooling the isotropic liquid to the liquid crystal temperature range. The thermal energy in the liquid crystal state is adequate to cause a partial breakdown of the ordered crystal; however, enough residual attraction between molecules remains to give a semi-ordered state. The second subclass, monotropic, can only be formed by supercooling the liquid phase. Most of the liquid crystals presently used are of the thermotropic type.

3.1.1 Historical Background

Liquid crystal behavior was first observed in 1888 by the Austrian botanist Friedrich Reinitzer [12], who noted that the compound "cholesteryl benzoate" appeared to have two distinct melting points. At 145°C the solid turned to a cloudy liquid and at 179°C the liquid became clear. Shortly thereafter the German physicist Lehmann [13] showed that the cloudy intermediate phase contained areas that seemed to have a crystal-like molecular structure. He suggested the name "liquid crystal" for this phase. In 1922, liquid crystals were classified by Friedel [13] as smectic, nematic, and cholesteric.

3.1.2 Liquid Crystal Structure

Thermotropic liquid crystals may be divided into two classes. One of these is the nematic liquid crystals, which have spontaneous orientation of their molecules with their long axes parallel (Fig. 4a). There is no long-range order in the spatial arrangement of molecules in nematic liquid crystals. Cholesteric liquid crystals are now recognized as a special case of nematic liquid crystals (Fig. 4b). Their molecules have an orientation order similar to that of nematic liquid crystals, but superimposed on their parallel orientation is a spontaneous and continuous twist. The second class of thermotropic liquid crystals is the smectic liquid crystals. In smectic liquid crystals of type A, the centers of gravity of the molecules are arranged in planes perpendicular to the preferred direction of the long axes of the molecules (Fig. 4c) and therefore perpendicular to the optical axis. There is no spatial long-range order of the molecules in the planes.

3.1.3 Cholesteric Liquid Crystal Structure

The molecular layers in a cholesteric substance are very thin (~3Å) with the long axes of the molecules parallel to the plane of the layers. The individual molecules are essentially flat, with a side chain of methyl groups (CH_3) projecting upward from the plane of each molecule. (Refer to Fig. 5.) This unusual configuration causes the direction of the long axes of the molecules in each layer to be displaced slightly from the

NEMATIC STRUCTURE

A

TWISTED NEMATIC STRUCTURE
(CHOLESTERIC STRUCTURE)

B

SMECTIC STRUCTURE A

C

TILTED SMECTIC STRUCTURE

D

TWISTED SMECTIC STRUCTURE

E
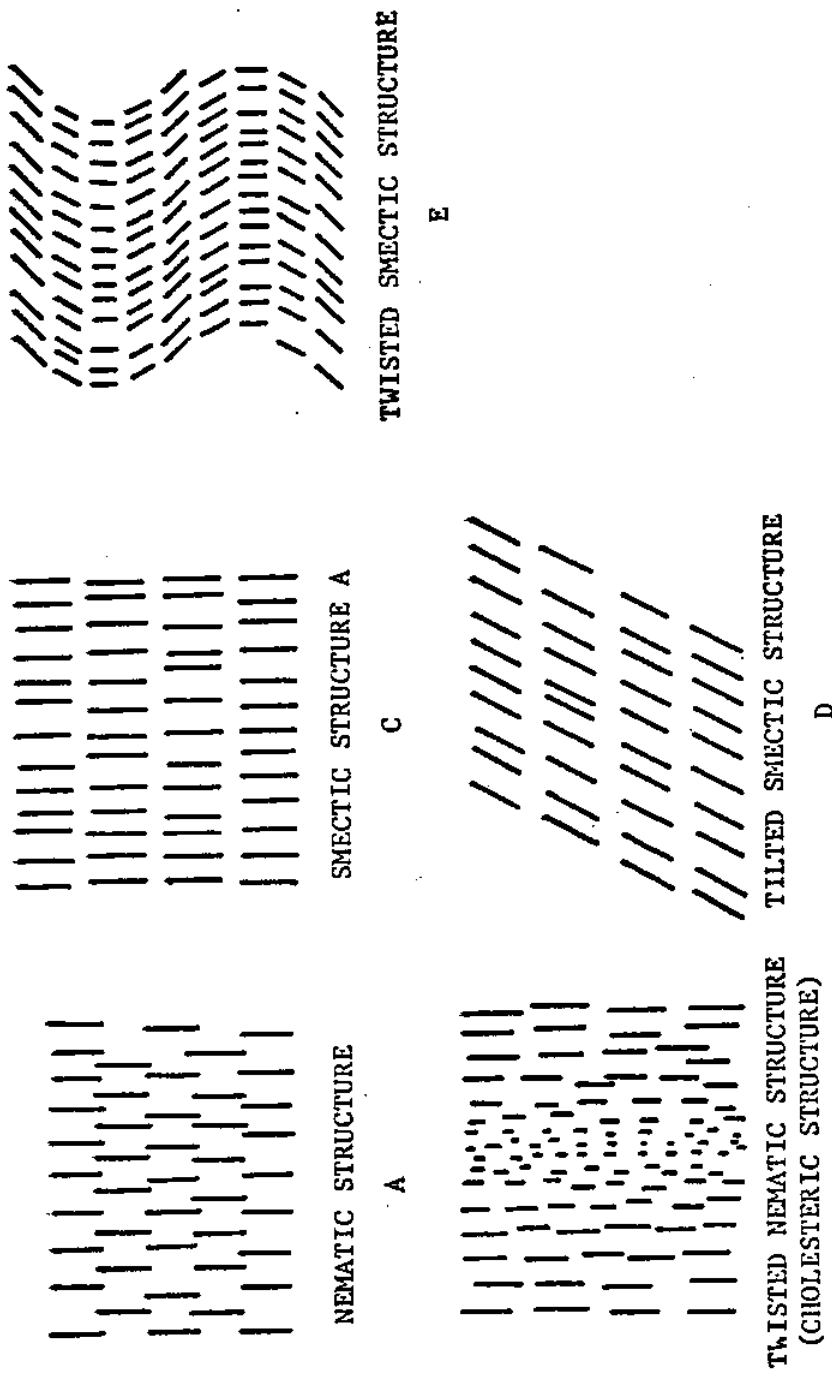
Fig. 4. A. Schematic diagram of molecular arrangement in uniformly oriented nematic liquid

Uniformly oriented structure has infinite-fold symmetry axis

B. Schematic diagram of molecular arrangement in uniformly oriented cholesteric liquid

Infinite-fold screw axis

C. Schematic diagram of smectic liquid Infinite-fold symmetry axis

D. Schematic diagram of molecular arrangement in tilted smectic structure

E. Schematic diagram of molecular arrangement in twisted smectic structure [14]
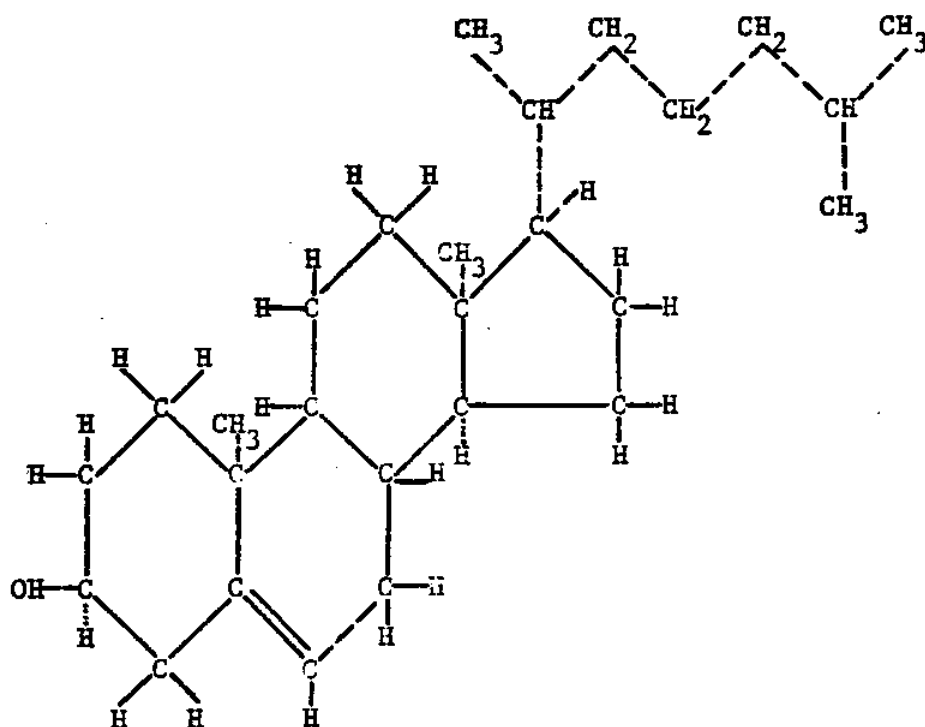
Fig. 5. The structural formula of cholesteryl. Molecule of cholesteryl is essentially flat with a side chain of methyl (CH_3) groups projecting upward from the plane of the molecule. Although cholesteryl by itself does not exhibit a liquid crystal phase, many compounds that contain cholesteryl do: compounds in this category are called cholesteric [16].

corresponding direction in adjacent layers. This displacement, which averages about 15 minutes or arc per layer, is cumulative through successive layers, so that the overall displacement traces out a helical path. (See Fig. 6.) The pitch of the helical path is usually temperature-dependent, and the temperature dependence may be positive or negative. The twist in the cholesteric molecular structure can be observed in the optical characteristics of homogeneously ordered layers.

Some of these optical observations are as follows: (a) Over a small wavelength range — about $\lambda_R = pn$, where p is the pitch of rotation and n is the average refractive index — irradiation of the sample parallel to the axis of rotation shows that one circularly polarized beam is transmitted while the other is totally reflected. (b) Outside this small wavelength range, irradiation parallel to the axis of rotation gives a strong optical rotatory power. If the wavelength λ_R lies in the visible region, the total reflection gives rise to bright colors. Since the pitch of the helical structure is strongly temperature-dependent, the color observed may also provide a temperature identification [14].

3.2 OPTICAL PROPERTIES OF CHOLESTERIC LIQUID CRYSTALS

The unique molecular structure of cholesteric liquid crystals gives rise to a number of interesting optical properties which are summarized in the next few paragraphs.

The cholesteric structure is uniaxial and optically negative while
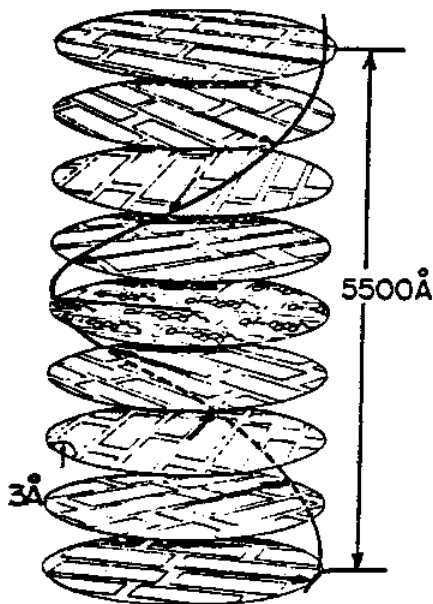
Fig. 6.   Cholesteric liquid crystals resemble smectic li-
          quid crystals in that the molecules are arranged
          in layers; within each layer, however, the para-
          llel alignment of molecules is more reminiscent
          of the nematic phase. The molecular layers are
          very thin, with the long axes of the molecules
          parallel to the plane of the layers. Because of
          the peculiar shape of the cholesteryl molecules,
          the direction of the long axes of the molecules
          in each layer is displaced slightly from the cor-
          responding direction in the adjacent layers; the
          overall displacement traces out a helical path.
          Roughly every 300th layer is depicted [23].
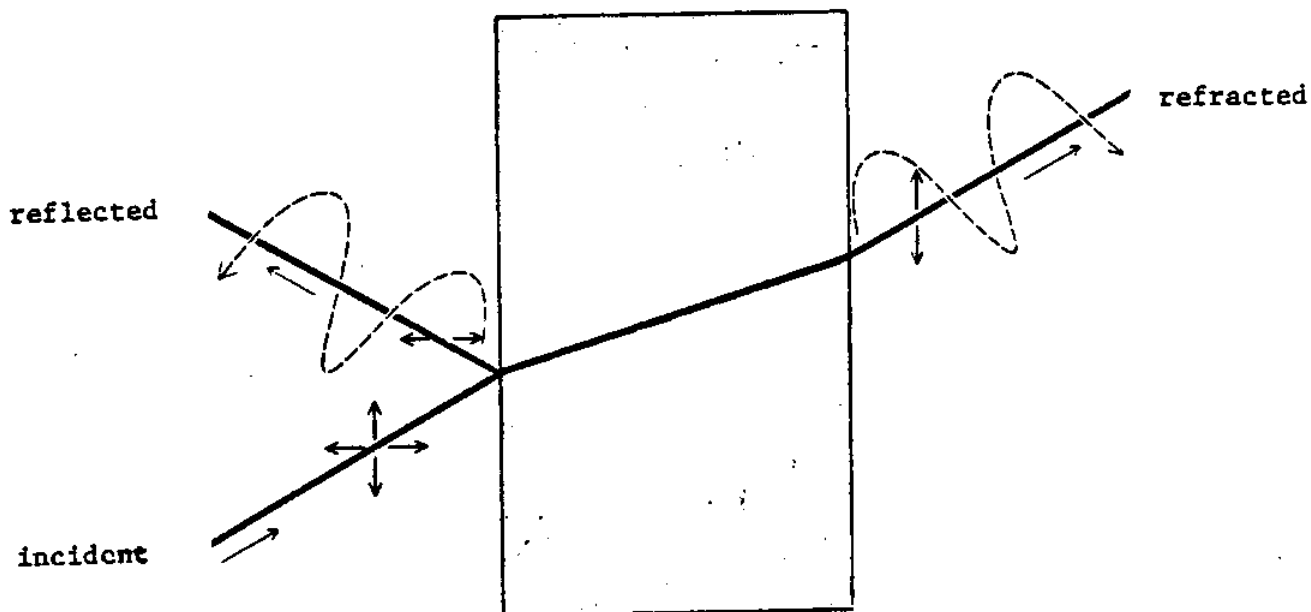
Fig. 7. CIRCULAR DICHROISM is a typically crystalline optical property exhibited by cholesteric liquid crystals. When unpolarized light is directed at at cholesteric substance, the light is broken into two components, one with the electric vector rotating clockwise and the other with the electric vector rotating counterclockwise; one of these components is transmitted and the other is reflected [13].

refracted

incident
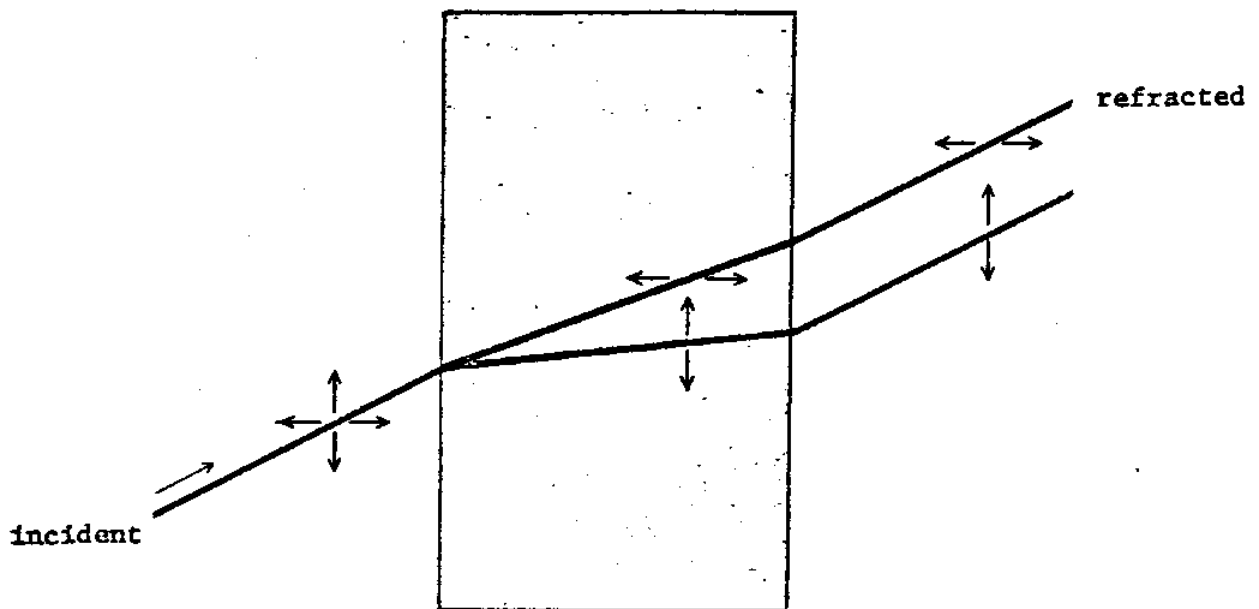
Fig. 8. BIREFRINGENCE, or double refraction, is an optical
phenomenon characteristic of solid crystals and
most liquid crystal substances. When a beam of
unpolarized light encounters a birefringent sub-
stance (left), it is split into two polarized
compounds whose transverse vibrations are at right
angles to each other. The two components are re-
fracted at different angles through the substance
and emerge as parallel beams of polarized light
(right) [13].

other liquid crystal structures are optically positive. In an optically

positive liquid crystal, the velocity of light transmitted perpendicular

to the layers is less than that transmitted parallel to the layers, but

in an optically negative liquid crystal, light propagated perpendicular

to the molecular layer has a maximum velocity. Thus, for the cholesteric

phase, there is a single optical axis normal to the surface, along which

the index of refraction is a minimum.

The cholesteric structure is optically active, rotating the plane

of polarization through an angle proportional to the thickness of the

transmitting material, with rotatory powers many times that of common

optically active materials. The plane of linearly polarized light is

rotated through an angle several hundred times that of familiar optically

active materials such as sucrose or optically active quartz.

When illuminated with white light, the cholesteric structure scatters

the light to give an iridescent color which varies with substance tempera-

ture and angle of incident beam.

The cholesteric structure is circularly dichroic for some wavelength

regions; that is, one circularly polarized component of the incident beam

is transmitted without attenuation, whereas the other is scattered [13].

(See Fig. 7.) Either the right- or the left-hand circular polarized com-

ponent may be affected.

Another optical property shared by solid crystals and most liquid

crystal substances is birefringence, or double refraction [13]. (See

Fig. 8.) When a beam of unpolarized light encounters a birefringent sub-

stance, it is split into two polarized components whose transverse vibrations are at right angles to each other. The two components are refracted at different angles through the substance and emerge as parallel beams of polarized light.

3.2.1 Temperature-Color Relationships

Under white light illumination, thin films of cholesteric liquid crystals placed on a black background and heated will pass through the color spectrum, or a portion of it. Within specific temperature ranges, the color transformations are repeatable and occur at predictable temperatures. The colors reflected from cholesteric liquid crystal films are considered to be caused by Bragg diffraction from molecular layers whose orientation axes are aligned within the film. Layer alignment occurs once every complete revolution of the helix.

Thermal energy disturbs the weak bonding forces between the molecular layers in a cholesteric film. Temperature variations increase or decrease the angle of rotation between layers, changing the helical pitch, or distance between aligned Bragg diffraction layers. According to Bragg's law [15], constructive interference will occur in the diffracted beam from a crystal when the path difference for rays from adjacent planes is an integral multiple of a specific wavelength as shown in Fig. 9, or when

$$2d \sin \theta = n\lambda \quad ,$$

where

d = molecular alignment-layer spacing
θ = Bragg angle
n = 0, 1, 2, 3, ...
λ = reflected wavelength due to reinforcement.

If the Bragg angle -- that is, the angle of incidence and reflection, θ -- is held constant, the wavelength receiving maximum reinforcement is entirely dependent upon the layer spacing d. Because Bragg diffraction layer spacing in the cholesteric phase is dependent on temperature, there is a fixed relationship between temperature and the wavelength of light reflected from a cholesteric liquid crystal film.

3.2.2 Angle-Color Relationships

The wavelength of maximum scattering in a cholesteric liquid crystal is affected by the angle from which it is illuminated and the angle from which it is observed. At any temperature, the wavelength of maximum scattering depends on the angle of incidence and the angle of scattering. Scattering in cholesteric materials behaves as if it were coming from a number of regularly spaced or ordered planes existing in a medium having a refractive index of about 1.5. For a given angle of incidence and observation, maximum reflection will occur in those regions whose molecular layers are at the Bragg angle θ with respect to the incident light. (See Fig. 10.)

The wavelength of maximum reflection as a function of angle for a constant temperature is given by [16]
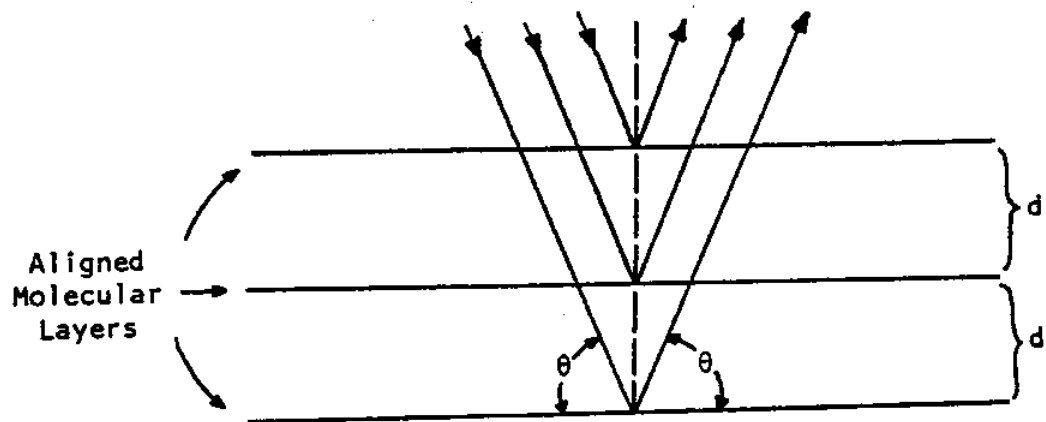
Fig. 9. Bragg Diffraction in a Crystalline Solid [15].
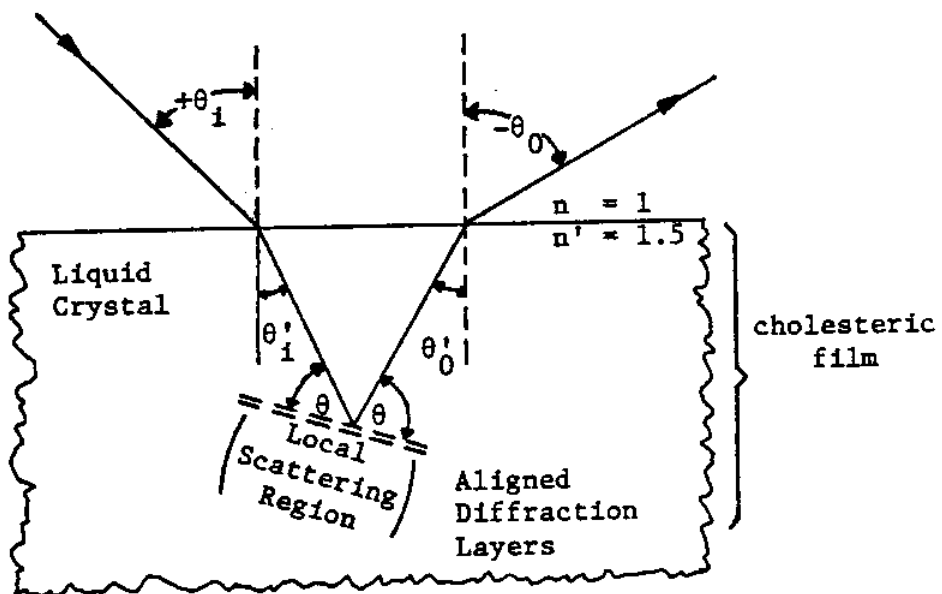
Fig. 10. Bragg Diffraction in a cholesteric film [16].

$$\lambda = \lambda_n \cos \tfrac{1}{2} [\sin^{-1}(\tfrac{n}{n'} \sin \theta_i) + \sin^{-1}(\tfrac{n}{n'} \sin \theta_o)]$$

$$= \lambda_n \sin \theta \quad ,$$

where

λ = wavelength of maximum reflection
λ_n = wavelength of maximum reflection for normal incidence and observation
n = index of refraction of the surrounding medium
n' = index of refraction of the liquid crystal
θ_i = angle of incidence
θ_o = angle of observation
θ = Bragg angle.

Figs. 11 and 12 show the dominant wavelength of the reflected light as a function of viewing angle for a material at a constant temperature.

3.3 LIQUID CRYSTAL SYSTEMS

By mixing two liquid crystals, blends are obtained with color responses intermediate between those of the initial materials, the properties obtained being governed by phase rule considerations [17]. (See Fig. 13.) The temperature at which the colors appear depends upon the melting point of the liquid crystal. Mixtures of cholesteric compounds exhibit color sensitivities over ranges as small as 0.1°C or as large as 30°C.

One of the most frequently used systems in nondestructive testing appears to be the mixture of oleyl cholesteryl carbonate and cholesteryl nonanoate; this system has the advantage ot not crystallizing for a long period of time [16]. The color-play range of this system increases in

Viewing Angle θ_s
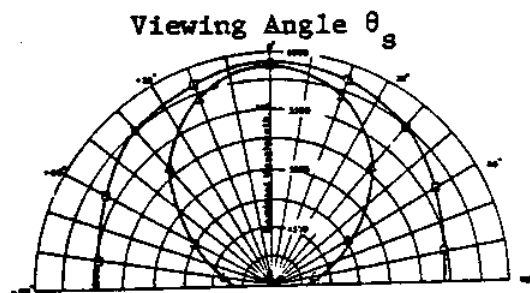
Fig. 11. A polar plot of scattering as a function of angle. The triangles represent the color which reflected when the angle of incidence is equal to the angle of scattering. The squares represent the wavelength of maximum scattering when the sample is illuminated at normal incidence and the scattering angle is changed [16].
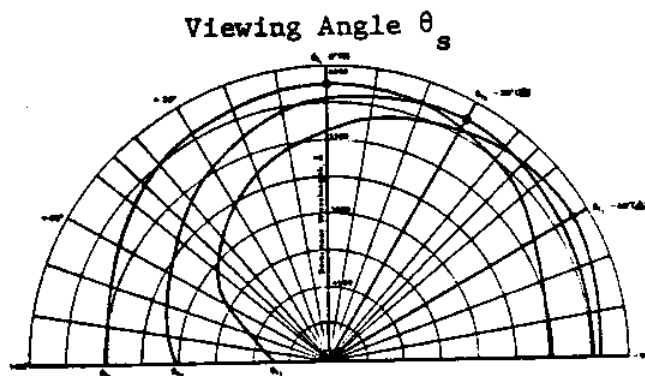
Viewing Angle θ_s

Fig. 12. The color of cholesteric liquids as a function of viewing angle for three fixed angles of illumination [16].
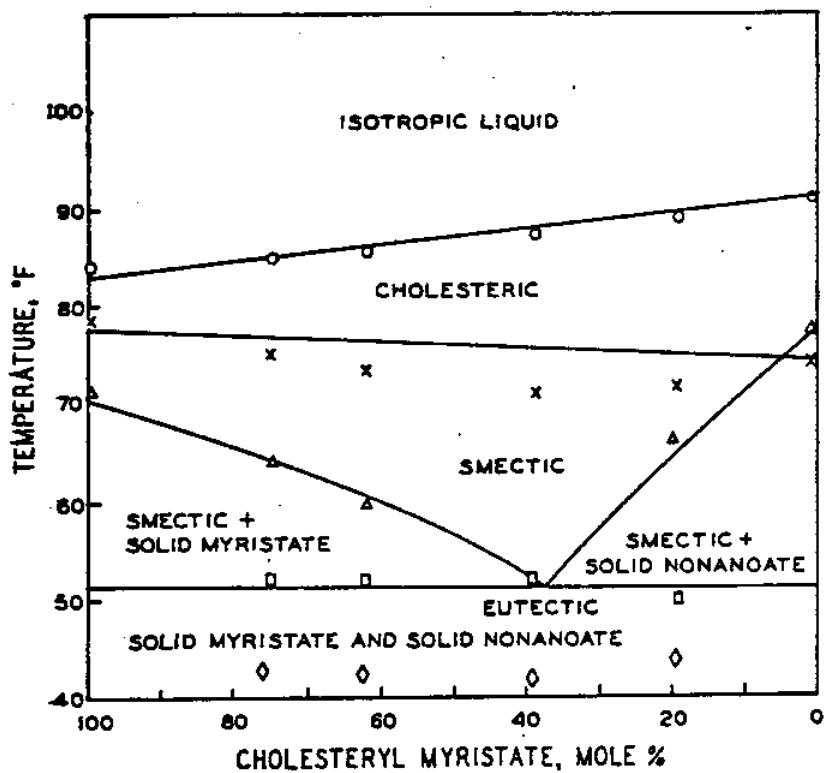
Fig. 13. Cholesteric liquid crystal ranges
          obtained on mixing cholesteryl non-
          anoate with cholesteryl myristate.
          (Refer to Figs. 2 and 3.) [17]

a monotonic manner when the fraction of cholesteryl nonanoate in the system is increased. (See Fig. 14.) Problems that occur in this system are primarily with the purity of the oleyl cholesteryl carbonate and with the oxidation of the material.

Other common systems are the various mixtures of cholesteryl pelargonate and cholesteryl butyrate. Pure cholesteryl pelargonate has a color-play range of 15°C. When 5 percent cholesteryl butyrate is added, the color-play range of the system becomes 1°C. (See Fig. 15.) Also, cholesteryl butyrate shows a decrease in color-play range when mixed with 5 percent cholesteryl pelargonate [9]. The present state of the art in preparing compositions for specific uses is such that liquid crystals can be formulated to produce colors up to 150°C with color ranges of 1°C to 30°C or more.

3.3.1 Available Types of Liquid Crystals

There are three types of temperature-sensitive liquid crystals available: pure compounds, premixed formulations for specific ranges, and encapsulated formulations for specific ranges in protective coatings. Some of these are "memory" temperature cholesterics which undergo nonreversible (with respect to temperature) transformations. These materials remain solid colors at temperatures below their trigger temperatures; at the trigger temperature the coatings become transparent. The color will not reappear on cooling through the trigger temperature unless the coating is reoriented by brushing.

3.3.2 Factors Affecting Response

Liquid crystal response can be affected by a variety of stimuli such as heat, electrical fields, magnetic fields, and shear forces. The colors are also sensitive to some organic vapors and to gases such as ammonia and oxides of nitrogen.

Liquid crystals are extremely sensitive to their environment and are adversely affected by airborne contaminants [20], atmospheric oxygen, and ultraviolet radiation [21]. Airborne contaminants can convert the molecular ordering of liquid crystals from the color-reflecting plane texture to a noncolored focal-conic texture. Eventually, the surface tension effects of dirt particles cause withdrawal of the liquid crystal away from the particle to produce a crater in the film.

Oxidative degradation becomes a problem during extended use of these materials. Some liquid crystal components are more sensitive to degradation than others so that care should be exercised in formulating compositions for high temperature or extended use. In these cases, antioxidants can be added to impede degradation. The effect of ultraviolet radiation on the response of cholesteric liquid crystals can be alleviated by adding small amounts of UV stabilizers to the liquid crystal. (See Fig. 16.)

3.4 LIQUID CRYSTAL CALIBRATION TECHNIQUES

Depending on the degree of accuracy required, there are several methods that can be used to calibrate temperature-sensitive cholesteric liquid
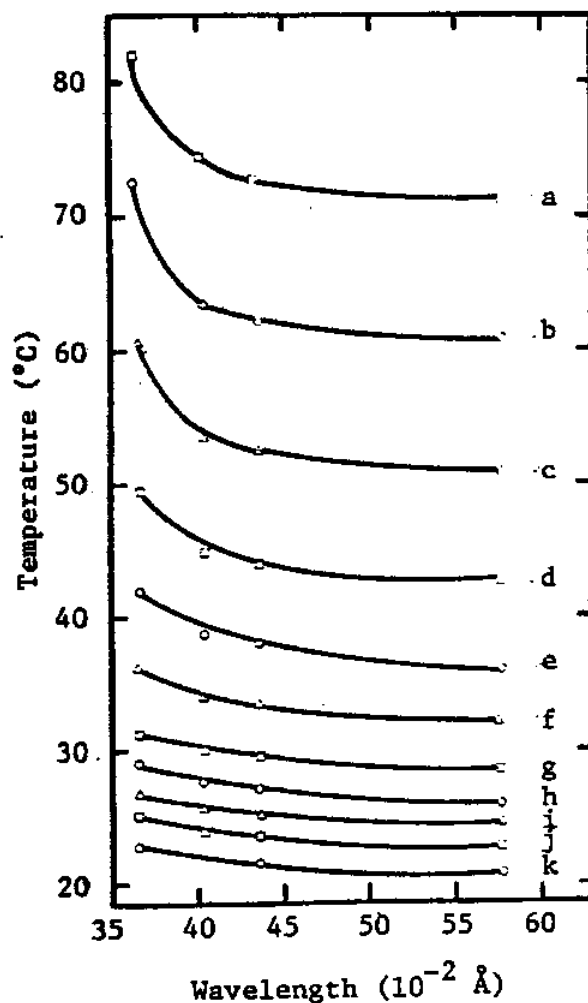
Fig. 14. The wavelength of maximum scattering plotted as a
function of temperature for various mixtures of
cholesteryl nonanoate and cholesteryl oleyl carbo-
nate. Curve a represents 100% cholesteryl nonano-
ate. Curve k represents 100% cholesteryl oleyl
carbonate. Curves b through j represent changing
the content of cholesteryl oleyl carbonate in
cholesteryl nonanoate by 10% steps [16].
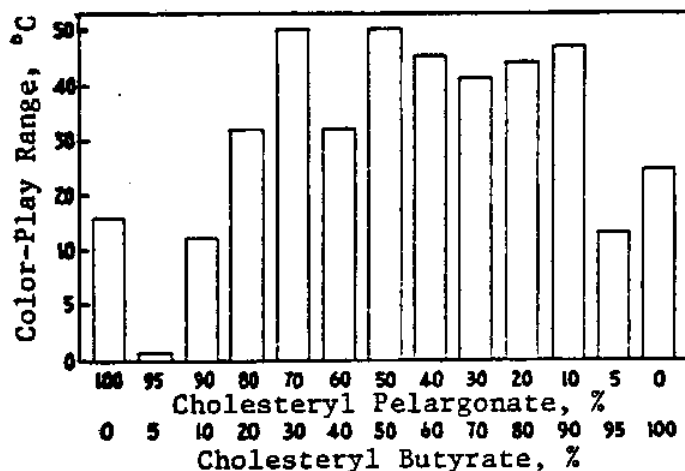
Fig. 15. Color-play range of mixtures of
cholesteryl pelargonate and chole-
steryl butyrate [18].
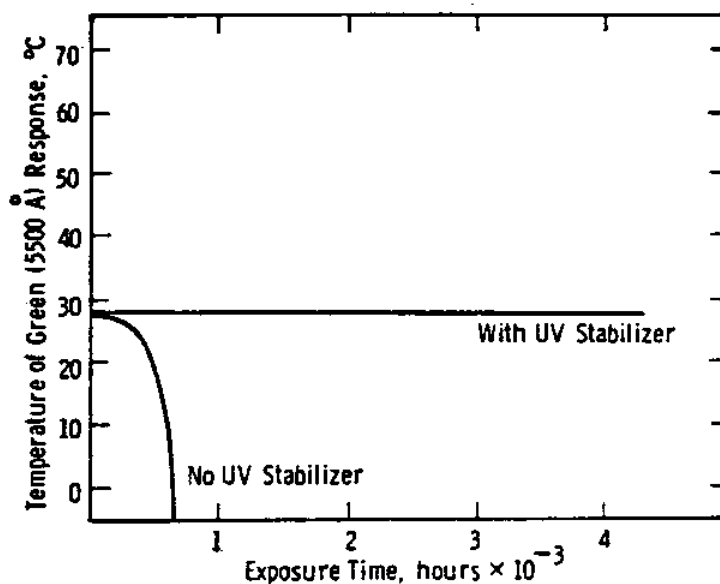
Fig. 16. Response of a cholesteric liquid
crystal exposed to ultraviolet (UV)
radiation, with and without UV
stabilizer [21].

crystals. The simplest method is to spray a sample onto a thin black mylar sheet and place the bulb of a heated mercury thermometer in contact with the opposite side of the sheet. As the thermometer cools, the coated area adjacent to the bulb will pass through the color spectrum and color transformation points can be correlated with the thermometer readings.

A water-filled rosemount constant temperature bath, capable of establishing and maintaining temperature to within 0.01°C, was employed in a liquid crystal calibration procedure by Cooper, et al. [19]. The bath temperature was monitored and controlled with a platinum resistance thermometer. Color was determined by direct visual observation. All liquid crystal formulations calibrated were applied to a piece of the material to which they would later be applied for data collection. The liquid-crystal-coated substrates were enclosed in small clear plastic bags to seal them from the damaging effects of the water. The package was then suspended in the water bath. The temperature of the bath was slowly raised until the event temperature range was reached. Careful adjustment of the bath temperature provided an accurate measure of the temperatures corresponding to the onset of red, then of green, etc., and finally of blue. This procedure may be repeated in reverse order by slowly lowering the bath temperature. Using this procedure, temperature and color may be calibrated to within an estimated accuracy of 0.1°C.

A very accurate technique was used by Fergason [16] in order to determine the temperature dependence of cholesteric materials. His device is sketched in Fig. 17. If the cholesteric phase is illuminated by mono-
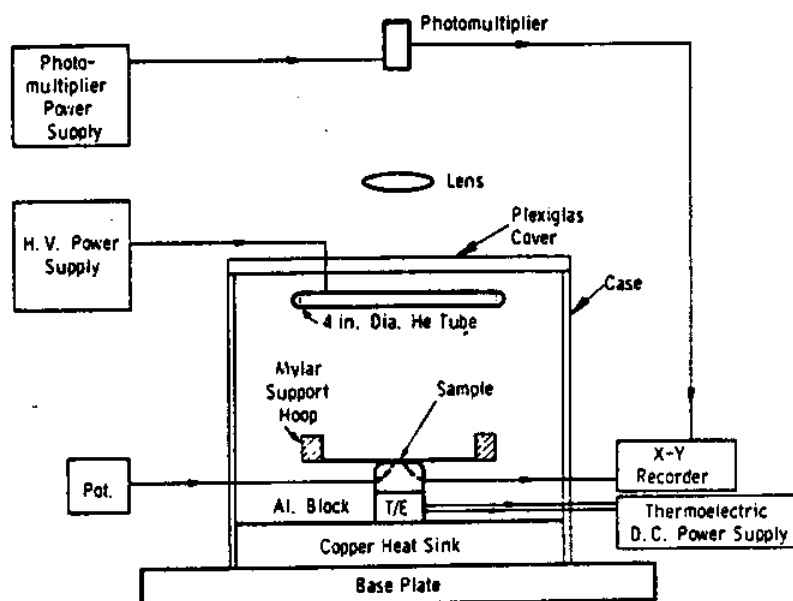
Fig. 17. A block diagram of the apparatus
for calibration of liquid crystals
[23].

chromatic light and the temperature varied so that the wavelength of maximum scattering passes through the wavelength of the source, the intensity of the light scattered will increase to a maximum and then decrease. If the source is a discharge lamp with a number of discrete emission lines, these will be visible as peaks of intensity. The line which is thus reflected is readily visible by observing the color of the cholesteric phase.

The apparatus shown in Fig. 17 makes use of these principles by illuminating the phase with one of the lamps described in Table 1. The temperature of the aluminum block is varied by using a thermoelectric unit which is driven by a variable d-c power supply. The block may be heated or cooled depending on the direction of current flow in the thermoelectric unit. The temperature range of this device as shown here is 120°C to -20°C. The temperature of the aluminum block is measured by a thermistor which drives the X axis of an X-Y recorder. As a cross reference and calibration source, a thermocouple is also used. Errors in this system occur in absolute measurements of temperature rather than temperature differences. The intensity of the light scattered is measured by a photodetector and fed to the Y axis of the recorder. The information which may be obtained in this manner is the temperature of each of the phase changes and the temperatures of scattering peaks. The plane texture of the cholesteric phase is formed by casting a film from a suitable solvent, usually hexane or petroleum ether, onto a substrate film, the back of which has previously been blackened. Fig. 18 shows a typical output of this apparatus for the illuminations.

TABLE I. Spectral Lamps for Wavelength
vs. Temperature Measurements
[23].

Light source	Wavelength (Å)
Hg	
UV	3663
Purple	4046
Blue	4358
Green	5460
Yellow	5780
He	
UV	3888
Blue	4685
Green	5015
Yellow	5875
Red	6560
Cd	
Blue	4799
Green	5085
Red	6438
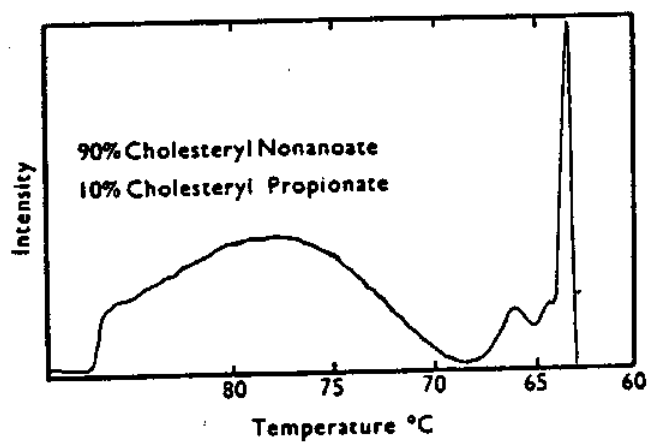
Fig. 18. Typical output of the apparatus
in Fig. 17 for the illumination
[23].

3.5 HANDLING

The handling method of liquid crystals is very important. The full potential of these interesting materials has not yet been realized because of the difficulty in forming surface films from these grease-like organic fluids. The usual method is to dissolve them in a solvent, then paint or spray the solution onto a pre-blackened surface. From a practical point of view, the liquid crystal layer should be about 0.001 in. thick. This film thickness is optimum because thinner layers give less intense colors and thicker layers reduce the resolution and speed of response as well as being a waste of material.

The liquid crystal layer is highly susceptible to degradation and tends to have a limited life during the test. Under ordinary room conditions, testing can continue from three to four hours before the film surface becomes marred. However, if it is desirable to leave the liquid crystal on for long periods of time, encapsulated cholesteric liquid crystals should be used because they are easily handleable films with a self-contained black background. Such a film can be instantly applied and removed from the surface, so that the need for an elaborate clean-up procedure is eliminated. Encapsulation also improves their resistance to environmental damage. But along with their many advantages, there are also several disadvantages. The film thickness required is greater when using encapsulated material, and therefore the heat capacity of the system is increased. Moreover, since the beads represent discrete elements, resolution is degraded slightly [16].

CHAPTER IV

THEORETICAL ANALYSIS

4.1 INTRODUCTION

In this chapter a theoretical basis for choosing the liquid crystal system to define the quantitative features of a delamination flaw in fiber reinforced laminates is established. Thermal testing is based upon the detection of surface temperature gradients induced by internal variations or defects in the test object which alter the object's normal heat flow pattern. The liquid crystals are used for mapping temperature gradients rather than measuring actual temperatures. The choice of liquid crystal system for thermographic mapping depends upon the temperature differences to be analyzed. For example, a system with a color-play range of 1°C is capable of detecting temperature differences as small as 0.1°C. For temperature differences of the order of 1°C, a system with a color-play range of about 5°C is preferable.

A heat source with a uniform radiant heat flux is used in the experimental thermal testing of composite laminates. The theoretical model consists of a flat plate laminate having thickness ℓ and which is initially at the ambient temperature T_∞ throughout. The laminate which has an interlaminar flaw is shown in Fig. 19. As indicated in Fig. 20, the plate is suddenly subjected to a net uniform radiant heat flux q". It is assumed that (1) the heat conduction through the plate is one-dimensional in the thickness direction, (2) the heat transfer coefficient h is the same for both surfaces of the laminate, and (3) the properties of the laminate and any material contained in the flaw are constant. Region I without the
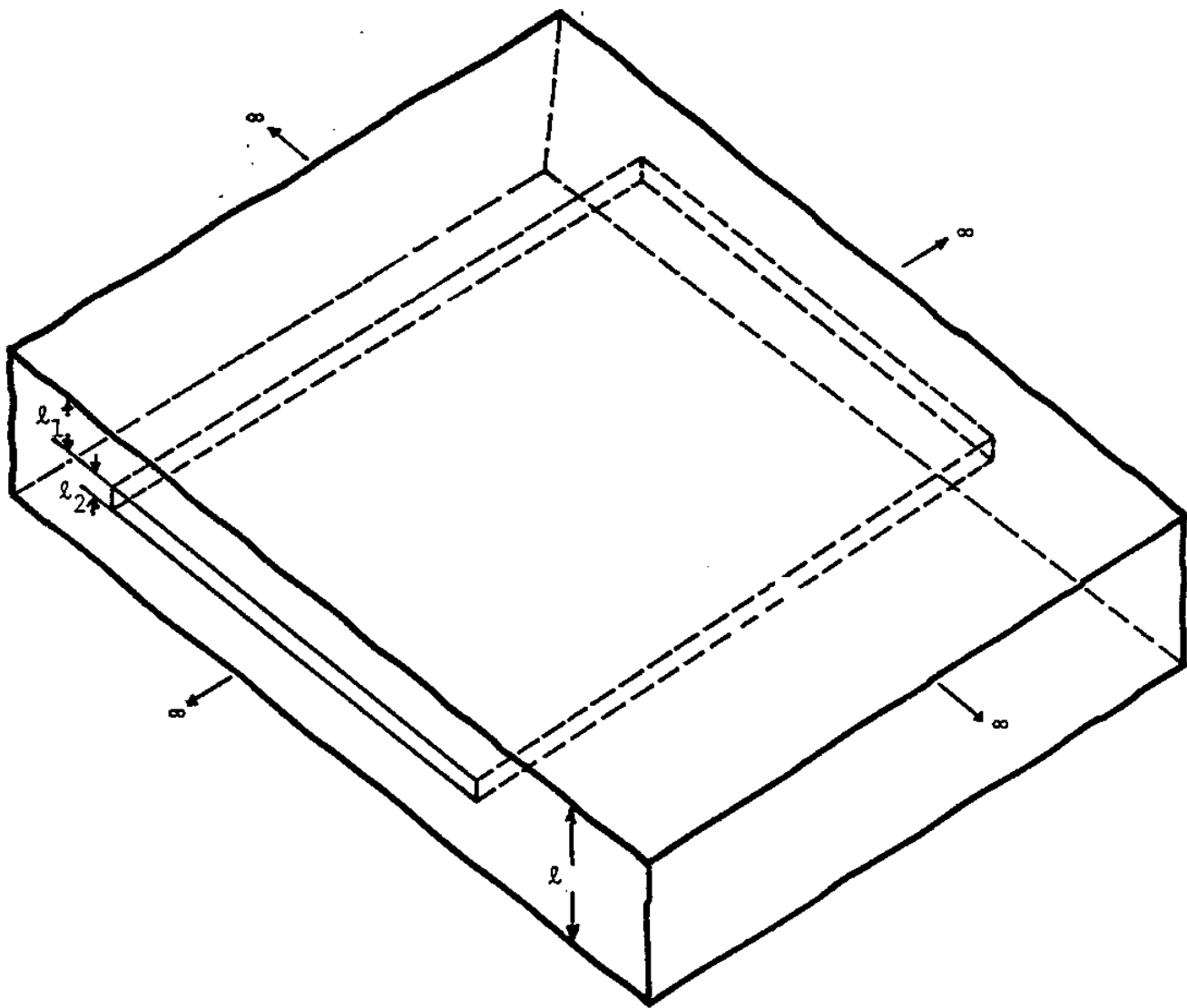
Fig. 19.   Isometric schematic of model of laminate con-
taining interlaminar flaw.

Fig. 20. Cross section of model of laminate con-
taining interlaminar flaw, showing geo-
metric and thermal variables.
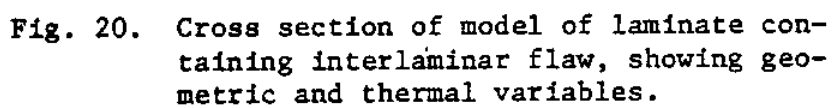
flaw and Region II with the flaw are defined, and because of the one-dimensional heat conduction assumption, the temperature distributions in Regions I and II are independent[†]. The temperature distributions in Regions I and II are different because of the presence of the flaw in Region II. The absolute value of the temperature difference on the surfaces of Regions I and II, ΔT, is defined by

$$\Delta T(t) = \left| T_{Is}(t) - T_{IIs}(t) \right| \qquad (1)$$

where the subscript s emphasizes that the temperatures of concern are at the surface. Thus, the color-play range and transition temperature of the liquid crystal system which is well suited for detecting a given flaw is related to ΔT and the corresponding surface temperatures, respectively.

4.2 CALCULATION OF T_{Is}

Region I is the unflawed part of the laminate. Heat conduction in this region is governed by [25]

$$\frac{\partial^2 T_I(x,t)}{\partial x^2} = \frac{1}{\alpha} \frac{\partial T_I(x,t)}{\partial t} \qquad \text{for } t > 0 \text{ and } 0 \le x \le \ell \qquad (2)$$

where $T_I(x,t)$ is the transient temperature distribution, α is the thermal diffusivity of the laminate material, t is time, and x is the coordinate in the thickness direction. The surface temperature T_{Is} is defined as

---

[†]This is a good assumption except for a transition zone between the two regions. The effect of this transition zone is actually illustrated in Fig. 20 where the surface temperature variation between Regions I and II is continuous rather than discontinuous.

$$T_{Is}(t) = T_I(0,t) \ . \tag{3}$$

The boundary conditions are

$$q'' - h[T_I(0,t) - T_\infty] + k \frac{\partial T_I(0,t)}{\partial x} = 0 \qquad \text{at } x = 0 \text{ and } t > 0 \tag{4}$$

$$h[T_I(\ell,t) - T_\infty] + k \frac{\partial T_I(\ell,t)}{\partial x} = 0 \qquad \text{at } x = \ell \text{ and } t > 0 \tag{5}$$

where eqns. (4) and (5) are simply statements of the conservation of energy at the boundaries $x = 0$ and $x = \ell$, respectively, and where k is the thermal conductivity of the laminate. The initial condition is

$$T_{Ii}(x,0) = T_\infty \qquad \text{at } t = 0 \text{ and } 0 \le x \le \ell \ . \tag{6}$$

The boundary condition in eqn. (4) is nonhomogeneous. In order to transform this nonhomogeneous boundary condition into a homogeneous boundary condition, let

$$\theta(x,t) \equiv T_I(x,t) - T_\infty \tag{7}$$

where $\theta(x,t)$ can be written as the sum of a steady-state part $\theta_s(x)$ and a transient part $\theta_t(x,t)$ as [25]

$$\theta(x,t) = \theta_s(x) + \theta_t(x,t) \ . \tag{8}$$

Substitution of eqn. (7) into eqns. (2), (4), (5), and (6) gives, respectively,

$$\frac{\partial^2 \theta(x,t)}{\partial x^2} = \frac{1}{\alpha} \frac{\partial \theta(x,t)}{\partial t} \tag{9}$$

$$q'' - h\theta(0,t) + k \frac{\partial \theta(0,t)}{\partial x} = 0 \tag{10}$$

$$h\theta(\ell,t) + k \frac{\partial \theta(\ell,t)}{\partial x} = 0 \tag{11}$$

$$\theta_i(x,0) = 0 . \tag{12}$$

In the steady state, eqns. (9), (10), and (11) become, respectively,

$$\frac{\partial^2 \theta_s(x)}{\partial x^2} = 0 \tag{13}$$

$$q'' - h\theta_s(0) + k \frac{\partial \theta_s(0)}{\partial x} = 0 \tag{14}$$

$$h\theta_s(\ell) + k \frac{\partial \theta_s(\ell)}{\partial x} = 0 \tag{15}$$

which have the solution [25]

$$\theta_s(x) = \frac{q''}{h[2 + Bi]} [1 + Bi - Bi(\frac{x}{\ell})]; \quad Bi \equiv \frac{h\ell}{k} . \tag{16}$$

Substitution of eqn. (16) into eqn. (8) gives an expression which if substituted into eqns. (9), (10), (11), and (12) yields, respectively,

$$\frac{\partial^2 \theta_t(x,t)}{\partial x^2} = \frac{1}{\alpha} \frac{\partial \theta_t(x,t)}{\partial t} \tag{17}$$

$$-h\theta_t(0,t) + k \frac{\partial \theta_t(0,t)}{\partial x} = 0 \tag{18}$$

$$h\theta_t(\ell,t) + k \frac{\partial \theta_t(\ell,t)}{\partial x} = 0 \tag{19}$$

$$\theta_{ti}(x,0) = -\theta_s(x) . \tag{20}$$

Eqn. (17) is a homogeneous partial differential equation and its boundary conditions are also homogeneous. Therefore, this equation can be solved by the method of separation of variables as [26]

$$\theta_t(x,t) = X(x)\phi(t) . \tag{21}$$

The product solution given by eqn. (21) converts eqns. (17), (18), (19),

and (20) to the following two sets of ordinary differential equations.

$$\frac{d^2X(x)}{dx^2} + \lambda_n^2 X(x) = 0 \tag{22}$$

$$-hX(0) + k\frac{dX(x)}{dx} = 0 \qquad \text{at } x = 0 \tag{23}$$

$$hX(\ell) + k\frac{dX(x)}{dx} = 0 \qquad \text{at } x = \ell \tag{24}$$

$$\frac{d\phi(t)}{dt} + \alpha\lambda_n^2\phi(t) = 0 \tag{25}$$

$$\phi(t) = 0 \qquad \text{for } t \to \infty . \tag{26}$$

The general solution of eqn. (22) is

$$X(x) = C_1\sin(\lambda_n x) + C_2\cos(\lambda_n x)$$

which if substituted into eqns. (23) and (24) gives

$$\lambda_n kC_1 - hC_2 = 0 \tag{27}$$

$$[h \sin(\lambda_n\ell) + k\lambda_n\cos(\lambda_n\ell)]C_1 + [h \cos(\lambda_n\ell) - k\lambda_n\sin(\lambda_n\ell)]C_2 = 0 . \tag{28}$$

The unknown eigenvalues λ_n are obtained from the requirement that the algebraic eqns. (27) and (28) have a nontrivial solution. Thus, the determinant of the coefficients C_1 and C_2 must be equal to zero, and therefore the eigenvalues are the roots of the transcendental equation

$$((\lambda_n\ell)^2 - (Bi)^2)\sin(\lambda_n\ell) - 2Bi\lambda_n\ell\cos(\lambda_n\ell) = 0 . \tag{29}$$

The solution of eqn. (25) is [26]

$$\phi(t) = C_3e^{-\alpha\lambda_n^2 t} \tag{30}$$

and thus the product solution eqn. (21) may be written as

$$\theta_t(x,t) = \sum_{n=1}^{\infty} [a_n \sin(\lambda_n x) + b_n \cos(\lambda_n x)] e^{-\alpha \lambda_n^2 t} \quad . \tag{31}$$

Substituting the initial condition eqn. (20) into eqn. (31) gives

$$\theta_t(x,0) = -\theta_s(x) = \sum_{n=1}^{\infty} [a_n \sin(\lambda_n x) + b_n \cos(\lambda_n x)] \tag{32}$$

where the Fourier coefficients are defined as [27]

$$a_n = \frac{\displaystyle\int_0^{\ell} (-\theta_s(x))\sin(\lambda_n x)\, dx}{\displaystyle\int_0^{\ell} \sin^2(\lambda_n x)\, dx}$$

$$= -\frac{2q'' \left[1 + Bi - \cos(\lambda_n \ell) - \left(\dfrac{Bi}{\lambda_n \ell}\right)\sin(\lambda_n \ell)\right]}{h(2 + Bi)[\lambda_n \ell - \sin(\lambda_n \ell)\cos(\lambda_n \ell)]} \tag{33}$$

$$b_n = \frac{\displaystyle\int_0^{\ell} (-\theta_s(x))\cos(\lambda_n x)\, dx}{\displaystyle\int_0^{\ell} \cos^2(\lambda_n x)\, dx}$$

$$= \frac{2q'' \left[\left(\dfrac{Bi}{\lambda_n \ell}\right)\cos(\lambda_n \ell) - \sin(\lambda_n \ell) - \dfrac{Bi}{\lambda_n \ell}\right]}{h(2 + Bi)[\lambda_n \ell + \sin(\lambda_n \ell)\cos(\lambda_n \ell)]} \quad . \tag{34}$$

Therefore, combining eqns. (7), (16), and (31), all evaluated at $x = 0$, the surface temperature in Region I as a function of time is given by

$$T_{Is}(t) = T_{\infty} + \frac{q'' (1 + Bi)}{h(2 + Bi)} + \sum_{n=1}^{\infty} b_n e^{-\alpha \lambda_n^2 t} \quad . \tag{35}$$

4.3 CALCULATION OF T_{IIs}

Region II is the region of the laminate which contains the flaw. Region II is modeled as three parallel layers and therefore heat conduction in this region is governed by [28]

$$\frac{\partial^2 T_{IIi}(x,t)}{\partial x^2} = \frac{1}{\alpha_i} \frac{\partial T_{IIi}(x,t)}{\partial t} \qquad \text{in } x_i \leq x \leq x_{i+1}, \ t > 0 \qquad (36)$$
$$i = 1,2,3$$

where $T_{IIi}(x,t)$ is the transient temperature distribution in layer i and α_i is the thermal diffusivity of layer i. The x_i coordinates are shown in Fig. 20. The surface temperature at x_1 is T_{IIs} which is

$$T_{IIs}(t) = T_{II1}(0,t) . \qquad (37)$$

The boundary conditions are

$$q'' - h[T_{II1}(x_1,t) - T_\infty]$$

$$+ k_1 \frac{\partial T_{II1}(x_1,t)}{\partial x} = 0 \qquad \begin{array}{l}\text{at the outer surface} \\ x_1; t > 0\end{array} \qquad (38)$$

$$k_3 \frac{\partial T_{II3}(x_4,t)}{\partial x}$$

$$+ h[T_{II3}(x_4,t) - T_\infty] = 0 \qquad \begin{array}{l}\text{at the outer surface} \\ x_4; t > 0\end{array} \qquad (39)$$

and the continuity conditions are

$$T_{IIi}(x_{i+1},t) = T_{II,i+1}(x_{i+1},t) \qquad \begin{array}{l}\text{continuity of temperature} \\ \text{at the interface, } i = 1,2\end{array} \qquad (40)$$

$$k_1 \frac{\partial T_{IIi}(x_{i+1}, t)}{\partial x}$$

$$= k_{i+1} \frac{\partial T_{II,i+1}(x_{i+1}, t)}{\partial x} \qquad \text{continuity of temperature} \qquad (41)$$
$$\text{at the interface, } i = 1, 2$$

where the k_i are the thermal conductivities. Note that eqn. (40) has been written with the assumption that there is no thermal contact resistance at the interfaces x_2 and x_3. The initial conditions are

$$T_{IIi}(x, 0) = T_\infty \qquad \text{in } x_i \le x \le x_{i+1} \qquad (42)$$
$$i = 1, 2, 3 \quad \text{for } t = 0 .$$

The boundary conditions in eqns. (38) and (39) are nonhomogeneous. In order to transform these into homogeneous boundary conditions, let

$$\theta_i(x, t) = T_{IIi}(x, t) - T_\infty \qquad (43)$$

where the $\theta_i(x,t)$ can be written as the sum of steady-state parts $\theta_{si}(x)$ and transient parts $\theta_{ti}(x,t)$ as [25]

$$\theta_i(x, t) = \theta_{si}(x) + \theta_{ti}(x, t) \qquad \text{for } i = 1, 2, 3 . \qquad (44)$$

Substitution of eqn. (43) into eqns. (36) and (38) through (42) gives, respectively,

$$\frac{\partial^2 \theta_i(x,t)}{\partial x^2} = \frac{1}{\alpha_i} \frac{\partial \theta_i(x,t)}{\partial t} \qquad i = 1, 2, 3; \ x_i \le x \le x_{i+1}; \ t > 0 \qquad (45)$$

$$q'' - h\theta_1(x_1, t) + k_1 \frac{\partial \theta_1(x_1, t)}{\partial x} = 0 \qquad (46)$$

$$k_3 \frac{\partial \theta_3(x_4, t)}{\partial x} + h\theta_3(x_4, t) = 0 \qquad (47)$$

$$\theta_i(x_{i+1}, t) = \theta_{i+1}(x_{i+1}, t) \qquad i = 1, 2 \qquad (48)$$

$$k_i \frac{\partial \theta_i(x_{i+1}, t)}{\partial x} = k_{i+1} \frac{\partial \theta_{i+1}(x_{i+1}, t)}{\partial x} \qquad i = 1,2 \qquad (49)$$

$$\theta_i(x,0) = 0 \qquad i = 1,2,3; \; x_i \leq x \leq x_{i+1}; \; t = 0 . \qquad (50)$$

In the steady state, eqns. (45) through (49) become, respectively,

$$\frac{\partial^2 \theta_{si}(x)}{\partial x^2} = 0 \qquad i = 1,2,3; \; x_i \leq x \leq x_{i+1} \qquad (51)$$

$$q'' - h\theta_{s1}(x_1) + k_1 \frac{\partial \theta_{s1}(x_1)}{\partial x} = 0 \qquad (52)$$

$$k_3 \frac{\partial \theta_{s3}(x_4)}{\partial x} + h\theta_{s3}(x_4) = 0 \qquad (53)$$

$$\theta_{si}(x_{i+1}) = \theta_{s,i+1}(x_{i+1}) \qquad i = 1,2 \qquad (54)$$

$$k_i \frac{\partial \theta_{si}(x_{i+1})}{\partial x} = k_{i+1} \frac{\partial \theta_{s,i+1}(x_{i+1})}{\partial x} \qquad i = 1,2 \qquad (55)$$

which have the solutions [25]

$$\theta_{s1} = \hat{\theta}_1 - \frac{(x - x_1)}{(x_2 - x_1)}(\hat{\theta}_1 - \hat{\theta}_2) \qquad x_1 \leq x \leq x_2 \qquad (56)$$

$$\theta_{s2} = \hat{\theta}_2 - \frac{(x - x_2)}{(x_3 - x_2)}(\hat{\theta}_2 - \hat{\theta}_3) \qquad x_2 \leq x \leq x_3 \qquad (57)$$

$$\theta_{s3} = \hat{\theta}_3 - \frac{(x - x_3)}{(x_4 - x_3)}(\hat{\theta}_3 - \hat{\theta}_4) \qquad x_3 \leq x \leq x_4 \qquad (58)$$

where

$$\hat{\theta}_1 = \frac{q''(1 + Bi_1 + Bi_2 + Bi_3)}{h(2 + Bi_1 + Bi_2 + Bi_3)} \quad ; \quad Bi_1 = \frac{h(x_2 - x_1)}{k_1} \qquad (59)$$

$$\hat{\theta}_2 = \frac{q''(1 + Bi_2 + Bi_3)}{h(2 + Bi_1 + Bi_2 + Bi_3)} \quad ; \quad Bi_2 = \frac{h(x_3 - x_2)}{k_2} \qquad (60)$$

$$\overset{\circ}{\theta}_3 = \frac{q''(1 + Bi_3)}{h(2 + Bi_1 + Bi_2 + Bi_3)} \quad ; \quad Bi_3 = \frac{h(x_4 - x_3)}{k_3} \qquad (61)$$

$$\overset{\circ}{\theta}_4 = \frac{q''}{h(2 + Bi_1 + Bi_2 + Bi_3)} \quad . \qquad (62)$$

Substitution of the steady-state solutions given in eqns. (56), (57), and (58) into eqn. (44), and then substitution of each of the resulting expressions into eqns. (45) through (50) give, respectively,

$$\frac{\partial^2 \theta_{ti}(x,t)}{\partial x^2} = \frac{1}{\alpha_i} \frac{\partial \theta_{ti}(x,t)}{\partial t} \qquad i = 1,2,3; \; x_i \le x \le x_{i+1} \qquad (63)$$

$$-h\theta_{t1}(x_1,t) + k_1 \frac{\partial \theta_{t1}(x_1,t)}{\partial x} = 0 \qquad (64)$$

$$\theta_{ti}(x_{i+1},t) = \theta_{t,i+1}(x_{i+1},t) \qquad i = 1,2 \qquad (65)$$

$$k_i \frac{\partial \theta_{ti}(x_{i+1},t)}{\partial x} = k_{i+1} \frac{\partial \theta_{t,i+1}(x_{i+1},t)}{\partial x} \qquad i = 1,2 \qquad (66)$$

$$h\theta_{t3}(x_4,t) + k_3 \frac{\partial \theta_{t3}(x_4,t)}{\partial x} = 0 \qquad (67)$$

$$\theta_{ti}(x,0) = -\theta_{si}(x) \qquad i = 1,2,3; \; x_i \le x \le x_{i+1} \quad . \qquad (68)$$

Eqns. (63) are homogeneous partial differential equations and the associated boundary conditions are homogeneous also. Thus, the equations may be solved by the method of separation of variables by assuming solutions of the form [29]

$$\theta_{ti}(x,t) = \sum_{n=1}^{\infty} A_n X_{in}(x) e^{-\alpha_i \beta_{in}^2 t} \qquad \text{in layer i, } i = 1,2,3 \; . \qquad (69)$$

The solutions given in eqns. (69) convert the formulation of the problem

to the set of eigenvalue problems

$$\frac{d^2X_{1n}(x)}{dx^2} + \beta_{1n}^2 X_{1n}(x) = 0 \qquad \text{in layer } i, \ i = 1,2,3 \qquad (70)$$

with the boundary conditions

$$-k_1 \frac{dX_{1n}(x_1)}{dx} + hX_{1n}(x_1) = 0 \qquad (71)$$

$$X_{1n}(x_{i+1}) = X_{i+1,n}(x_{i+1}) \qquad i = 1,2 \qquad (72)$$

$$k_i \frac{dX_{1n}(x_{i+1})}{dx} = k_{i+1} \frac{dX_{i+1,n}(x_{i+1})}{dx} \qquad i = 1,2 \qquad (73)$$

$$k_3 \frac{dX_{3n}(x_4)}{dx} + hX_{3n}(x_4) = 0 \ . \qquad (74)$$

The solutions of the above eigenvalue problems are of the form

$$X_{1n} = C_{1n}\cos(\beta_{1n}x) + D_{1n}\sin(\beta_{1n}x) \qquad x_i \le x \le x_{i+1} \ . \qquad (75)$$

$$i = 1,2,3$$

The substitution of eqn. (75) in eqns. (71) through (74) gives

$$[h\cos(\beta_{1n}x_1) + k_1\beta_{1n}\sin(\beta_{1n}x_1)]C_{1n}$$

$$+ [h\sin(\beta_{1n}x_1) - k_1\beta_{1n}\cos(\beta_{1n}x_1)]D_{1n} = 0 \qquad (76)$$

$$[\cos(\beta_{1n}x_2)]C_{1n} + [\sin(\beta_{1n}x_2)]D_{1n}$$

$$+ [-\cos(\beta_{2n}x_2)]C_{2n} + [-\sin(\beta_{2n}x_2)]D_{2n} = 0 \qquad (77)$$

$$[-\frac{k_1}{k_2}\beta_{1n}\sin(\beta_{1n}x_2)]C_{1n} + [\frac{k_1}{k_2}\beta_{1n}\cos(\beta_{1n}x_2)]D_{1n}$$

$$+ [\beta_{2n}\sin(\beta_{2n}x_2)]C_{2n} + [-\beta_{2n}\cos(\beta_{2n}x_2)]D_{2n} = 0 \qquad (78)$$

$$[\cos(\beta_{2n}x_3)]C_{2n} + [\sin(\beta_{2n}x_3)]D_{2n}$$

$$+ [-\cos(\beta_{3n}x_3)]C_{3n} + [-\sin(\beta_{3n}x_3)]D_{3n} = 0 \qquad (79)$$

$$[-\frac{k_2}{k_3}\beta_{2n}\sin(\beta_{2n}x_3)]C_{2n} + [\frac{k_2}{k_3}\beta_{2n}\cos(\beta_{2n}x_3)]D_{2n}$$

$$+ [\beta_{3n}\sin(\beta_{3n}x_3)]C_{3n} + [-\beta_{3n}\cos(\beta_{3n}x_3)]D_{3n} = 0 \qquad (80)$$

$$[h\cos(\beta_{3n}x_4) - k_3\beta_{3n}\sin(\beta_{3n}x_4)]C_{3n}$$

$$+ [h\sin(\beta_{3n}x_4) + k_3\beta_{3n}\cos(\beta_{3n}x_4)]D_{3n} = 0 \qquad (81)$$

or

$$\begin{bmatrix} A & B & 0 & 0 & 0 & 0 \\ C & D & E & F & 0 & 0 \\ G & H & I & J & 0 & 0 \\ 0 & 0 & K & L & M & N \\ 0 & 0 & \emptyset & P & Q & R \\ 0 & 0 & 0 & 0 & S & T \end{bmatrix} \begin{bmatrix} C_{1n} \\ D_{1n} \\ C_{2n} \\ D_{2n} \\ C_{3n} \\ D_{3n} \end{bmatrix} = 0 \qquad (82)$$

where

$$A = [h\cos(\beta_{1n}x_1) + k_1\beta_{1n}\sin(\beta_{1n}x_1)]$$

$$B = [h\sin(\beta_{1n}x_1) - k_1\beta_{1n}\cos(\beta_{1n}x_1)]$$

$$C = [\cos(\beta_{1n}x_2)]$$

$$\qquad\qquad\qquad\qquad\qquad\qquad (83)$$
$$\qquad\qquad\qquad\qquad\qquad\text{(continued)}$$

$$D = [\sin(\beta_{1n}x_2)]$$

$$E = [-\cos(\beta_{2n}x_2)]$$

$$F = [-\sin(\beta_{2n}x_2)]$$

$$G = [- \frac{k_1}{k_2} \beta_{1n} \sin(\beta_{1n} x_2)]$$

$$H = [\frac{k_1}{k_2} \beta_{1n} \cos(\beta_{1n} x_2)]$$

$$I = [\beta_{2n} \sin(\beta_{2n} x_2)]$$

$$J = [-\beta_{2n} \cos(\beta_{2n} x_2)]$$

$$K = [\cos(\beta_{2n} x_3)]$$

$$L = [\sin(\beta_{2n} x_3)]$$

$$M = [-\cos(\beta_{3n} x_3)]$$

$$N = [-\sin(\beta_{3n} x_3)]$$

$$\emptyset = [- \frac{k_2}{k_3} \beta_{2n} \sin(\beta_{2n} x_3)]$$

$$P = [\frac{k_2}{k_3} \beta_{2n} \cos(\beta_{2n} x_3)]$$

$$Q = [\beta_{3n} \sin(\beta_{3n} x_3)]$$

$$R = [-\beta_{3n} \cos(\beta_{3n} x_3)]$$

$$S = [h \cos(\beta_{3n} x_4) - k_3 \beta_{3n} \sin(\beta_{3n} x_4)]$$

$$T = [h \sin(\beta_{3n} x_4) + k_3 \beta_{3n} \cos(\beta_{3n} x_4)] \; .$$

(continued)
(83)

Evaluation of the coefficients C_{in} and D_{in} from eqns. (82) cannot be performed yet because the system includes the unknown eigenvalues β_{in}, which are determined by the following considerations. Consider the inter-face at x_i between layers (i-1) and i. Because there can be no energy

storage in the infinitesimal thickness of the interface, the time behavior of temperature at the interface x_i must be the same on either side of x_i. This requirement is satisfied by [30]

$$\alpha_i \beta_{in}^2 = \alpha_{i+1} \beta_{i+1,n}^2 \qquad \text{for } i = 1,2 \qquad (84)$$

By means of relation (84) it is possible to express all but one of the β_{in} in terms of that remaining one, say, β_{1n}. Because the six equations in the system (82) are homogeneous equations, the coefficients C_{in} and D_{in} may be determined by expressing them in terms of any one of them, say, C_{1n}. Hence,

$$D_{1n} = \left[-\frac{A}{B} \right] C_{1n} \qquad (85)$$

$$C_{2n} = \left[\frac{-ADJ + AFH + BCJ - BFG}{BFI - BEJ} \right] C_{1n} \qquad (86)$$

$$D_{2n} = \left[\frac{ADI - AEH - BCI + BEG}{BFI - BEJ} \right] C_{1n} \qquad (87)$$

$$C_{3n} = \left[\frac{[-ADJ + AFH + BCJ - BEJ][-\emptyset T] + [ADI - AEH - BCI + BEG][-PT]}{[BFI - BEJ][QT - SR]} \right] C_{1n} \qquad (88)$$

$$D_{3n} = \left[\frac{[-ADJ + AFH + BCJ - BFG][S\emptyset] + [ADI - AEH - BCI + BEG][SP]}{[BFI - BEJ][QT - SR]} \right] C_{1n} . \qquad (89)$$

An additional relationship to determine the unknown eigenvalue β_{1n} may be obtained from the requirement that the system of six algebraic equations (82) have a nontrivial solution if the determinant of the coefficients C_{in} and D_{in} vanish. By equating this determinant to zero, the following transcendental equation is obtained:

$$[LQT - LRS - MPT + NPS][ADI - AEH - BCI + BEG]$$
$$+ [KQT - KRS - M\emptyset T + N\emptyset S][-ADJ + AFH + BCJ - BFG] = 0 \qquad (90)$$

where the positive roots of eqn. (90) give the eigenvalues $\beta_{11} < \beta_{12} <$ $\ldots < \beta_{1n} < \ldots$. For each of these eigenvalues there are corresponding values of C_{1n}, D_{1n}, and the eigenfunctions $X_{1n}(x)$ which can be determined.

In general, for a region containing more than one layer, the eigenfunctions $X_{1n}(x)$ are not orthogonal with respect to the usual weighting functions derived from a one-region Sturm-Louisville problem [31]. However, an orthogonal set $G_n(x)$ can be constructed from the non-orthogonal set $X_{1n}(x)$ by multiplying the X_{1n} in each layer i by the orthogonality factor W_i which is called the discontinuous weighting function for layer i. Hence [30],

$$G_n(x) = W_i X_{1n}(x) \qquad \text{in layer i} \qquad (91)$$

where the discontinuous weighting functions are

$$W_i = \left(\frac{k_i}{\alpha_i}\right)^{1/2} . \qquad (92)$$

Tittle [32] has shown that the discontinuous weighting function is unchanged whether there is perfect thermal contact or a linear thermal contact resistance at the interface.

So far, the eigenfunctions and the eigenvalues for use in the solution given by eqn. (69) have been determined, but the unknown coefficients A_n are yet to be determined. Now, the initial condition (68) will be used to find the A_n. The initial condition function $\theta_t(x,0)$ may be expressed as a sum of three subfunctions $\theta_{ti}(x,0)$ in the form

$$\theta_t(x,0) = \sum_{i=1}^{3} \theta_{ti}(x,0) \qquad (93)$$

where the subfunctions $\theta_{ti}(x,0)$ are defined as [30]

$$\theta_{ti}(x,0) = \theta_t(x,0) \qquad \text{in layer i} \qquad (94\text{-a})$$

$$\theta_{ti}(x,0) = 0 \qquad \text{in all other layers .} \qquad (94\text{-b})$$

Each subfunction $\theta_{ti}(x,0)$ can be expanded into a series of orthogonal functions $G_n(x)$ in the form

$$\theta_{ti}(x,0) = \sum_{n=1}^{\infty} B_{in} G_n(x) \ . \qquad (95)$$

Each expansion must be made over the entire range $x_1 \le x \le x_4$, spanning all three layers. The unknown coefficients B_{in} in the expansion (95) are determined by a generalized Fourier analysis over the entire range of the three layers; therefore,

$$B_{in} = \frac{\displaystyle\int_{\substack{\text{three}\\\text{layers}}} \theta_{ti}(x,0)G_n(x)w(x)\ dx}{\displaystyle\int_{\substack{\text{three}\\\text{layers}}} [G_n(x)]^2 w(x)\ dx} \qquad (96)$$

where $w(x)$ is the usual one region Sturm-Louisville orthogonality function and which, in rectangular cartesian coordinates, is

$$w(x) = 1 \ .$$

Substitution of eqns. (91), (93), and (94) into eqn. (96) gives

$$B_{in} = \frac{W_i \int_{\text{layer } i} \theta_t(x,0) X_{in}(x)\, dx}{\sum_{i=1}^{3} W_i^2 \int_{\text{layer } i} X_{in}^2(x)\, dx} \; . \tag{97}$$

Using eqns. (75) and (93), eqn. (97) may be evaluated to give

$$B_{1n} = \frac{T_1}{\Delta} \tag{98}$$

$$B_{2n} = \frac{T_2}{\Delta} \tag{99}$$

$$B_{3n} = \frac{T_3}{\Delta} \tag{100}$$

where

$$
T_i = W_i \left\{ \frac{-\theta_i C_{in}}{\beta_{in}} [\sin(\beta_{in} x_{i+1}) - \sin(\beta_{in} x_i)] \right.
$$

$$
+ \frac{\theta_i D_{in}}{\beta_{in}} [\cos(\beta_{in} x_{i+1}) - \cos(\beta_{in} x_i)]
$$

$$
+ \frac{(\theta_{i+1} - \theta_i)}{(x_{i+1} - x_i)} \left\{ C_{in} \left[\left(\frac{x_{i+1}\sin(\beta_{in} x_{i+1}) - x_i\sin(\beta_{in} x_i)}{\beta_{in}} \right) \right. \right.
$$

$$
\left. + \left(\frac{\cos(\beta_{in} x_{i+1}) - \cos(\beta_{in} x_i)}{\beta_{in}^2} \right) \right]
$$

$$
+ D_{in} \left[\left(\frac{-x_{i+1}\cos(\beta_{in} x_{i+1}) + x_i\cos(\beta_{in} x_i)}{\beta_{in}} \right) \right.
$$

$$
\left. \left. \left. + \left(\frac{\sin(\beta_{in} x_{i+1}) - \sin(\beta_{in} x_i)}{\beta_{in}^2} \right) \right] \right] \right\}
$$

and

$$\Delta = \sum_{i=1}^{3} W_i^2 \left(\frac{C_{in}D_{in}}{2\beta_{in}}[\cos(2\beta_{in}x_i) - \cos(2\beta_{in}x_{i+1})] \right.$$

$$- \frac{(D_{in}^2 - C_{in}^2)}{4\beta_{in}}[\sin(2\beta_{in}x_{i+1}) - \sin(2\beta_{in}x_i)]$$

$$\left. + \frac{(C_{in}^2 + D_{in}^2)}{2}(x_{i+1} - x_i) \right) .$$

By substituting eqn. (91) into eqn. (95), the $G_{in}(x)$ functions may be replaced by $W_i X_{in}(x)$ so that

$$\theta_{t1}(x,0) = \sum_{n=1}^{\infty} B_{in}W_i X_{in}(x) . \qquad x_1 \leq x \leq x_4 \qquad (101)$$

If eqn. (69) is evaluated at $t = 0$, it becomes

$$\theta_t(x,0) = \sum_{n=1}^{\infty} A_n X_{in}(x) \qquad \text{in } x_1 \leq x \leq x_4 \qquad (102)$$

Using eqn. (101) in (93) and equating to eqn. (102) gives

$$A_n = \sum_{i=1}^{3} W_i B_{in} . \qquad (103)$$

Therefore, by substituting the values of B_{in} from eqn. (97) into eqn. (103), the A_n become

$$A_n = \frac{\displaystyle\sum_{i=1}^{3} W_i^2 \int_{\text{layer } i} \theta_t(x,0)X_{in}(x) \, dx}{\displaystyle\sum_{i=1}^{3} W_i^2 \int_{\text{layer } i} [X_{in}(x)]^2 \, dx} . \qquad (104)$$

-65-

Note that if eqns. (85) through (89) are substituted into eqn. (75), each of the resulting eigenfunctions $X_{1n}(x)$ will include the unknown coefficient C_{1n} as a product factor. So, when the $X_{1n}(x)$ are substituted into the solution (69) with the A_n as given in eqn. (104), the unknown coefficient C_{1n} will cancel. Therefore, the solution of eqns. (63) is complete since the terms in the relation (69) may be found in accordance with eqn. (104) for the A_n, eqns. (75) and (85) through (89) for the $X_{1n}(x)$, and eqns. (84) and (90) for the β_{1n}. Hence, the surface temperature in Region II as a function of time is given by combining eqns. (43), (44), and (69) as

$$T_{IIs}(t) = T_\infty + \frac{q''(1 + Bi_1 + Bi_2 + Bi_3)}{h(2 + Bi_1 + Bi_2 + Bi_3)} + \sum_{n=1}^{\infty} A_n e^{-\alpha_1 \beta_{1n}^2 t} . \qquad (105)$$

CHAPTER V

NUMERICAL CALCULATION PROCEDURE

In chapter IV, the analytical expressions for the calculation of $T_{Is}(t)$ and $T_{IIs}(t)$, the surface temperature in Regions I and II, respectively, were derived. (See Fig. 19.) In this chapter a computation algorithm for calculating the values of T_{Is}, T_{IIs}, and their difference ΔT is developed.

In the computer program, the analytical procedures for the calculation of T_{Is} and T_{IIs} as described in sections 4.2 and 4.3 are implemented. Fig. 21 shows the flowchart of the program. A printed list of the FORTRAN IV program appears in Appendix 1.

5.1 CALCULATION OF EIGENVALUES

In this section a procedure for solving eqns. (29) and (90) is established. Let

$$f(\lambda) = [(\lambda \ell)^2 - (Bi)^2]\sin(\lambda \ell) - 2Bi\lambda\ell\cos(\lambda \ell) \tag{106}$$

and

$$g(\beta_1) = [LQT - LRS - MPT + NPS][ADI - AEH - BCI + BEG]$$

$$+ [KQT - KRS - M\emptyset T + N\emptyset S][-ADJ + AFH + BCJ - BFG] \tag{107}$$

where eqns. (29) and (90) are $f(\lambda) = 0$ and $g(\beta_1) = 0$, respectively. Then the eigenvalues λ_n and β_{1n} from eqns. (29) and (90) are the values of λ and β_1 at the points of intersection of the curves of $f(\lambda)$ and $g(\beta_1)$ with the λ and β_1 axes, respectively. Figs. 22 through 25 show typical plots of

SUBROUTINE EIGF

ENTER →

Calculate A through T by using eqns. (83); then evaluate the left-hand side of eqn. (90) for β_1.

→ RETURN

SUBROUTINE COEF

ENTER →

By using eqns. (85) through (89), (98) through (100), and (103), calculate and store the coefficients A_n.

→ RETURN

SUBROUTINE TWOTI

ENTER →

By using a stepping procedure in which a sign change detects the stepping interval within which the root lies, calculate and store the roots λ_n of eqn. (29).

→

By using eqn. (34), calculate and store each coefficient b_n which corresponds to the eigenvalue λ_n.

→

By using eqn. (35), calculate and store $T_{Is}(t)$.

→ RETURN

MAIN PROGRAM

START → READ NEXT DATA CASE →

Read data: materials properties, geometrical variables, boundary and initial conditions, and maximum time.

→

By using a stepping procedure in which a sign change detects the stepping interval within which the root lies, calculate and store the roots β_{1n} of eqn. (90). CALL SUBROUTINE EIGF.

→

CALL SUBROUTINE COEF. Calculate and store the coefficients A_n which correspond to the eigenvalues β_{1n}.

→

By using eqn. (105), calculate and store $T_{IIs}(t)$; also calculate and store Fourier number (Fo) at the same time.

→

CALL SUBROUTINE TWOTI. By using eqn. (35), calculate and store $T_{Is}(t)$. Then, by using eqn. (1), at the same time calculate and store $\Delta T(t)$.

→

Plot $T_{Is}(t)$, $T_{IIs}(t)$, and $\Delta T(t)$ vs. Fo.

→ END

Fig. 21. Program Flowchart
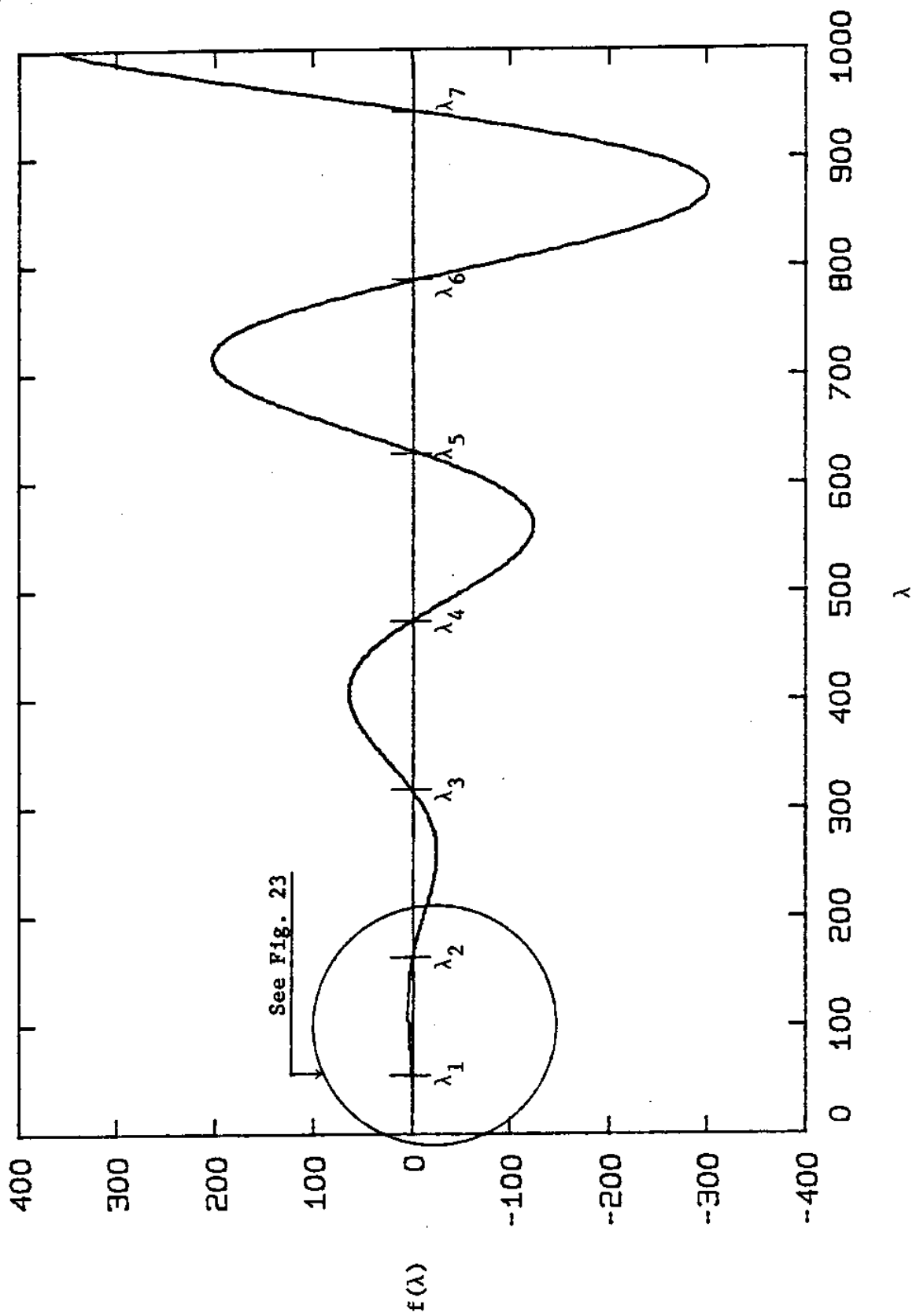
Fig. 22. Graphical representation of eigenfunction f(λ).
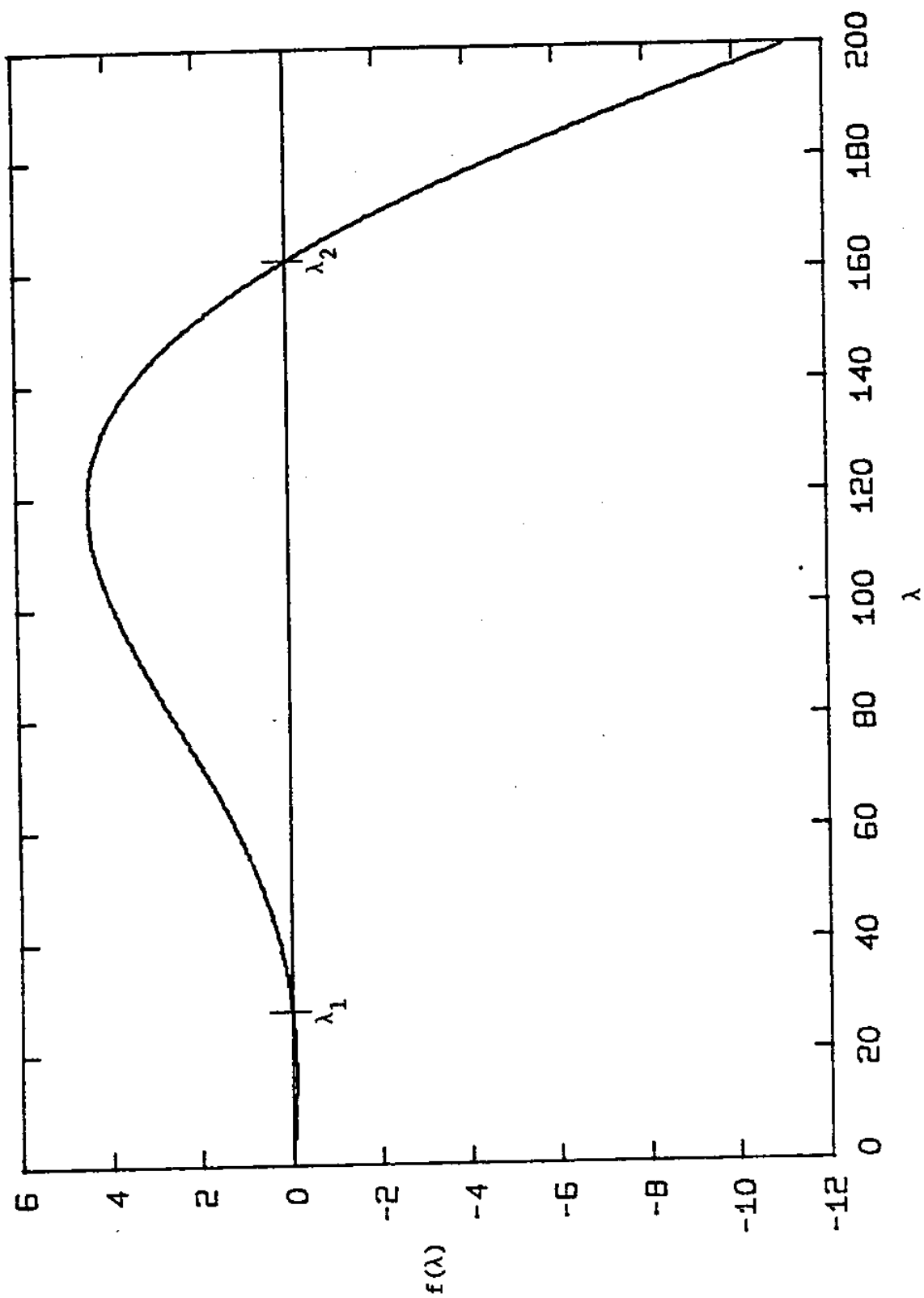
Fig. 23. Graphical representation of eigenfunction $f(\lambda)$ at low values of λ.
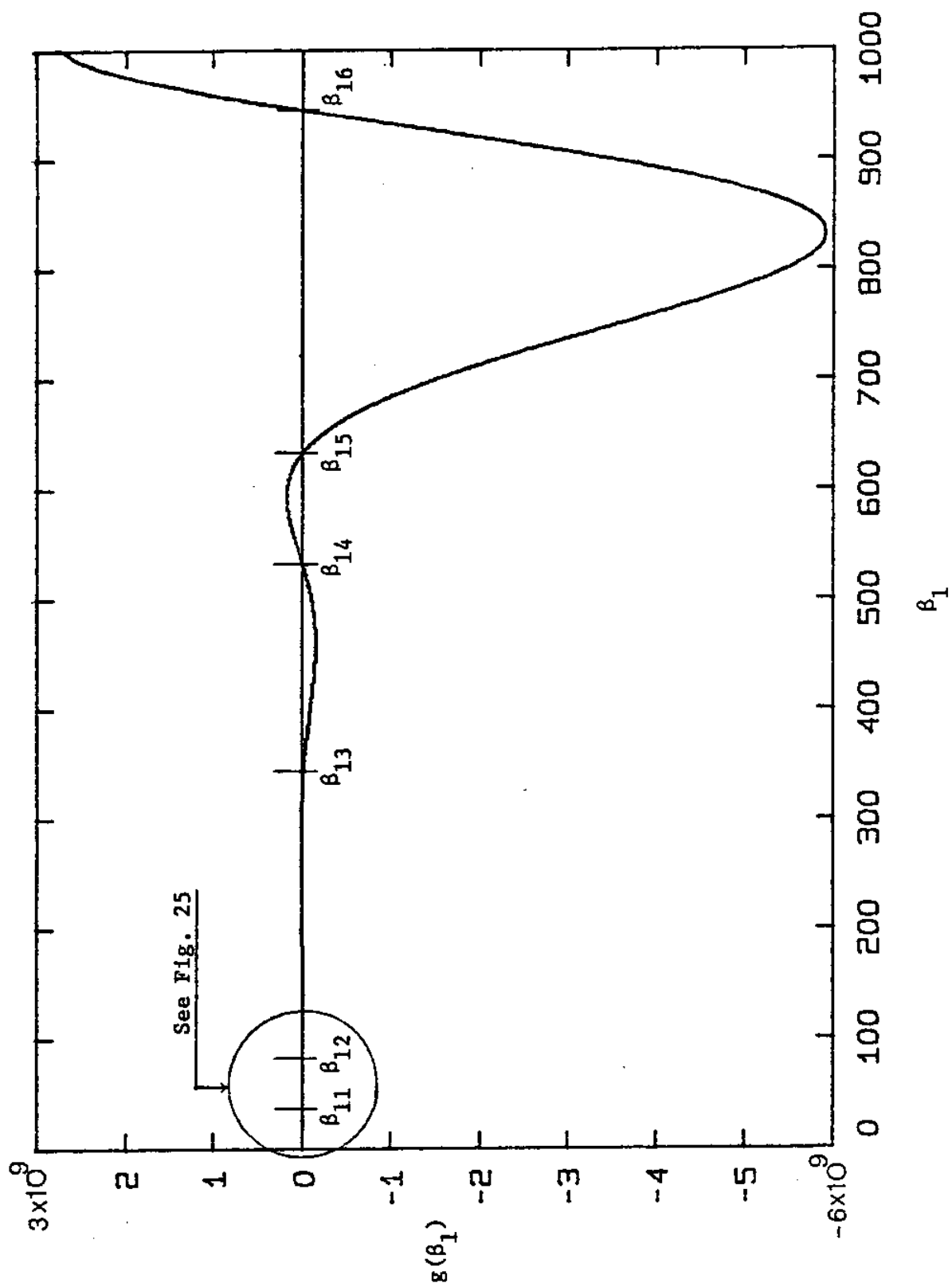
Fig. 24. Graphical representation of eigenfunction $g(\beta_1)$.
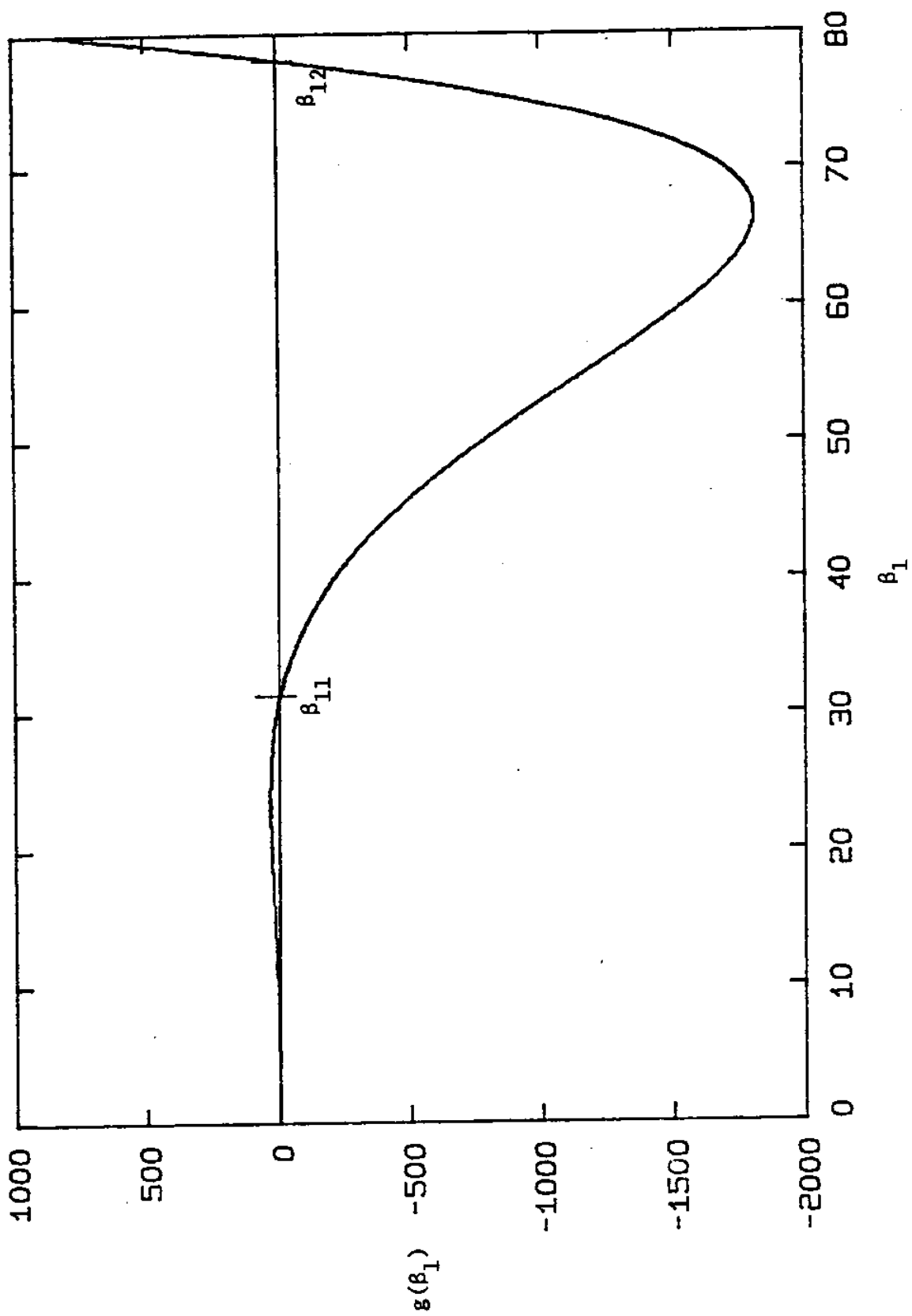
Fig. 25. Graphical representation of eigenfunction $g(\beta_1)$ at low values of β_1.

these functions. The oscillatory behavior of these functions may also be seen from their expressions as they are combinations of sines and cosines. Hence, the roots of eqns. (29) and (90) can be found by applying a stepping procedure, in which a sign change in $f(\lambda)$ or $g(\beta_1)$ detects the stepping interval within which a root lies. (See Figs. 22 through 25.) This procedure is quite satisfactory as the eigenvalues can be computed to any degree of desired accuracy.

5.2 NUMERICAL CALCULATION OF T_{Is} AND T_{IIs}

Once the eigenvalues have been computed, the numerical value of $T_{Is}(t)$ can be determined from eqn. (35). Eqn. (35) may be evaluated by using the defined ambient temperature T_∞ and heat flux q'', the computed Biot number Bi (eqn. (16)), and the Fourier coefficients b_n given in eqn. (34). Similarly, $T_{IIs}(t)$ can be evaluated from eqn. (105), where the Bi_j ($j = 1,2,3$) are defined in eqns. (59) through (61), the A_n are computed by the substitution of eqns. (92), (98), (99), and (100) into eqn. (103), and the β_{1n} are the roots of eqn. (90). Finally $\Delta T(t)$ can be calculated according to eqn. (1).

CHAPTER VI

RESULTS AND DISCUSSION

6.1 INTRODUCTION

In chapter V a computation algorithm for calculating the values of T_{Is}, T_{IIs}, and their difference ΔT was established. In this chapter the results of numerical calculations of T_{Is}, T_{IIs} and ΔT will be presented, which make it possible to determine the "optimal" testing conditions and the "best" liquid crystal system in relation to the parameters of the delamination and the laminate being inspected.

In Appendix 2 it is shown that

$$\theta^*_{Is} = f_1(Bi, Fo); \quad \theta^*_{is} \equiv k_1(T_{is} - T_\infty)/q''\ell \quad \text{for } i = I \text{ and } II \quad (108)$$

$$\theta^*_{IIs} = f_2(Bi, Fo, RK, RA, R1, R2); \quad RK \equiv k_2/k_1, \quad RA \equiv \alpha_2/\alpha_1 \quad (109)$$

$$\Delta\theta^* = |f(Bi, Fo, RK, RA, R1, R2)|; \quad R1 \equiv \ell_1/\ell, \quad R2 \equiv \ell_2/\ell \quad (110)$$

where θ^*_{Is}, θ^*_{IIs}, and $\Delta\theta^*$ are dimensionless temperatures corresponding to T_{Is}, T_{IIs}, and ΔT, respectively. Fo is the Fourier number which is defined as $Fo \equiv \alpha_1 t/\ell^2$. Note that the values of T_{Is} and T_{IIs} are calculated with the ambient temperature as the reference temperature, so in order to find the absolute value of temperature in each case, the ambient temperature should be added to the computed value. Thus, setting the ambient temperature T_∞ to zero, the dimensionless temperatures can be redefined as T^*_{Is} and T^*_{IIs} where

$$T^*_{Is} \equiv k_1 T_{Is}/q''\ell \tag{111}$$

$$T^*_{IIs} \equiv k_1 T_{IIs}/q''\ell \tag{112}$$

$$\Delta T^* = \Delta \theta^* = k_1 |(T_{Is} - T_{IIs})|/q''\ell \quad . \tag{113}$$

6.2 RESPONSES OF T^*_{Is}, T^*_{IIs}, and ΔT^* VERSUS Fo

Figs. 26 and 27 show typical responses of T^*_{Is}, T^*_{IIs}, and ΔT^* versus Fo, where Bi, RK, RA, R1, and R2 are fixed, and RK is less than unity; in other words, the thermal conductivity of the material contained in the delamination is less than the thermal conductivity of the material of the unflawed laminate. Note that Fo represents the dimensionless time. The Fo corresponding to the maximum value of ΔT^* is defined as $(Fo)_{\Delta T^*_{max}}$. At large values of Fo, T^*_{Is} and T^*_{IIs} tend toward their steady-state values and so ΔT^* tends toward a constant.

6.3 FACTORS INFLUENCING ΔT^*

6.3.1 Effect of Geometrical Parameters R1 and R2 on ΔT^*

Fig. 28 shows the response of ΔT^* versus Fo to different values of R1 and R2, where Bi, RK, and RA are fixed. From Fig. 28 the value of ΔT^* is less sensitive to changes in R1 than in R2. Also at large values of Fo, the value of ΔT^* is only sensitive to changes in R2. This behavior may be explained by the fact that at large values of Fo the temperatures
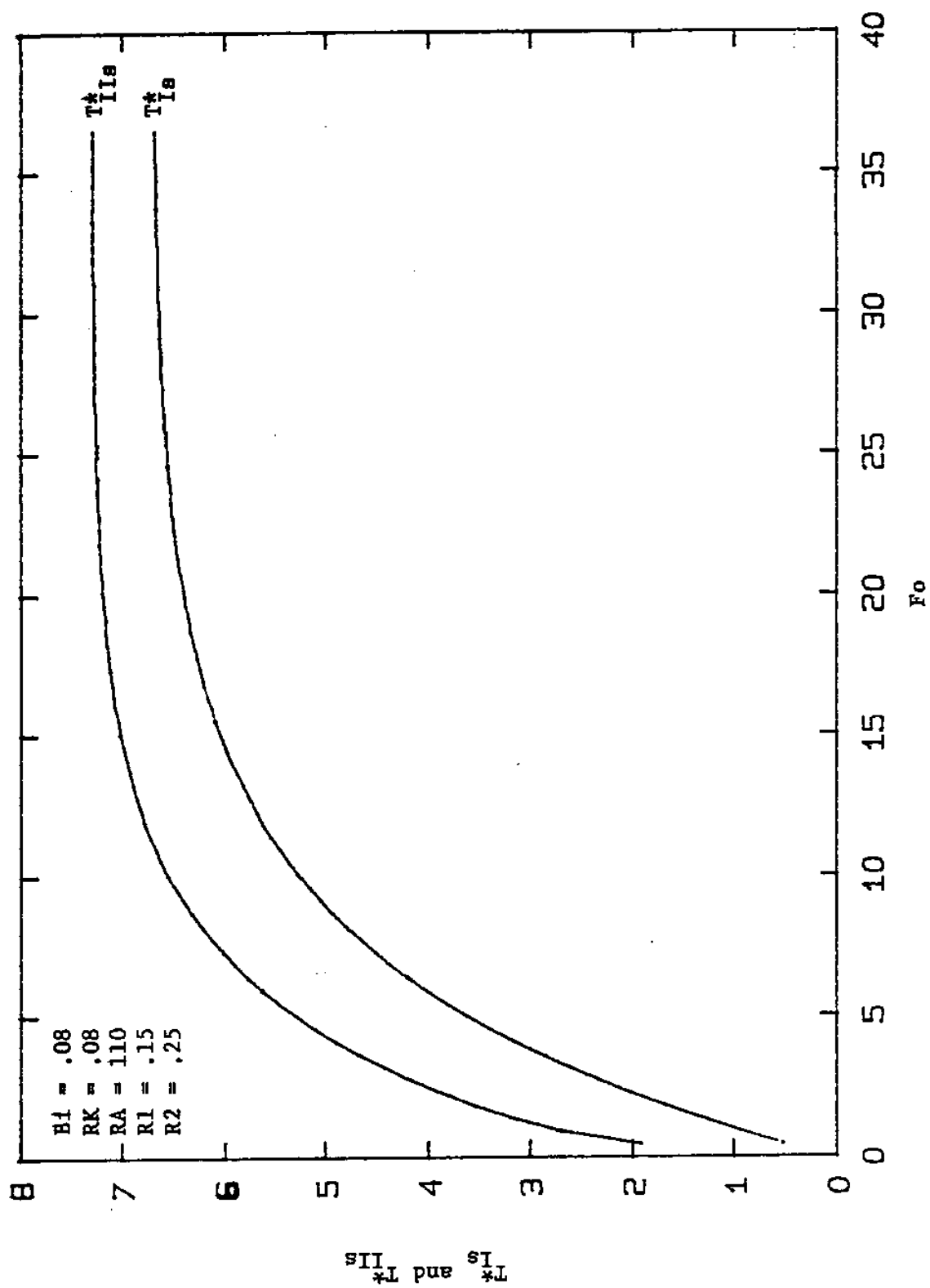
Fig. 26. Typical behavior of T^*_{Is} and T^*_{IIs} versus Fo.
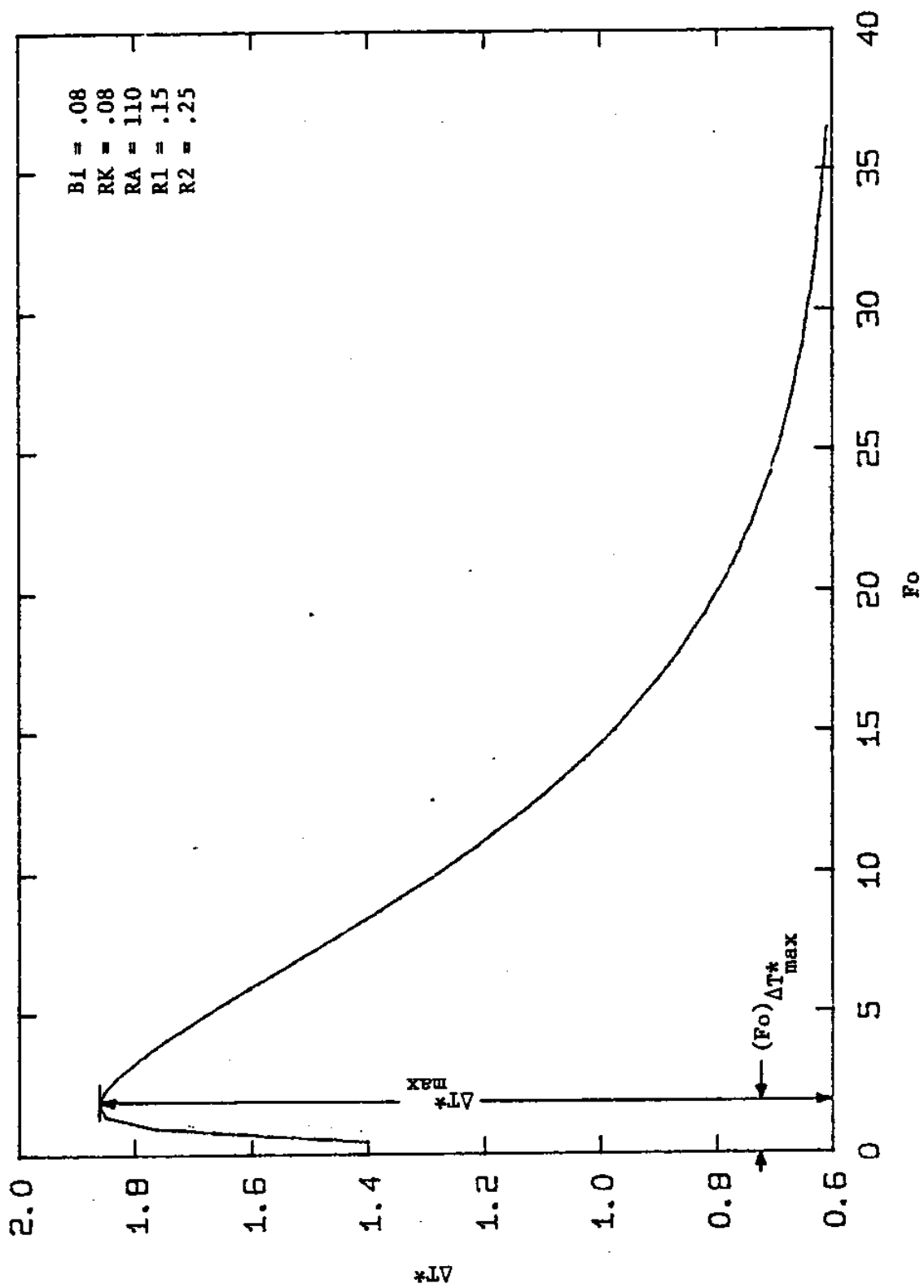
Fig. 27. Typical behavior of ΔT^* versus Fo.
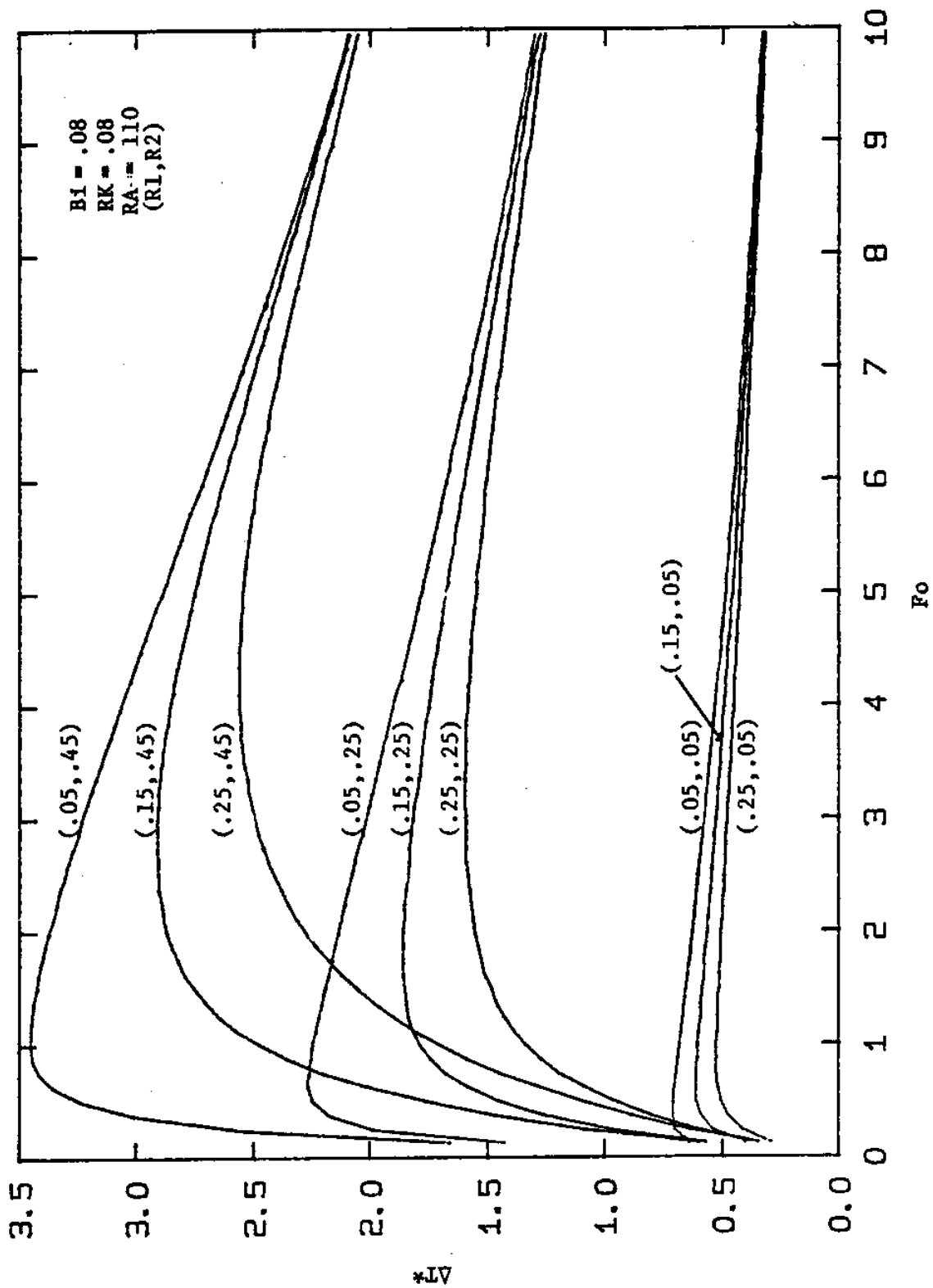
Fig. 28. Typical effect of geometrical parameters R1 and R2 on ΔT*.

tend to their steady-state values and at steady-state, the temperature response of T^*_{IIs} does not depend on the depth of defect in the laminate. Therefore, at large values of Fo, ΔT^* does not depend on Rl as it is only a function of the defect thickness.

Fig. 29 shows the variation of ΔT^*_{max} versus Rl when R2 is fixed and Fig. 30 shows the variation of ΔT^*_{max} versus R2 when Rl is fixed, where RK and RA are fixed in both cases. These figures show that the value of ΔT^*_{max} is also less sensitive to changes in Rl than in R2. From Figs. 29 and 30 it may be concluded that the relations between ΔT^*_{max} and both Rl and R2 are linear.

Figs. 31 and 32 show the variation of $(Fo)_{\Delta T^*_{max}}$ versus Rl and R2 when R2 and Rl are fixed, respectively, where RK and RA are also fixed in both cases. These figures show that the $(Fo)_{\Delta T^*_{max}}$ is sensitive to both Rl and R2 and increases as either Rl or R2 or both increase. The relations between $(Fo)_{\Delta T^*_{max}}$ and both Rl and R2 are linear also.

6.3.2 Effect of Biot Number on T^*_{Is}, T^*_{IIs}, and ΔT^*

Figs. 33, 34, and 35 respectively show the response of T^*_{Is}, T^*_{IIs}, and ΔT^* versus Fo for different values of Bi, where RK, RA, Rl, and R2 are fixed. These figures show that T^*_{Is}, T^*_{IIs}, and ΔT^* decrease as Bi increases.

Figs. 36 and 37 respectively show the variation of ΔT^*_{max} and $(Fo)_{\Delta T^*_{max}}$ versus Bi, where RK, RA, Rl, and R2 are fixed. These figures show that at small values of Bi, the values of ΔT^*_{max} and $(Fo)_{\Delta T^*_{max}}$ are sensitive to
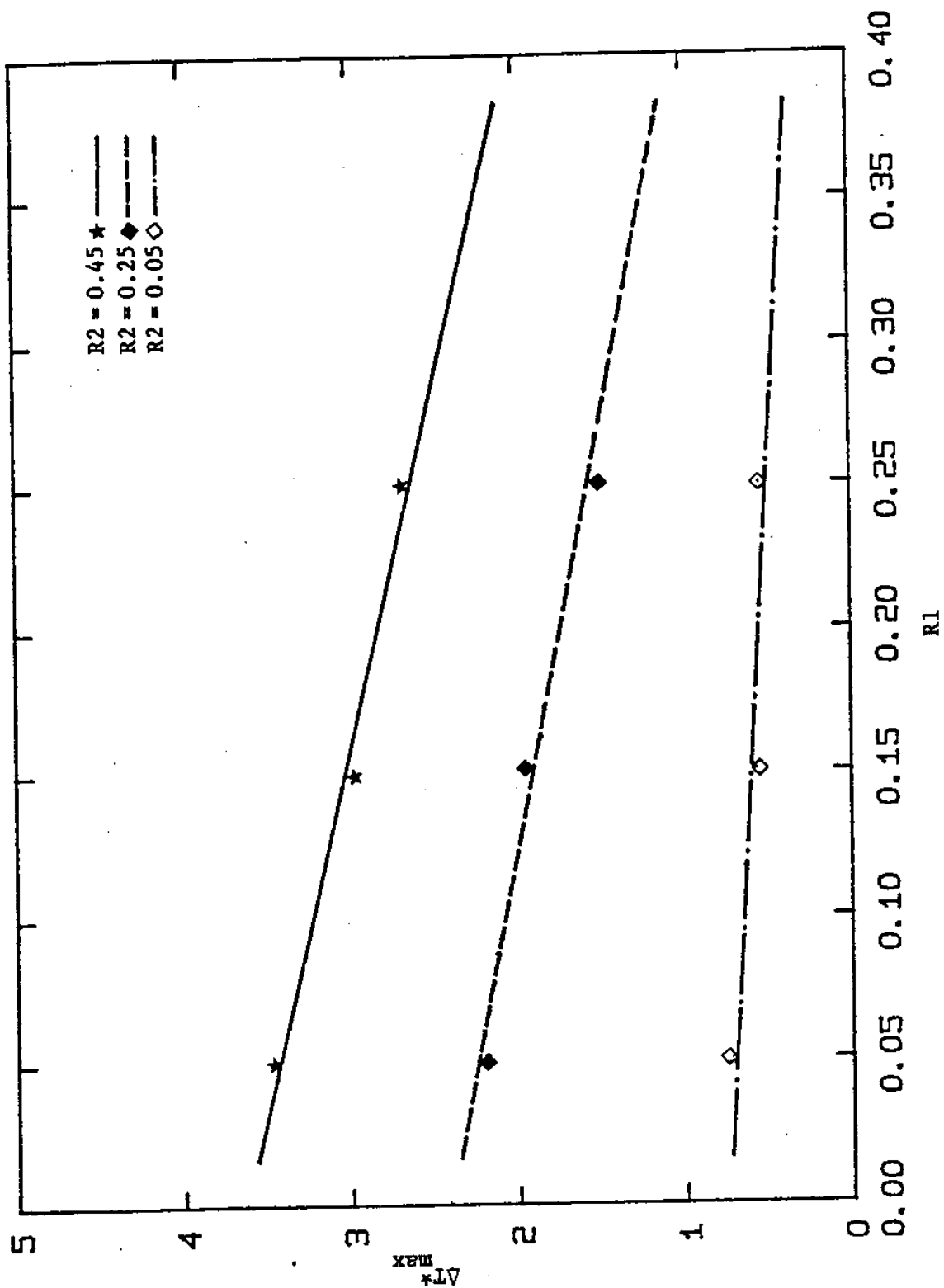
Fig. 29. Typical variation of ΔT^*_{max} versus R1 for different values of R2. (Data points are taken from Fig. 28.)
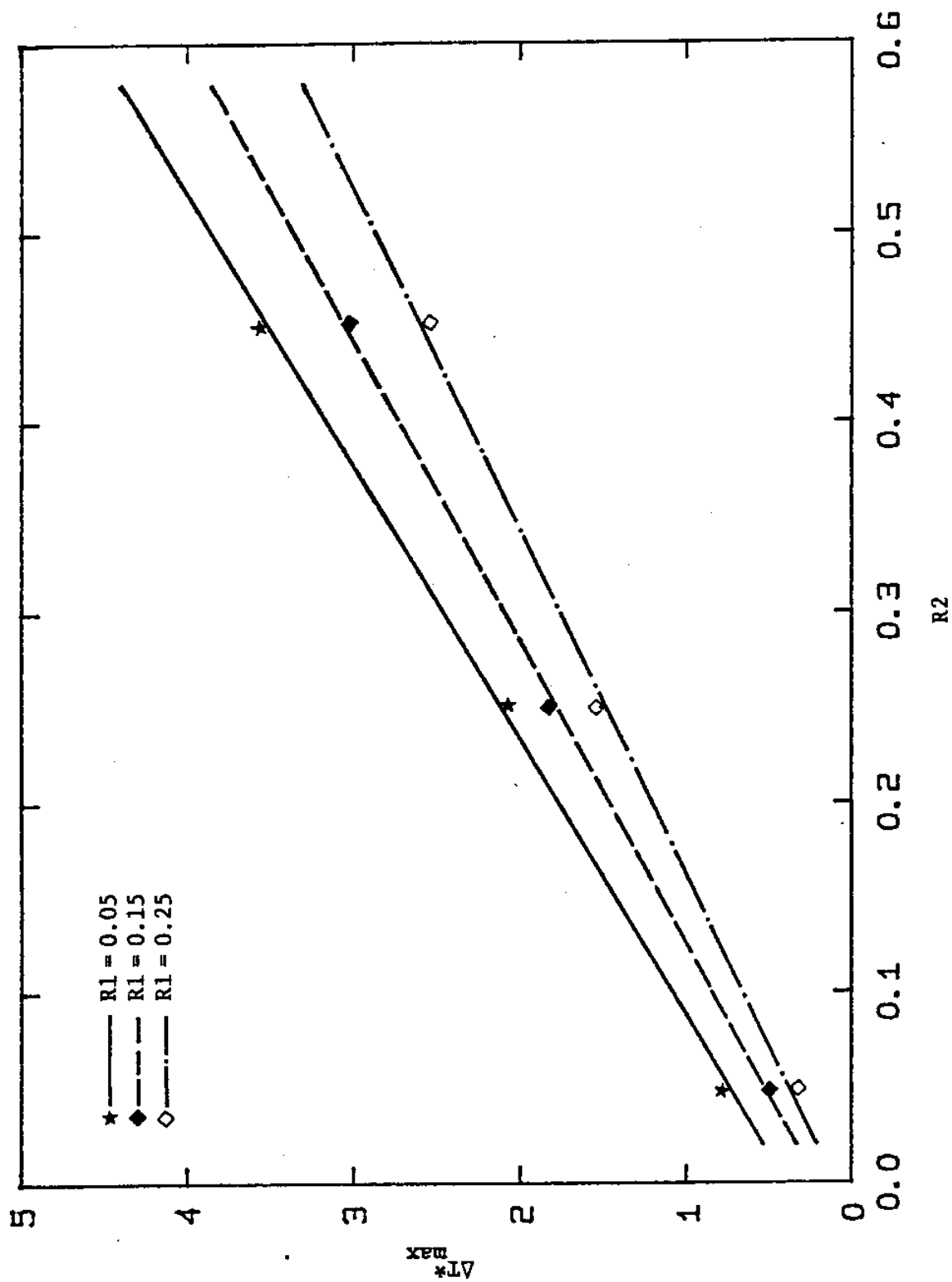
Fig. 30. Typical variation of ΔT^*_{max} versus R2 for different values of R1. (Data points are taken from Fig. 28.)
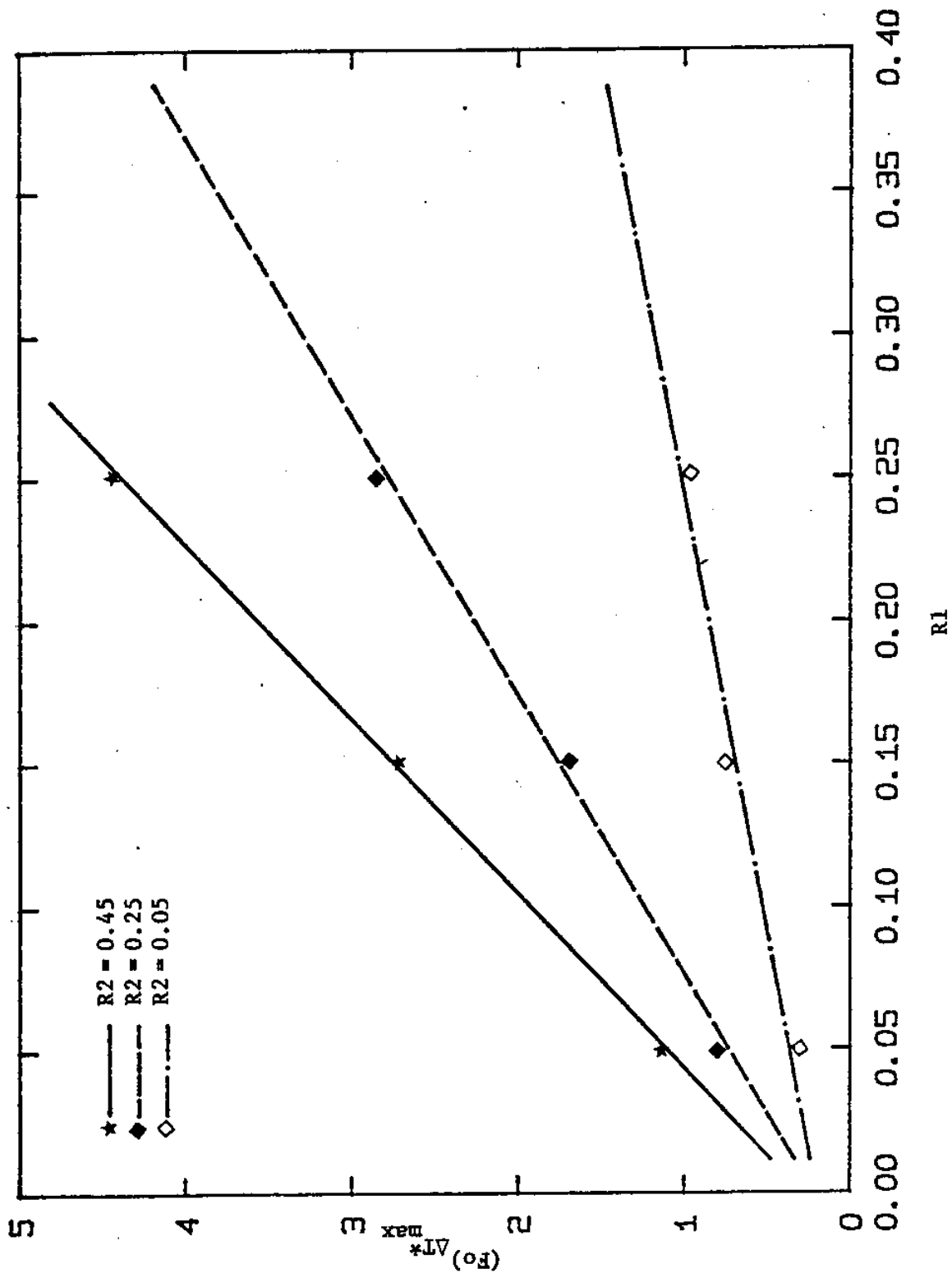
Fig. 31. Typical variation of nondimensional time corresponding to ΔT^*_{max} versus R1 for different values of R2. (Data points are taken from Fig. 28.)
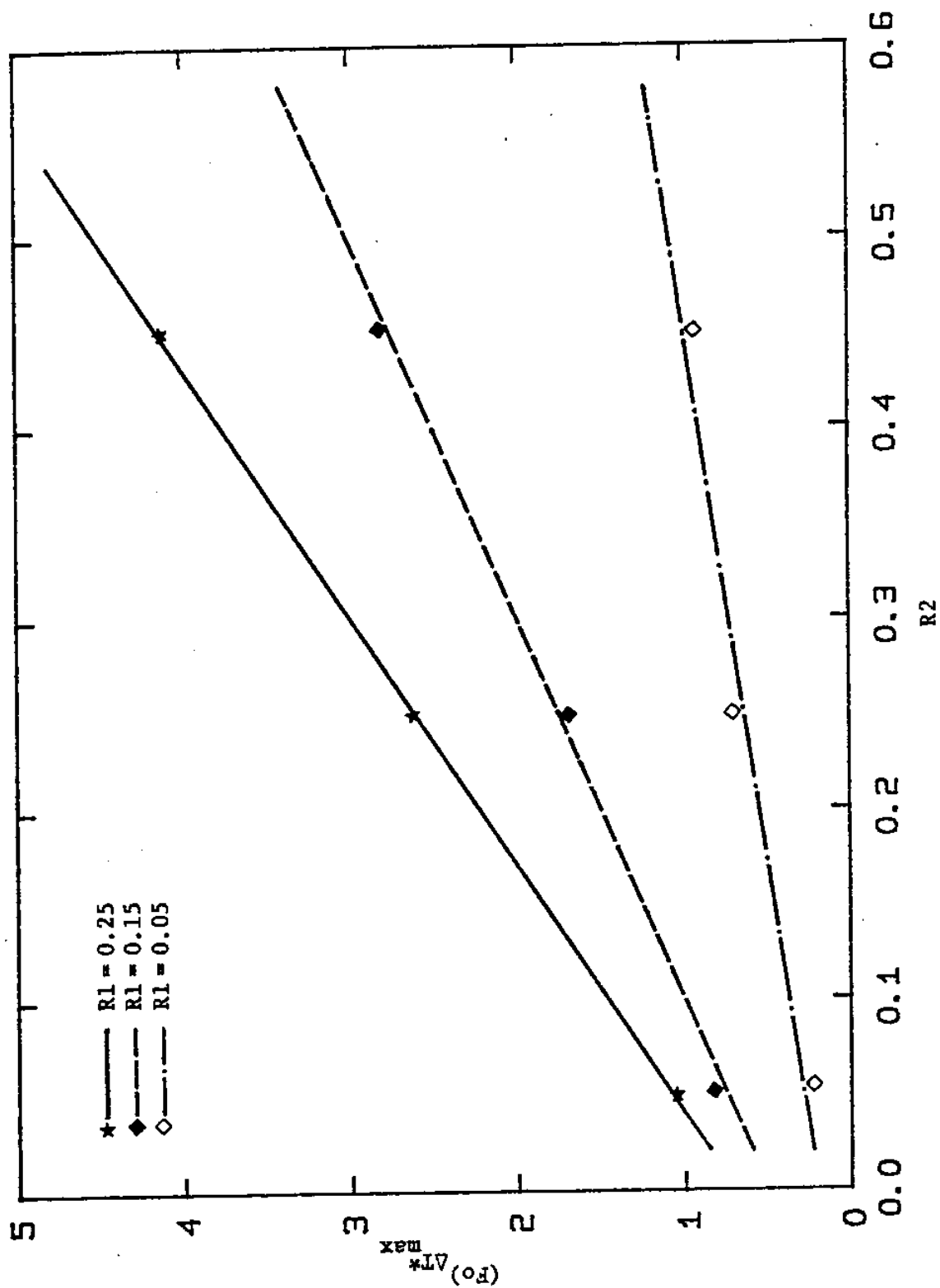
Fig. 32. Typical variation of nondimensional time corresponding to ΔT^*_{max} versus R2 for different values of R1. (Data points are taken from Fig. 28.)
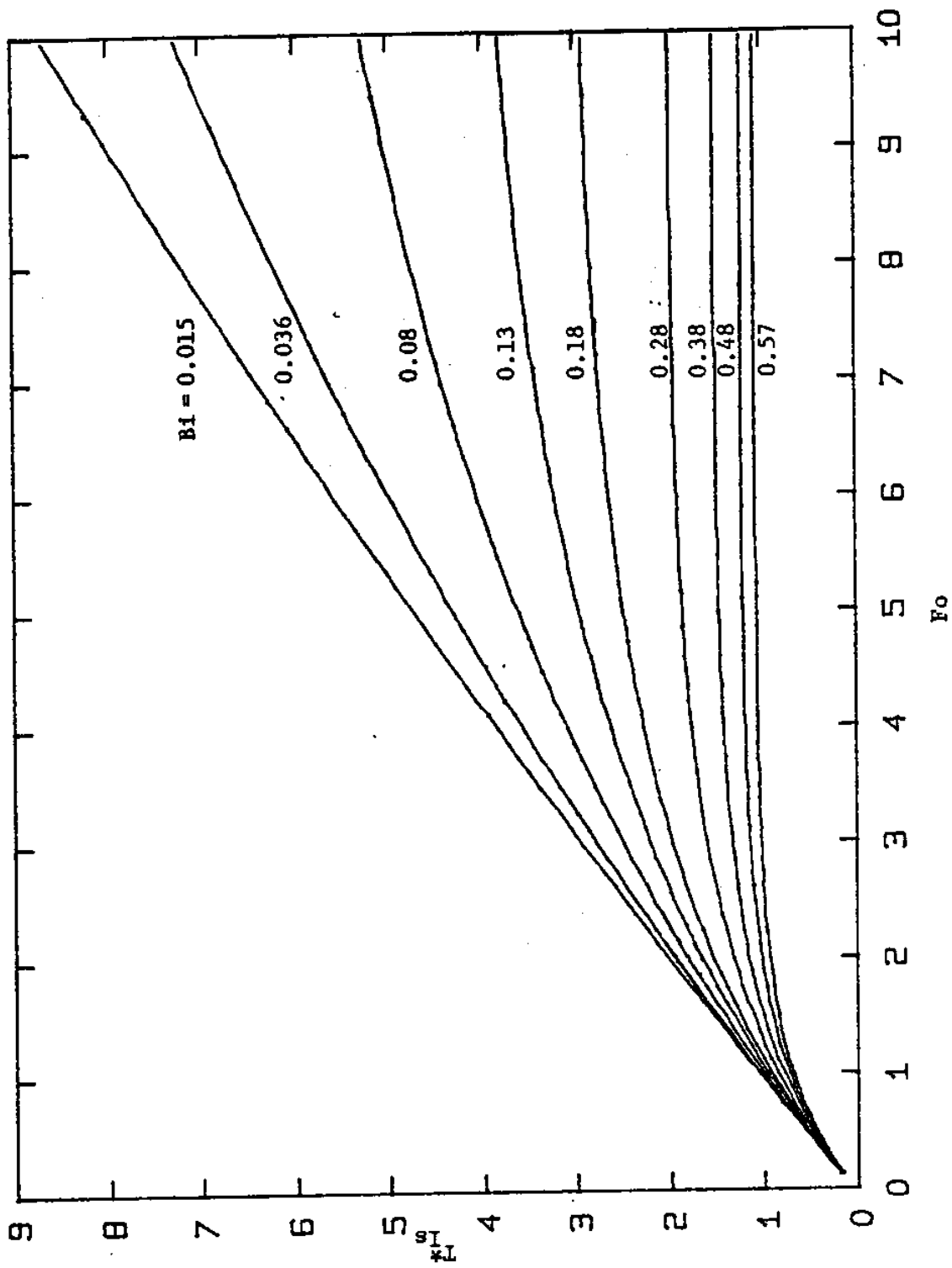
Fig. 33. Effect of Bi on T^*_{is}.
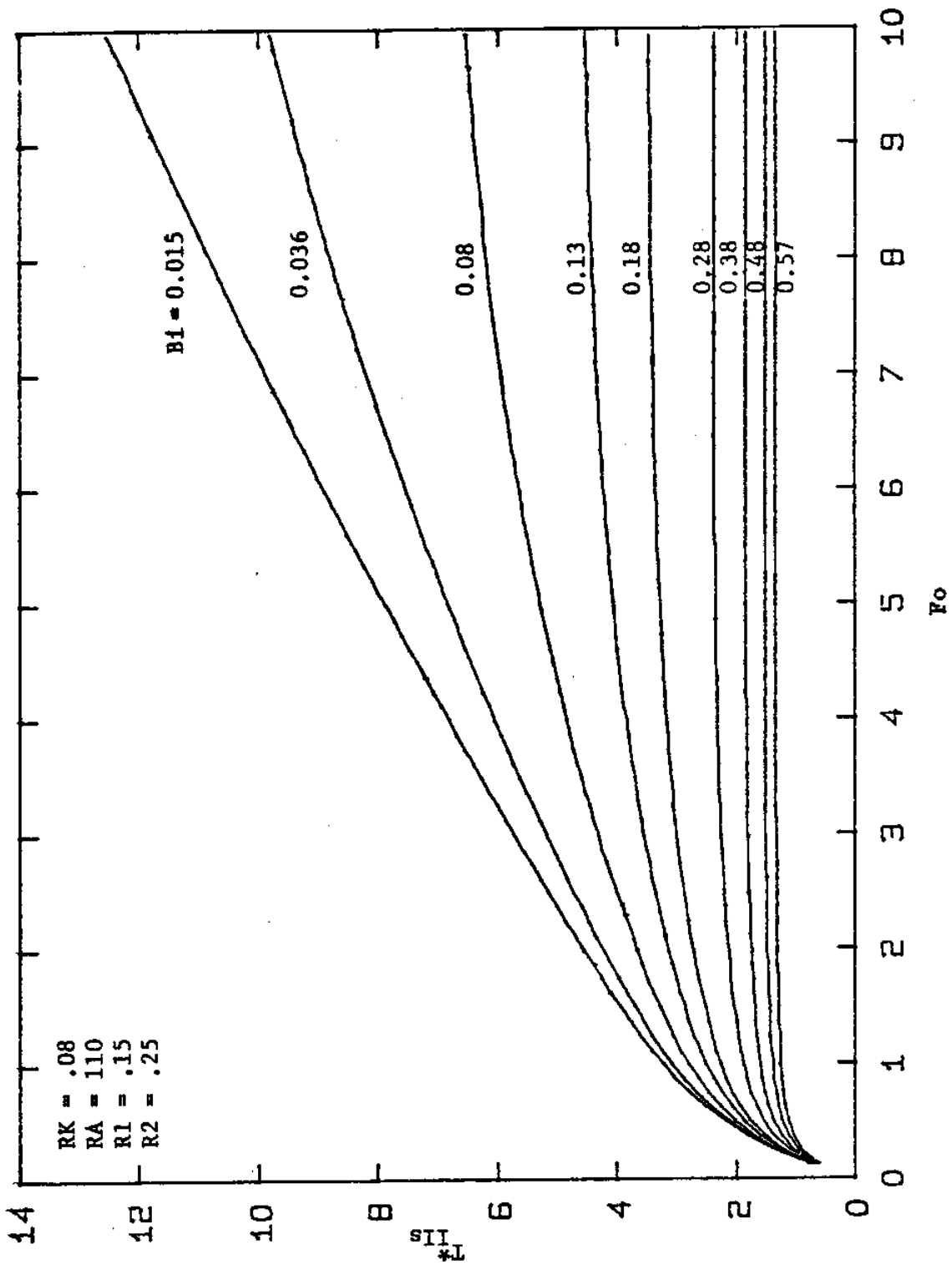
Fig. 34. Typical effect of B1 on T^*_{IIs}.
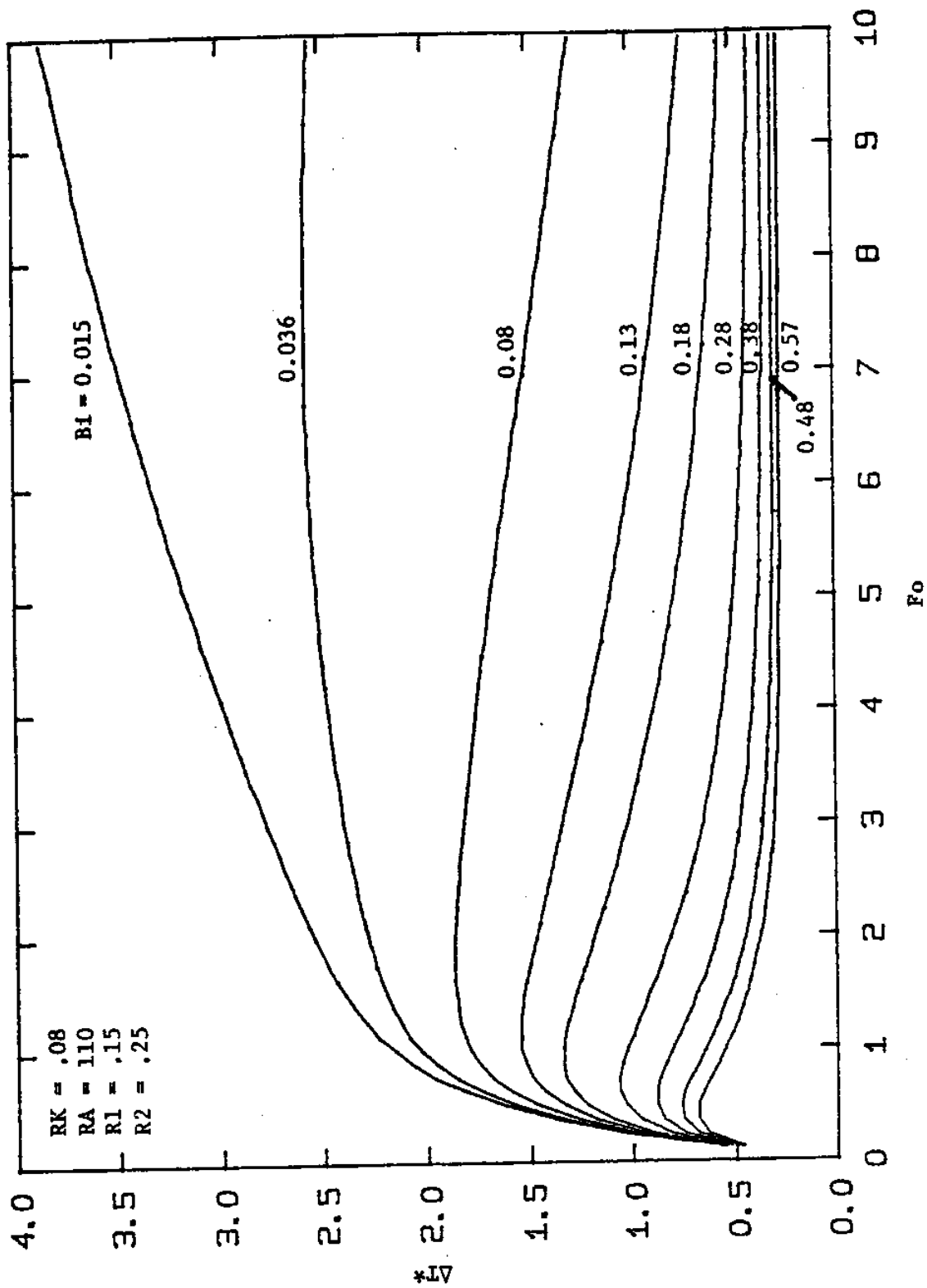
Fig. 35. Typical effect of Bi on ΔT*.
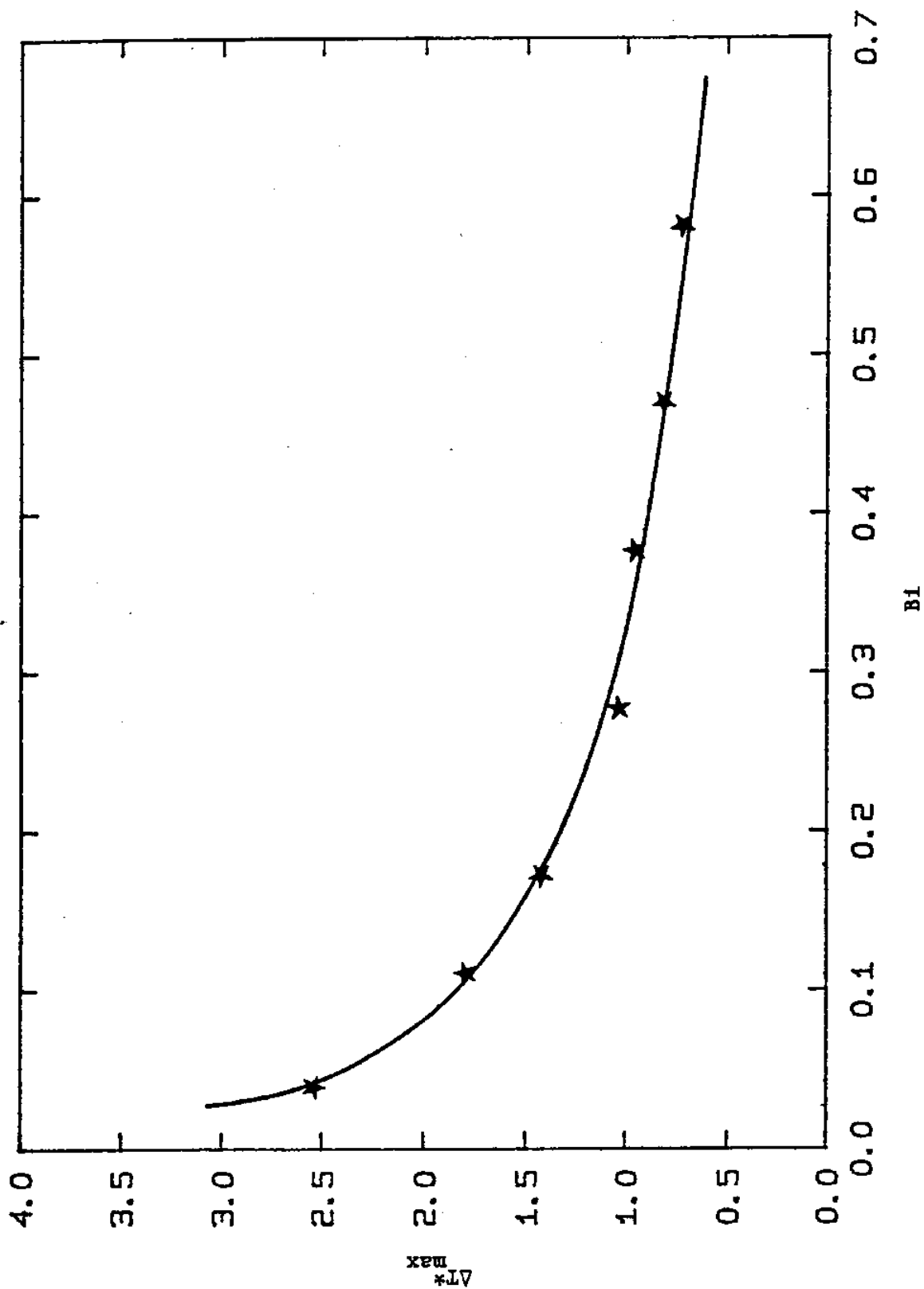
Fig. 36. Typical effect of B1 on ΔT^*_{max}. (Star data points are taken from Fig. 35.)
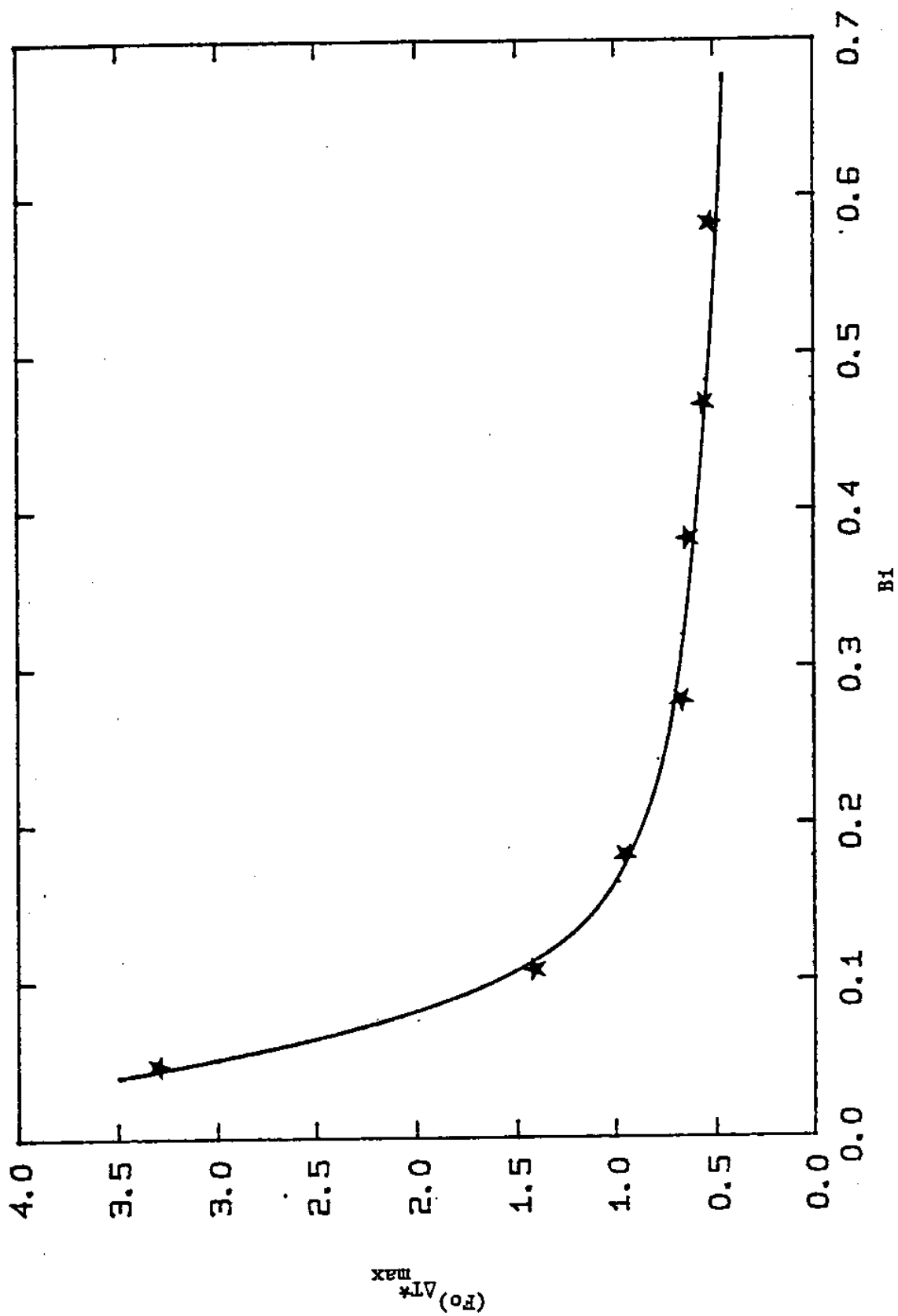
Fig. 37. Typical effect of Bi on the nondimensional time corresponding to ΔT^*_{max}. (Star data points are taken from Fig. 35.)

changes in Bi. However, at large values of Bi, the values of ΔT^*_{max} and $(Fo)_{\Delta T^*_{max}}$ are relatively insensitive to changes in Bi.

6.3.3 Effect of Thermal Conductivity Ratio RK on ΔT^*

Fig. 38 shows the response of ΔT^* versus Fo for different values of RK, where Bi, RA, R1, and R2 are fixed. This figure shows that as RK increases, the value of ΔT^* decreases as it also becomes less sensitive to changes in RK.

Figs. 39 and 40 show the variation of ΔT^*_{max} and $(Fo)_{\Delta T^*_{max}}$ versus RK, respectively, where Bi, RA, R1, and R2 are fixed. These figures show that at small values of RK, the values of ΔT^*_{max} and $(Fo)_{\Delta T^*_{max}}$ are sensitive to changes in RK. However, at large values of RK, the values of ΔT^*_{max} and $(Fo)_{\Delta T^*_{max}}$ are relatively insensitive to changes in RK.

6.3.4 Effect of Thermal Diffusivity Ratio RA on ΔT^*

Fig. 41 shows the response of ΔT^* versus Fo for different values of RA, where Bi, RK, R1, and R2 are fixed. This figure shows that the values of ΔT^* increase slightly as RA increases. Thus, it may be concluded that ΔT^* is almost independent of RA, especially at small values of Fo.

Figs. 42 and 43 show the respective variations of ΔT^*_{max} and $(Fo)_{\Delta T^*_{max}}$ versus RA, where Bi, RK, R1, and R2 are fixed. Also, these figures show that the values of ΔT^*_{max} and $(Fo)_{\Delta T^*_{max}}$ are almost independent of RA.

Fig. 38. Typical effect of RK on ΔT*.

The figure shows curves of ΔT^* versus Fo for various values of RK.

Legend:
- $B1 = .08$
- $RA = 110$
- $R1 = .15$
- $R2 = .25$

Curves labeled:
- $RK = 0.08$
- 0.16
- 0.24
- 0.32
- 0.48
- 0.62
- 0.74
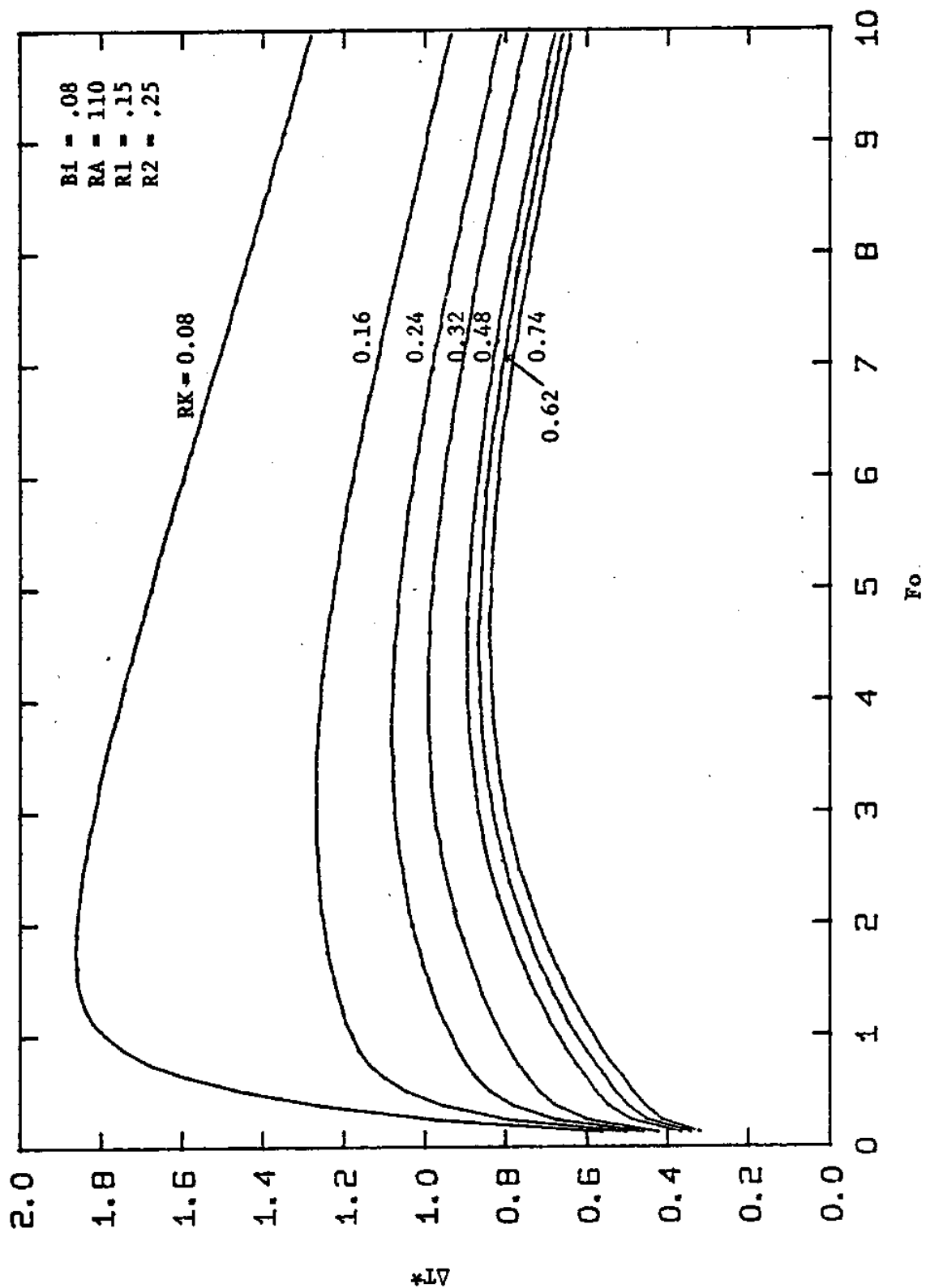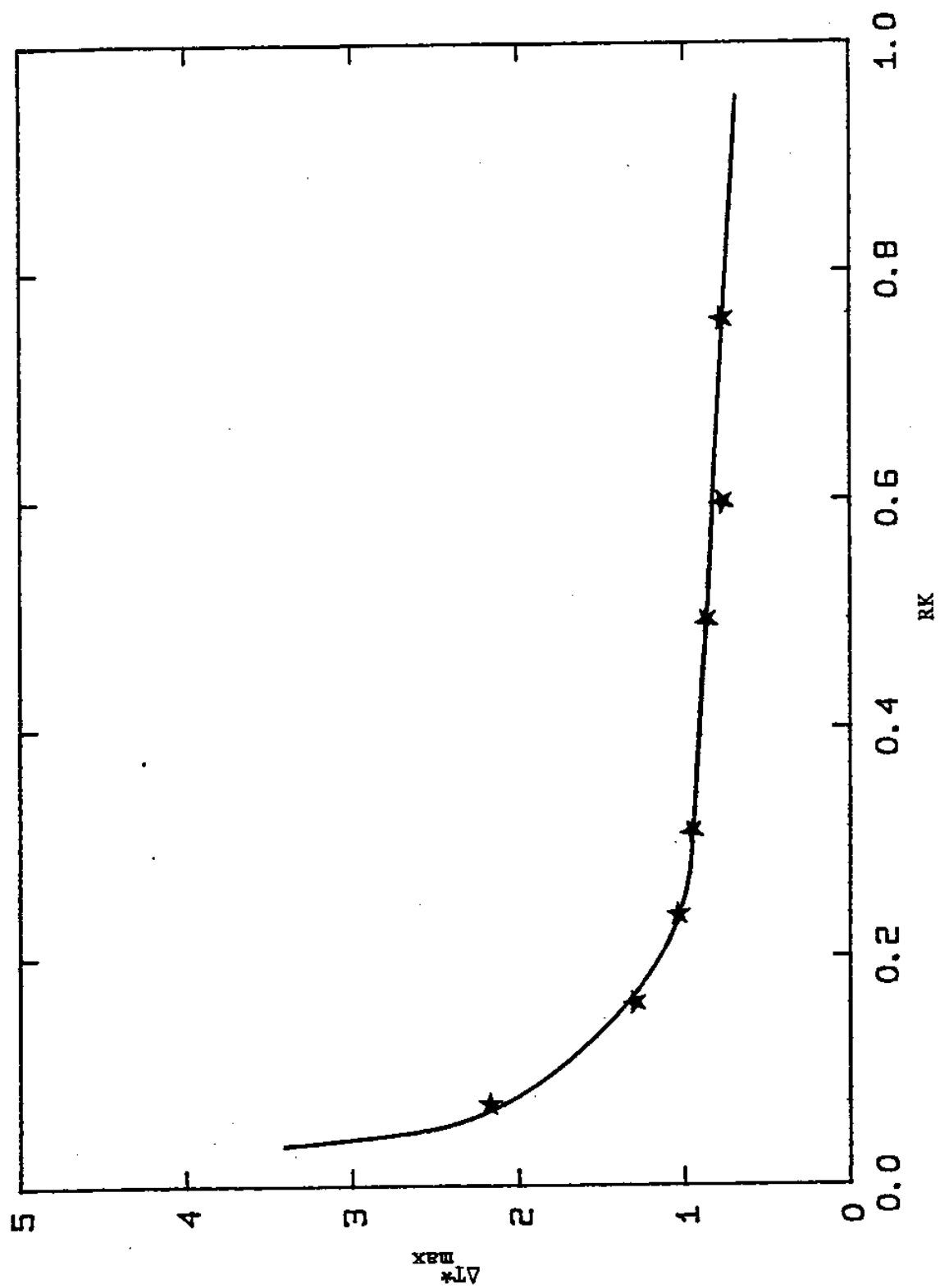
Fig. 39. Typical effect of RK on ΔT^*_{max}. (Star data points are taken from Fig. 38.)
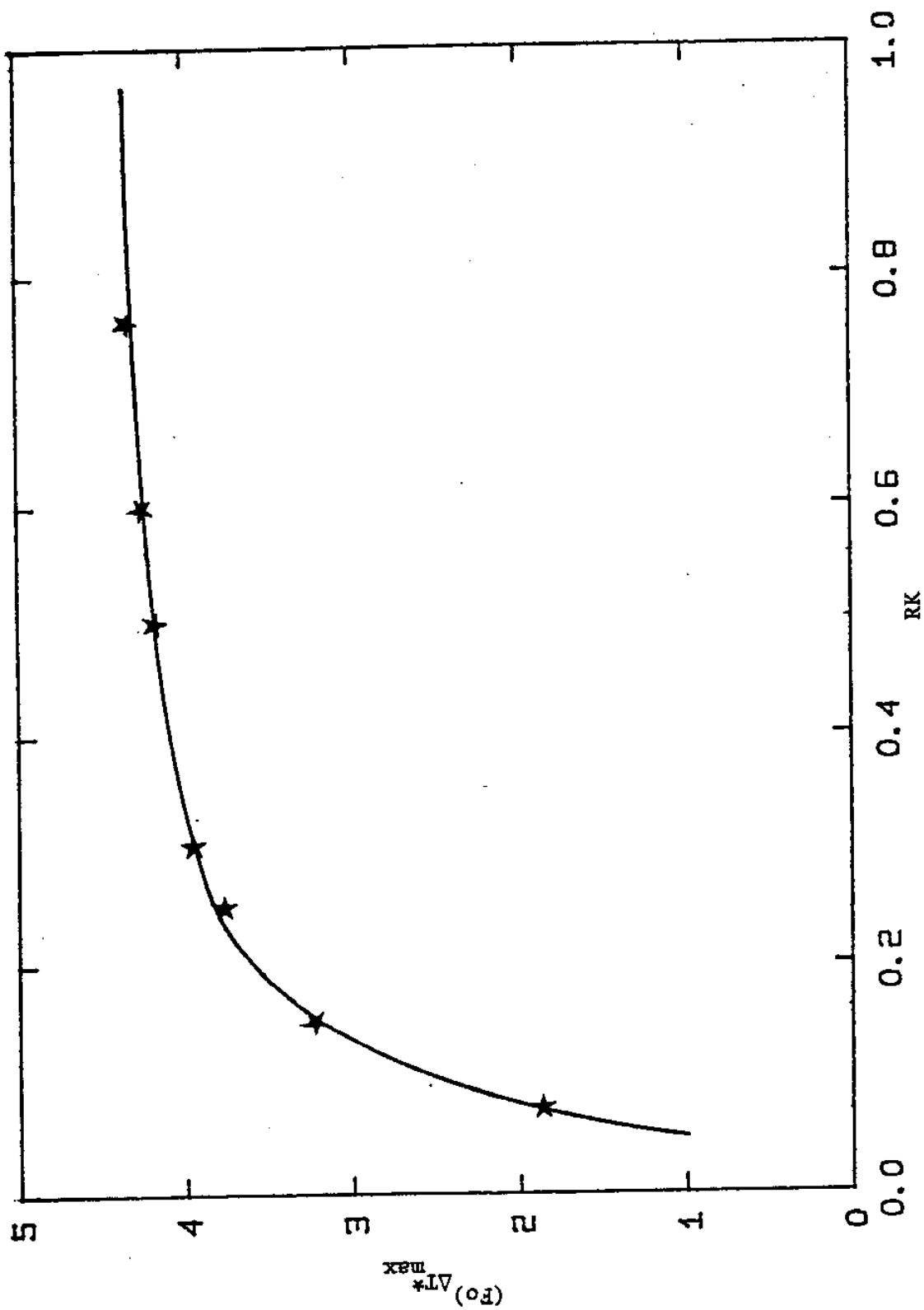
Fig. 40. Typical effect of RK on the nondimensional time corresponding to ΔT^*_{max}. (Star data points are taken from Fig. 38.)
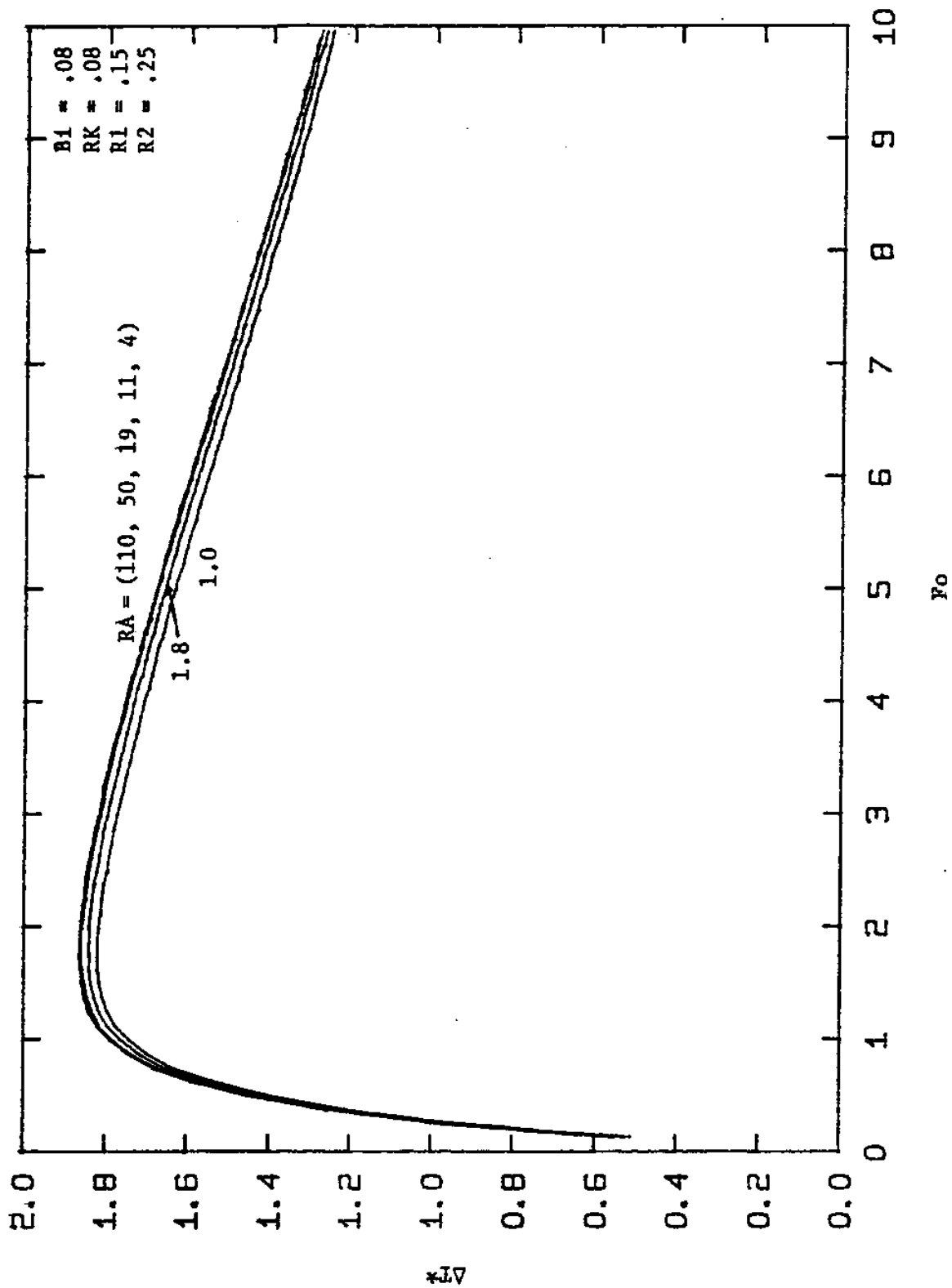
Fig. 41. Typical effect of RA on ΔT*.
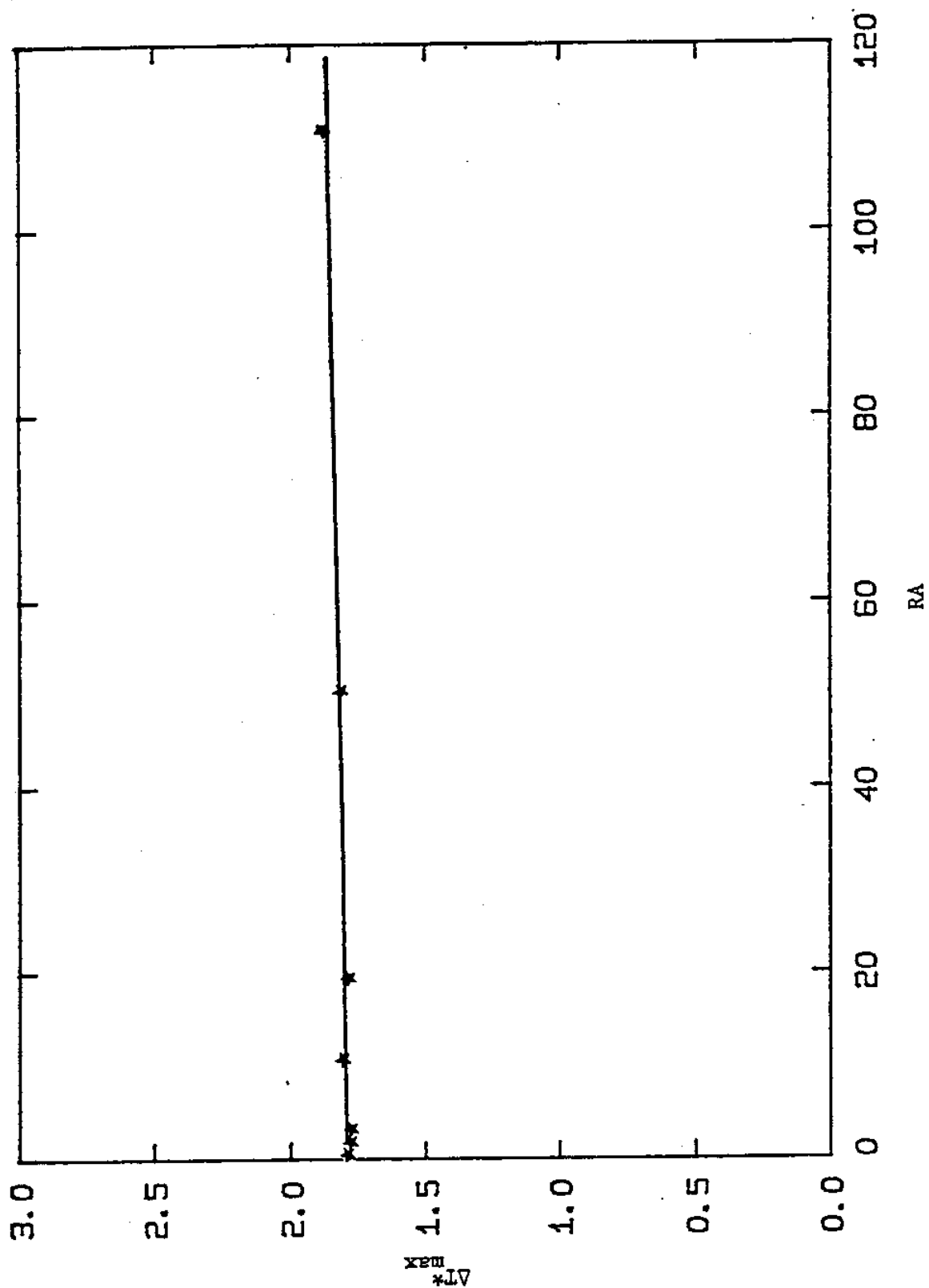
Fig. 42. Typical effect of RA on ΔT^*_{max}. (Star data points are taken from Fig. 41.)
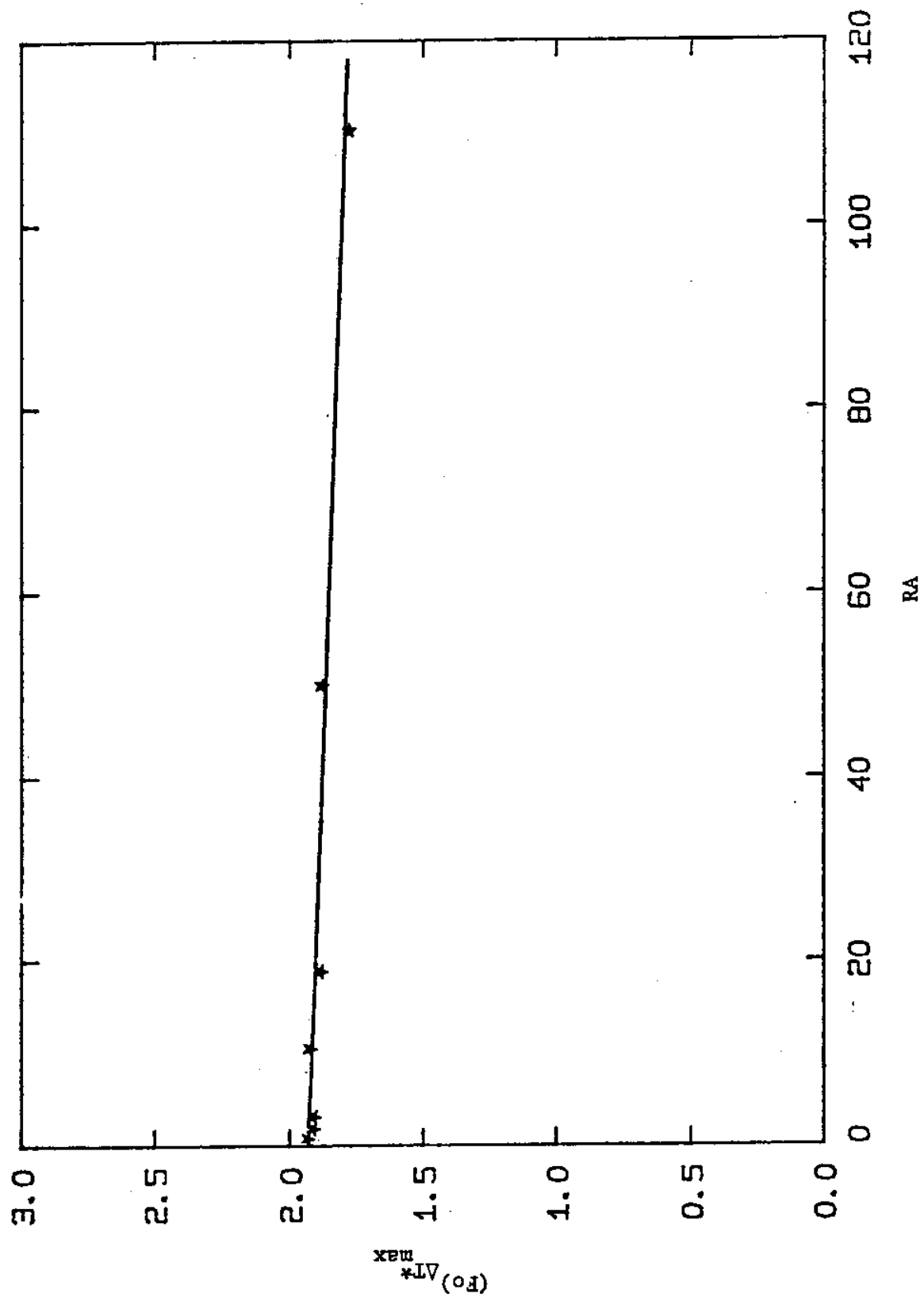
Fig. 43. Typical effect of RA on the nondimensional time corresponding to ΔT^*_{max}. (Star data points are taken from Fig. 41.)

## 6.3.5 Effect of Net Radiant Heat Flux q" on T_{Is}, T_{IIs}, and ΔT

In preceding sections the responses of T_{Is}^*, T_{IIs}^*, and ΔT^* versus Fo and the effect of variations of the parameters R1, R2, RK, RA, and Bi on these responses have been illustrated. It was also mentioned that the color-play range and the transition temperature of the liquid crystal system which is well suited for the detection of a given flaw is related to ΔT and the surface temperatures T_{Is} and T_{IIs}. Thus, the determination of testing conditions and the selection of the liquid crystal system for the detection of a given defect is related to R1, R2, RK, RA, Bi, k_1, ℓ and q".

Figs. 28, 33, and 44 respectively show typical responses of ΔT^*, T_{Is}^*, and T_{IIs}^* versus Fo to different values of R1 and R2, where Bi, RK, and RA are fixed. It has been shown that there are unique relationships between T_{Is}^*, T_{IIs}^*, and ΔT^* versus Fo when Bi, R1, R2, RK, and RA are fixed. (See eqns. (108) through (110).) However, the relationships between T_{Is}, T_{IIs}, and ΔT versus time are not unique for the same conditions which have been mentioned above because T_{Is}, T_{IIs}, and ΔT are also dependent on k_1, ℓ and q". (Refer to eqns. (111), (112), and (113).)

For specified values of k_1 and ℓ, that is, a given laminate, T_{Is}, T_{IIs}, and ΔT depend only on q". Eqns. (111) through (113) show that the relationships between T_{Is}, T_{IIs}, and ΔT, and q" are linear and all proportionality constants are the same. So, ΔT can be increased by increasing the value of the net radiant heat flux q". T_{Is} and T_{IIs} will be increased as well. As ΔT increases, the accuracy of the thermal testing also increases because larger temperature differences are more easily detected. Thus,
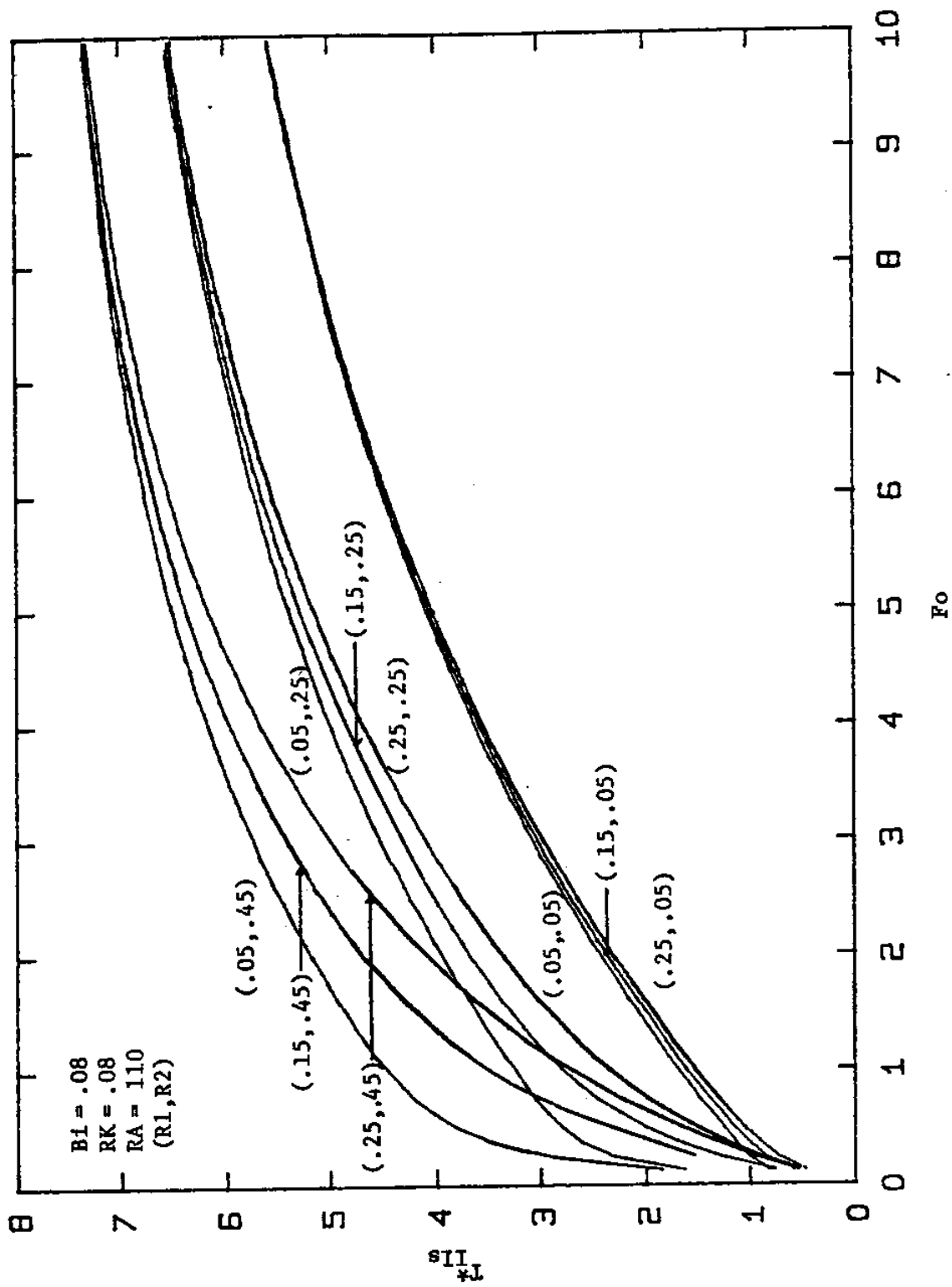
Fig. 44. Typical effect of geometrical parameters R1 and R2 on T^*_{IIs}.

the ideal situation is to use a heat source which provides the largest possible uniform radiant heat flux over the surface of the test laminate. However, in practice, there is a maximum acceptable temperature to which the laminate may be heated and this temperature must be in a range where liquid crystal materials are available. Recall from section 3.3 that liquid crystals of the cholesteric type have been observed from -40°C to 285°C. However, materials which have been found useful for thermography are presently limited from about 0°C to 150°C. Also, the rate of thermal change must be sufficiently slow to allow the liquid crystal to follow the temperature variations. (The rate of change of liquid crystal color with temperature has a time constant which may be as short as 30 milliseconds and as long as 0.1 sec.)

6.3.6 Effect of Heat Transfer Coefficient h on ΔT*

The effect of the heat transfer coefficient h on ΔT^* is the same as the effect of Bi on ΔT^* for a given laminate. (That is, for a specific ℓ and k_1, Bi is proportional to h.) So according to section 6.3.2, it may be concluded that the ideal situation is to have the smallest possible value for h. It is also known that the value of h is the summation of h_c and h_r, the convection and radiation heat transfer coefficients, respectively [34]. The smallest value for h can be obtained by providing natural convection heat transfer on the surfaces of the test laminate (that is, without blowing air onto the surfaces of the test object) and siffuciently low surface temperatures such that radiation effects are negligible (that is, less than

about 80°C).

6.4 CHOICE OF TESTING CONDITIONS AND LIQUID CRYSTAL SYSTEM

In this section the necessary and sufficient conditions for "optimal," "acceptable," "moderately acceptable," and "limiting" cases of testing conditions and for choosing the liquid crystal system will be established. For simplicity the color-play range and transition temperature of the liquid crystal system are called $\Delta T_{L.c.}$ and $T_{L.c.}$, respectively. Also, the temperatures of two colors (for example, green and red) are called $T_{L.c.i}$ and $T_{L.c.ii}$, respectively, and their difference is called $\Delta T_{L.c.i.ii}$ where

$$\Delta T_{L.c.i,ii} = |T_{L.c.i} - T_{L.c.ii}| \quad . \tag{114}$$

Also, define

$$\Delta T^*_{L.c.} \equiv k_1 \Delta T_{L.c.}/q''\ell \tag{115}$$

$$T^*_{L.c.} \equiv k_1 (T_{L.c.} - T_\infty)/q''\ell \tag{116}$$

$$\Delta T^*_{L.c.i,ii} \equiv k_1 \Delta T_{L.c.i,ii}/q''\ell \tag{117}$$

$$T^*_{L.c.i} \equiv k_1 (T_{L.c.i} - T_\infty)/q''\ell \tag{118}$$

$$T^*_{L.c.ii} \equiv k_1 (T_{L.c.ii} - T_\infty)/q''\ell \tag{119}$$

where $\Delta T^*_{L.c.}$, $T^*_{L.c.}$, $\Delta T^*_{L.c.i,ii}$, $T^*_{L.c.i}$, and $T^*_{L.c.ii}$ are dimensionless temperatures corresponding to $\Delta T_{L.c.}$, $T_{L.c.}$, $\Delta T_{L.c.i,ii}$, $T_{L.c.i}$, and $T_{L.c.ii}$, respectively.

6.4.1 "Optimal" Testing Conditions and Liquid Crystal System

For this case, the following performance indices should be satisfied, and are also the necessary and sufficient conditions for thermal testing with the liquid crystal:

$$T_{L.c.} > T_\infty \tag{120}$$

$$\Delta T^*_{max} = \Delta T^*(F_o) \gg \Delta T^*_{L.c.} \tag{121}$$

$$T^*_{L.c.} < T^*_{IIs}[(Fo)_{\Delta T^*_{max}}] < T^*_{L.c.} + \Delta T^*_{L.c.} \tag{122}$$

where $RK < 1$ (that is, $T^*_{IIs} > T^*_{Is}$). The conditions represented by eqns. (120), (121), and (122) define the "optimal" testing conditions.

6.4.2 "Acceptable" Testing Conditions and Liquid Crystal System

For this case, the following performance indices should be satisfied, and are also the necessary and sufficient conditions for thermal testing with the liquid crystal:

$$T_{L.c.} > T_\infty \tag{123}$$

$$\Delta T^*_{max} > \Delta T^*(Fo) > \Delta T^*_{L.C.} \tag{124}$$

$$T^*_{L.c.} < T^*_{IIs}(Fo) < T^*_{L.c.} + \Delta T^*_{L.c.} \tag{125}$$

where $RK < 1$ (that is, $T^*_{IIs} > T^*_{Is}$). The conditions represented by eqns. (123), (124), and (125) define the "acceptable" testing conditions.

6.4.3 "Moderately Acceptable" Testing Conditions and Liquid Crystal System

For this case, the following performance indices should be satisfied, and are also the necessary and sufficient conditions for thermal testing with the liquid crystal:

$$T_{L.c.} > T_\infty \tag{126}$$

$$\Delta T^*_{L.c.} > \Delta T^*(Fo) \geq \Delta T^*_{L.c.i,ii} \tag{127}$$

$$T^*_{L.c.i.} < T^*_{IIs}(Fo) \leq T^*_{L.c.i.} + \Delta T^*_{L.c.i,ii} \tag{128}$$

where $RK < 1$ (that is, $T^*_{IIs} > T^*_{Is}$) and $T^*_{L.c.i} < T^*_{L.c.ii}$. Also, $T_{L.c.i}$ and $T_{L.c.ii}$ are the temperatures corresponding to two nonadjacent colors. The conditions represented by eqns. (126), (127), and (128) define the "moderately acceptable" testing conditons.

6.4.4 "Limiting" Testing Conditions and Liquid Crystal System

For this case, the following performance indices should be satisfied, and are also the necessary and sufficient conditions for thermal testing with the liquid crystal:

$$T_{L.c.} > T_\infty \tag{129}$$

$$(\Delta T^*_{L.c.i,ii})_{nonadjacent} > \Delta T^*(Fo) \geq (\Delta T^*_{L.c.i,ii})_{adjacent} \tag{130}$$

$$T^*_{L.c.i.} < T^*_{IIs}(Fo) \leq T^*_{L.c.i.} + (\Delta T^*_{L.c.i,ii})_{adjacent} \tag{131}$$

where $RK < 1$ (that is, $T^*_{IIs} > T^*_{Is}$) and $T^*_{L.c.i} < T^*_{L.c.ii}$. Also, $T_{L.c.i}$ and $T_{L.c.ii}$ are the temperatures corresponding to two adjacent colors. The conditions represented by eqns. (129), (130), and (131) define the "limiting"

testing conditions.

6.5 EFFECT OF AMBIENT TEMPERATURE T_∞ ON CHOICE OF LIQUID CRYSTAL SYSTEM

It is clear from conditions (120), (123), (126), and (129) that the transition temperature of a chosen liquid crystal system should be greater than the ambient temperature T_∞. It is also concluded from eqns. (116), (118), and (119) that if T_∞ decreases by an amount δT_∞, the transition temperature of the liquid crystal system should be decreased by the same amount δT_∞, in order that the conditions (122), (125), (128), and (131) remain unchanged. Therefore, these conditions can be satisfied by choosing the transition temperature of the liquid crystal system in accordance with the ambient temperature. Also, in a control temperature environment, slight changes in the ambient temperature may be made in order to improve the testing conditions.

6.6 SPECIFICATIONS OF TESTING CONDITIONS AND LIQUID CRYSTAL SYSTEM

In order to specify the testing conditions and the liquid crystal system, it is necessary to specify q'', h, and T_∞ for the testing conditions, and $\Delta T_{L.c.}$ and $T_{L.c.}$ for the liquid crystal system. In general, for a given laminate and an assumed or known delamination, the parameters q'', h, $\Delta T_{L.c.}$, and $T_{L.c.}$ can be evaluated by satisfying the performance indices. Note that in evaluating q'', h, $\Delta T_{L.c.}$, and $T_{L.c.}$, the limitations which are

imposed by the conditions discussed in sections 6.3.5, 6.3.6, and 3.3 should be considered.

In order to satisfy the performance indices, it is necessary to evaluate ΔT^* and T^*_{IIs} for the laminate. For a given laminate and an assumed or known delamination, the values of ℓ, α_1, k_1, RK, R1, and R2 are known. Also, by considering the conditions which have been discussed in section 6.3.6, h can be evaluated. Hence, the value of Bi can be computed also. Therefore, the values of ΔT^* and T^*_{IIs} corresponding to the values of RK, Bi, R1, and R2 can be obtained from graphs, typically, such as Figs. 28 and 44, respectively. For this purpose, typical sets of graphs, such as Figs. 28 and 44, have been generated for ranges of RK and Bi and appear in Appendix 3.

Now, in order to evaluate the specifications of the testing conditions and the liquid crystal system, the performance indices, for example for the "optimal" testing conditions, can be rewritten as follows:

$$T_{L.c.} > T_\infty \tag{132}$$

$$\Delta T_{L.c.} \ll (q''\ell/k_1)\Delta T^*_{max} \tag{133}$$

$$T_{L.c.} < (q''\ell/k_1)T^*_{IIs}[(Fo)_{\Delta T^*_{max}}] < T_{L.c.} + \Delta T_{L.c.} \tag{134}$$

where ΔT^*_{max} and $T^*_{IIs}[(Fo)_{\Delta T^*_{max}}]$ have been evaluated for a given laminate. These conditions should be satisfied simultaneously by choosing the values of q'', $\Delta T_{L.c.}$, and $T_{L.c.}$. Those values, which satisfy the performance indices, determine the testing conditions and the liquid crystal system. The procedure for evaluating the specifications of the testing conditions

and the liquid crystal system for "acceptable", "moderately acceptable", and "limiting" testing conditions is the same as that represented in eqns. (132), (133), and (134), with the exceptions that ΔT^*_{max} should be replaced by ΔT^* and $(Fo)_{\Delta T^*_{max}}$ should be replaced by $(Fo)_{\Delta T^*}$. Note also that because eqns. (121), (124), (127), and (130) are inequalities, the specifications of the testing conditions ("optimal", "acceptable", "moderately acceptable", or "limiting") and the corresponding liquid crystal system are not unique.

If the specifications of the testing conditions and the liquid crystal system are given and those testing conditions are assumed to be any desirable case, such as "optimal" or "acceptable", information about the corresponding laminates and their interlaminar flaws, where those testing conditions are satisfied, can be obtained by working backwards through the above procedure. Rewriting, for example, the "optimal" testing conditions gives

$$T_{L.c.} > T_{\infty} \qquad (134)$$

$$\Delta T^*_{max} \gg (k_1/q''\ell)\Delta T_{L.c.} \qquad (135)$$

$$(k_1/q''\ell)T_{L.c.} < T^*_{IIs}[(Fo)_{\Delta T^*_{max}}] < (k_1/q''\ell)(T_{L.c.} + \Delta T_{L.c.}) \qquad (136)$$

where $\Delta T_{L.c.}$, $T_{L.c.}$, and q'' are given. Thus, any set of values for ℓ, R1, and R2 defines a laminate with its interlaminar flaw, if the conditions represented by eqns. (134), (135), and (136) are satisfied. Note also that the determination of the laminate and its interlaminar flaw, when the specifications of the testing conditions and the liquid crystal system are given, is not unique. Again, this is due to the presence of inequalities in the operating equations.

CHAPTER VII

EXPERIMENTAL RESULTS

7.1 TESTING UNIT AND EQUIPMENT

The radiant heating unit and the panel are shown in Fig. 45. The heating unit has two quartz-iodine lamps with a high-efficiency reflector which provides broad flat illumination which is capable of uniformly heating large areas [35]. The lamps (SMITH-VICTOR Model 750/1000 WATT) are symmetrically arranged to irradiate the panel uniformly with the light beams incident on the panel at approximately 30°.

The photographic recording systems is comprised of a 35 mm. single-lens reflex NIKON FM chrome camera body with a 135 mm. f/2.8 AUTOPROMASTER lens and a VIVITAR automatic 3X teleconverter MC 3X-3. No optical filter is used for lighting and photography. The same lamps were used for both irradiation and photography. The axis of the camera was perpendicular to the face of the test laminate. Kodacolor II C-135 (ASA 100) film was used.

The size of the test panel is 1 sq. ft. The lamps are placed approximately 3 ft. away. The camera is located approximately 5 ft. away.

7.2 PREPARATION OF TEST PANEL

Before applying the liquid crystal, the surface of the test laminate is cleaned with soap and water, then coated with a water-base black paint (FABER CASTELL Drawing Ink). The most important step in the testing procedure is the proper application of the liquid crystal. The coating thickness is judged by eye and is adequate if the entire surface of the panel

appears uniformly glossy when viewed obliquely. An aerosol spray with approximately 10% liquid crystal is used in the experiments. (The liquid crystal was supplied by Liquid Crystal Biosystems, Inc., 26101 Miles Ave., Cleveland, Ohio 49128.) Best results are obtained when approximately two or three coats of spray having a total thickness of about 0.001 in. are applied uniformly over the surface. The surface should not be allowed to dry between successive coats. Whereas the wavelength of light that is scattered does not depend upon the thickness of the liquid crystal, non-uniform coating thickness may cause an irregular color pattern even though no subsurface anomaly exists. The aerosol liquid crystal which is used scatters the entire color range from red to violet with a color-play range of 3°C from 31°C to 34°C. Fig. 47 shows the calibration results for this liquid crystal.

7.3 TEST PROCEDURE

The procedure for heating and photographing the laminate is described below. Before photographing the laminate, visual observations are made of the thermographic images produced during heating. The lamps are mounted as shown in Figs. 45 and 46 and aimed so as to uniformly irradiate the laminate. A laminate without any defects was used as a control panel to establish the uniformity of irradiation by means of the temperature-color response of the liquid crystal. An essentially uniform color over the entire panel surface which represents a uniform irradiation is achieved

10cm
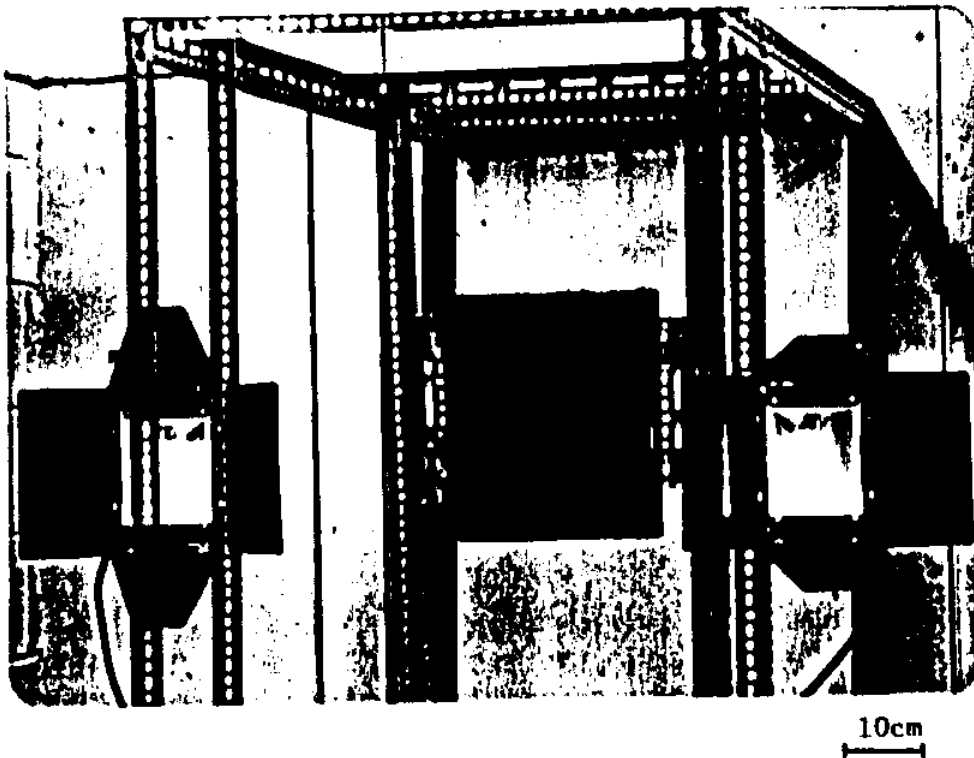
Fig. 45. Photograph of testing unit. (Lamps have
been rotated to show the reflectors.)

10cm
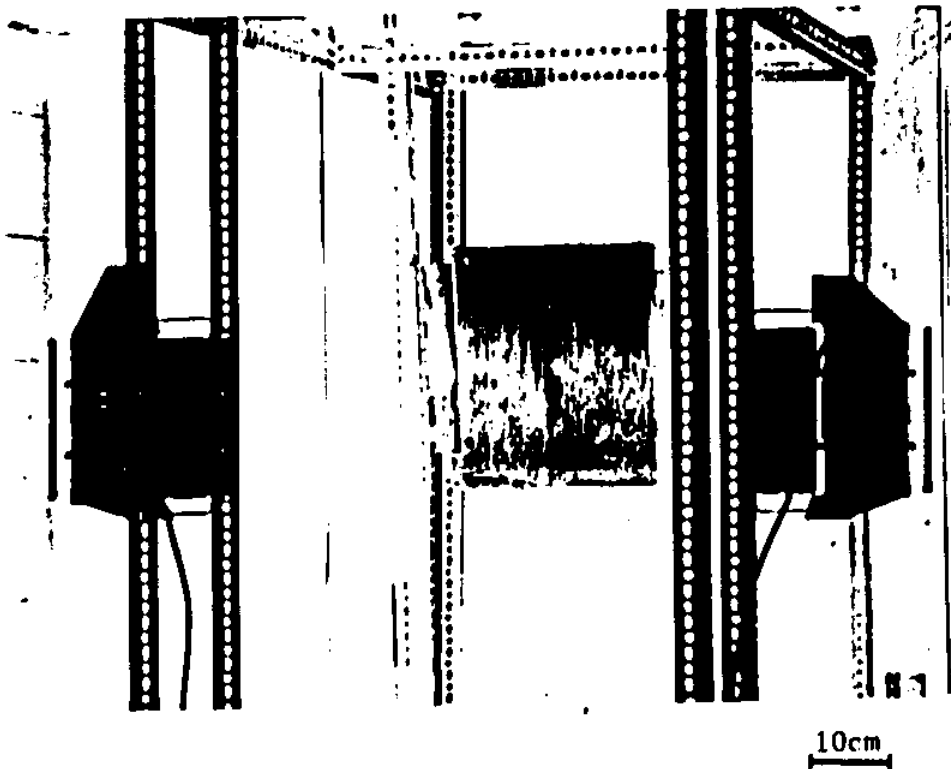
Fig. 46. Photograph of testing unit with lamps on.
(The whitish areas on the surface are due to glare
and do not affect either the color generation or
the color interpretation.)

(A color xerox of this page
is available for $1.00 from
the MIT Sea Grant Office.)

-107-
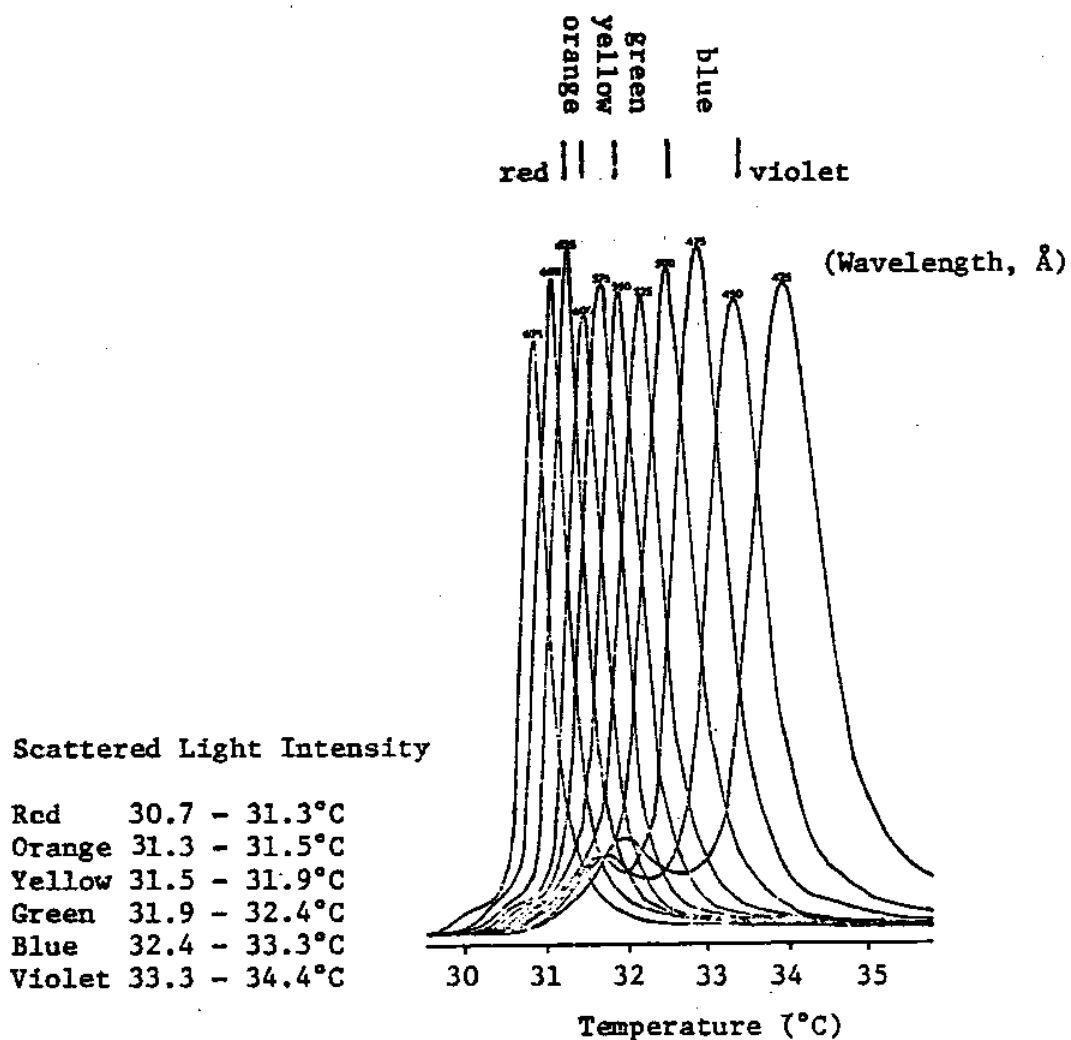
Fig. 47. Calibration results for the liquid crystal
system (with the color-play range of 3°C
from 31°C to 34°C).

Scattered Light Intensity

Red   30.7 - 31.3°C
Orange 31.3 - 31.5°C
Yellow 31.5 - 31.9°C
Green   31.9 - 32.4°C
Blue   32.4 - 33.3°C
Violet 33.3 - 34.4°C

by adjusting the position of the lamps. The, the test laminate is mounted on the stand with the face of the panel in a plane perpendicular to the floor and to the horizontal axis of the camera. The camera is focused and the camera controls (aperture and exposure time) are set for correct exposure according to the camera built-in light meter. Then the quartz-iodine lamps are turned on and a stop-watch is started. The panel is observed as the thermographic images images develop. At suitable times, photographs are taken to record the images as the surface temperature of the laminate increases and passes through the color-play range of the liquid crystal. The irradiation time corresponding to each photograph is recorded. Then the lamps are turned off and the panel is allowed to cool to the ambient temperature before conducting another photographic sequence.

Above its mesomorphic transition temperature, the liquid crystal appears wet, causing excessive glare. Most of this glare can be eliminated by adjusting the position of the lamps without affecting the uniformity of the panel irradiation. While the remaining glare has negligible effect upon the visual interpretation of the thermic pattern, this glare appears as small white regions in the photographs (this fact should be kept in mind in viewing subsequent photographs).

7.4 TEST RESULTS

The objective of the tests is to demonstrate some general features of the thermal testing of fiberglass composite laminates with liquid crystals. The results of several tests on fiberglass laminates with simulated defects

are described in this section. The defects are simulated by cutting patches out of a few succesive fiberglass prepreg layers before the laminate is formed using a hot press. In some of the cutouts paper is inserted while the other cutouts were left empty with the resulting flaw expected to be a combination of largely air with some resin.

A photograph of the thermographic image for a panel with a square defect is shown in Fig. 48. The photograph was taken 51 sec. after the initiation of heating. The geometrical variables, for the panel and defect, ℓ, R1, and R2 are 0.12 in., 0.25, and 0.30, respectively. The thermal properties of air are assumed for the material contained in the defect. The estimated value for q" is approximately 120 Btu/hr sq ft. ΔT^* and T^*_{IIs} that have been obtained from the results of this experiment are shown in Figs. 50 and 51.

Examination of the test results shows that the testing conditions were "acceptable." (See section 6.4.) Note that for the "acceptable" conditions, the originally black laminate surface is still black at the time of the photograph. Also, Fig. 48 shows that the lateral heat conduction is negligible because the thermographic image of a square shape defect is also a square of the same size. This result supports the one-dimensional heat conduction assumption which was made in chapter IV.

Fig. 49 shows a photograph of the thermographic image for the same laminate testing in Fig. 48 when it was tested for the same defect from the opposite face of the laminate (R1 and R2 are 0.45 and 0.30, respectively). The photograph was taken 56 sec. after the initiation of heating. The estimated value for q" was about 100 Btu/hr sq ft. ΔT^* and T^*_{IIs} that have been
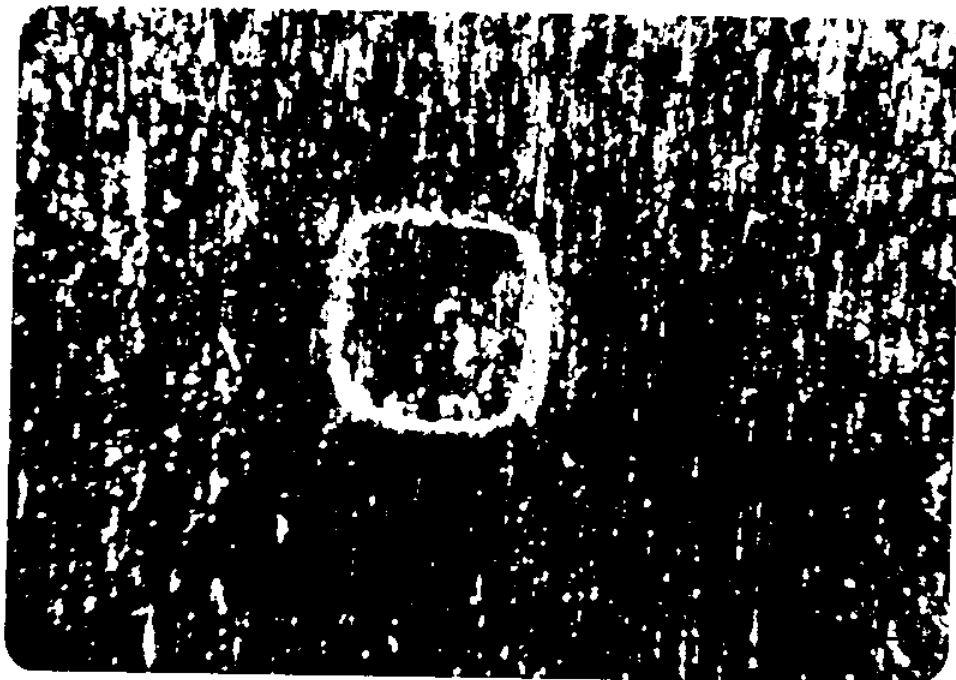
Fig. 43. Photograph of the thermographic image under "acceptable" testing conditions (R1=0.25, R2=0.30, ℓ=0.12 in., RK≈0.08).
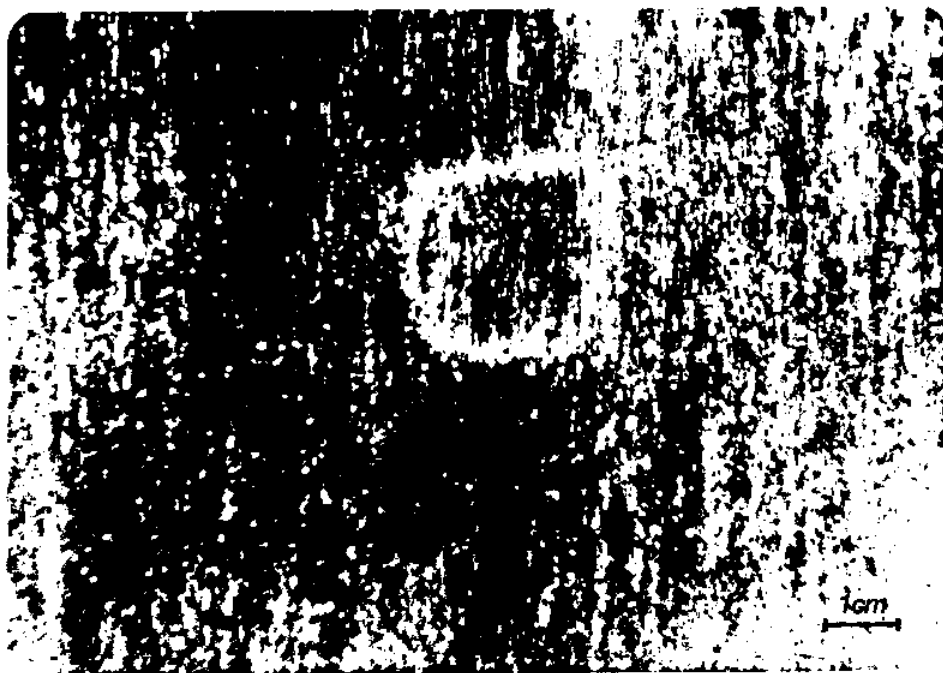
Fig. 49. Photograph of the thermographic image under "moderately acceptable" testing conditions (R1=0.45, R2=0.30, ℓ=0.12 in., RK≈0.08).

(A color xerox of this page is available for $1.00 from the MIT Sea Grant Office.)

-111-
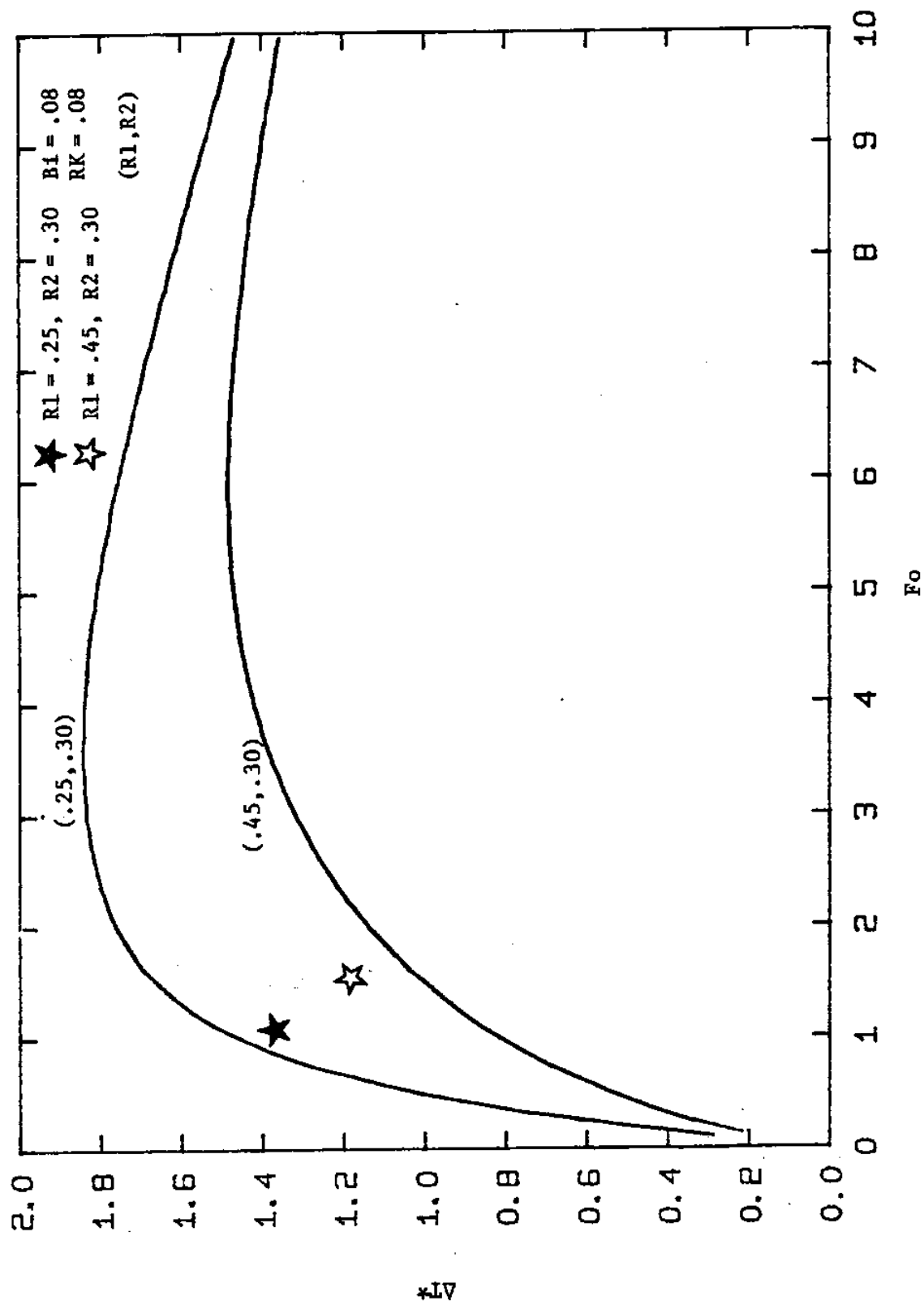
Fig. 50. Comparisons of theoretical results and the experimental data corresponding to Figs. 48 and 49.
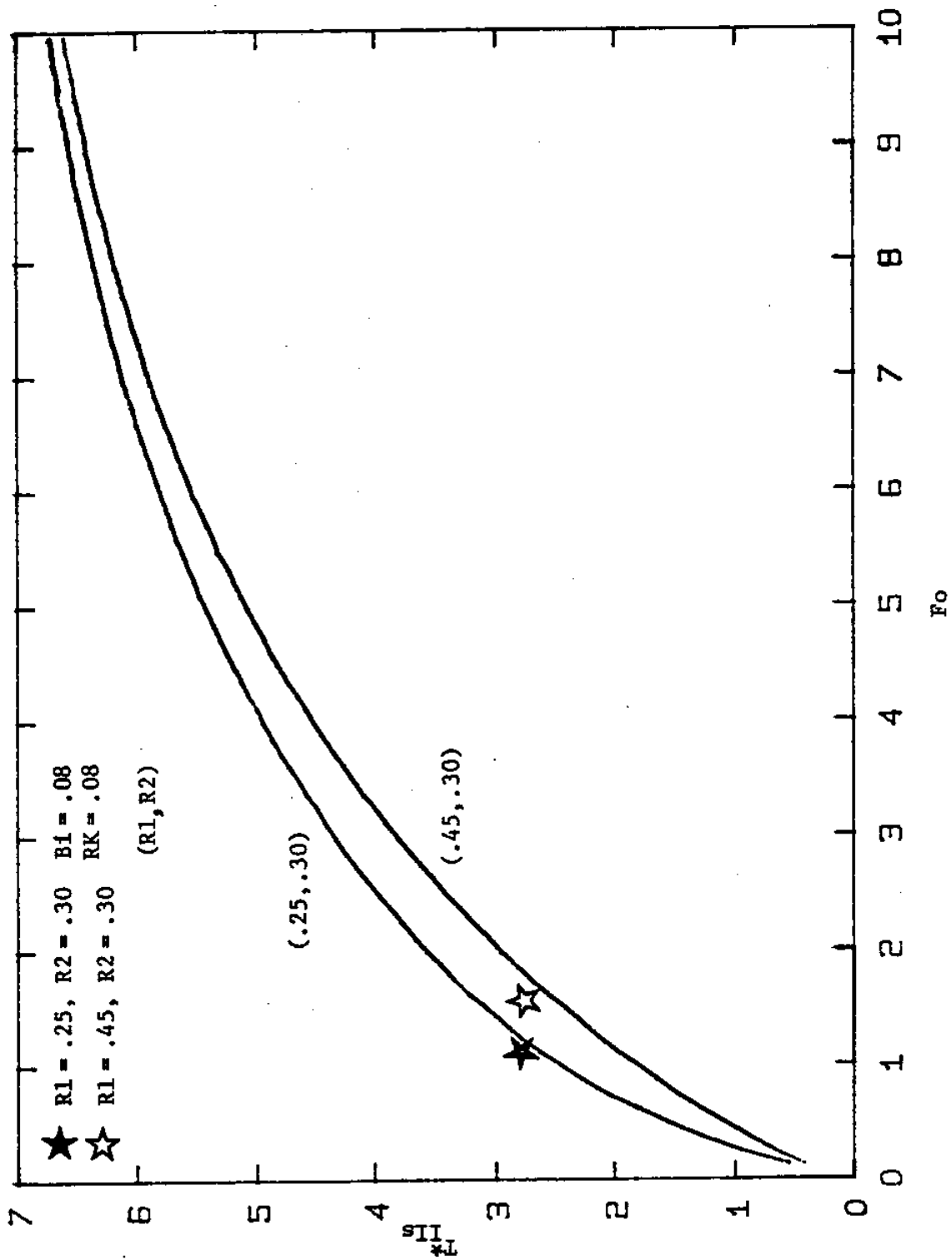
Fig. 51. Comparisons of theoretical results and the experimental data corresponding to Figs. 48 and 49.

obtained from the results of this experiment are also shown in Figs. 50 and 51. Examination of the test results showed that the testing conditions were "moderately acceptable".

A photograph of the thermographic image for a laminate with a circular defect is shown in Fig. 52. The photograph was taken 56 sec after the initiation of heating. The geometrical variables, for the panel and the defect, ℓ, R1, and R2 are 0.12 in., 0.25, and 0.30, respectively. The defect contained a paper inclusion. Examination of the test results shows that the testing conditions were "acceptable". In this case the defect can be detected easily and accurately.

Fig. 53 shows a photograph of the thermographic image for the same laminate tested in Fig. 52 when it was tested for the same defect from the opposite face of the laminate (R1 and R2 are 0.45 and 0.30 respectively). The photograph was taken 70 sec after the initiation of heating. Examination of the test results shows that the testing conditions were "moderately acceptable".

A photograph of the thermographic image for a laminate with a circular flaw (ℓ, R1, and R2 are 0.12 in., 0.25, and 0.15, respectively) is shown in Fig. 54. The defect contained a paper inclusion. The photograph was taken 45 sec after the initiation of heating. Fig. 55 is a photograph of the thermographic image of the same laminate and defect when tested from the opposite face of the laminate (R1 and R2 are 0.60 and 0.15, respectively). The photograph was taken 50 sec after the initiation of heating. Examination of the test results shows that the testing conditions depicted in Figs.
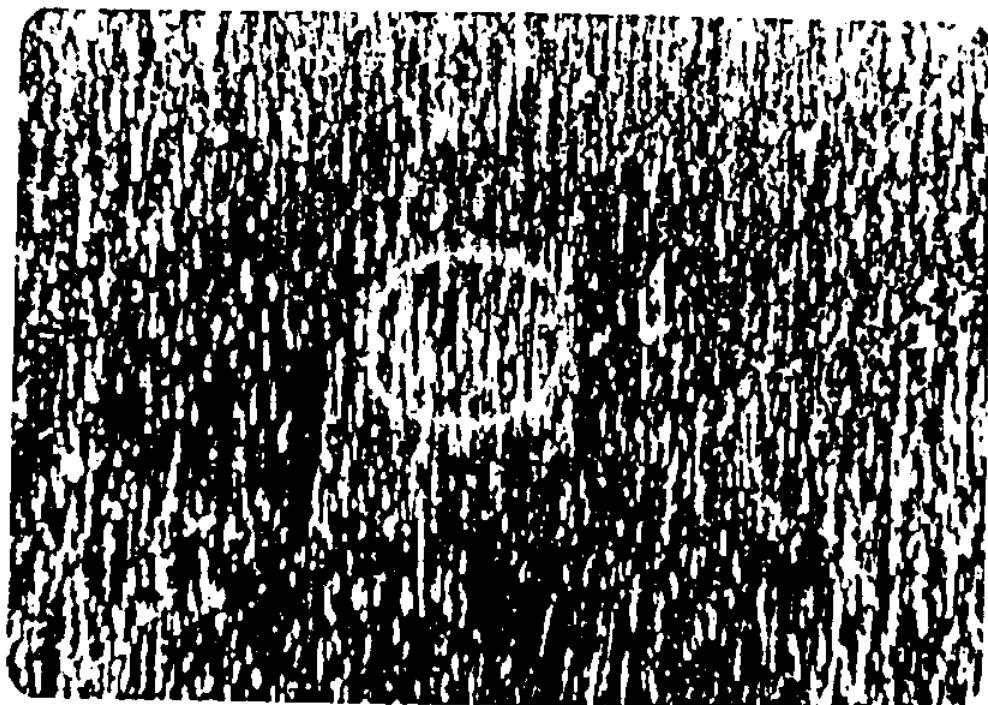
1 cm

Fig. 52. Photograph of the thermographic image under "accceptable"
testing conditions (R1=0.25, R2=0.30, ℓ=0.12 in., RK=0.40).
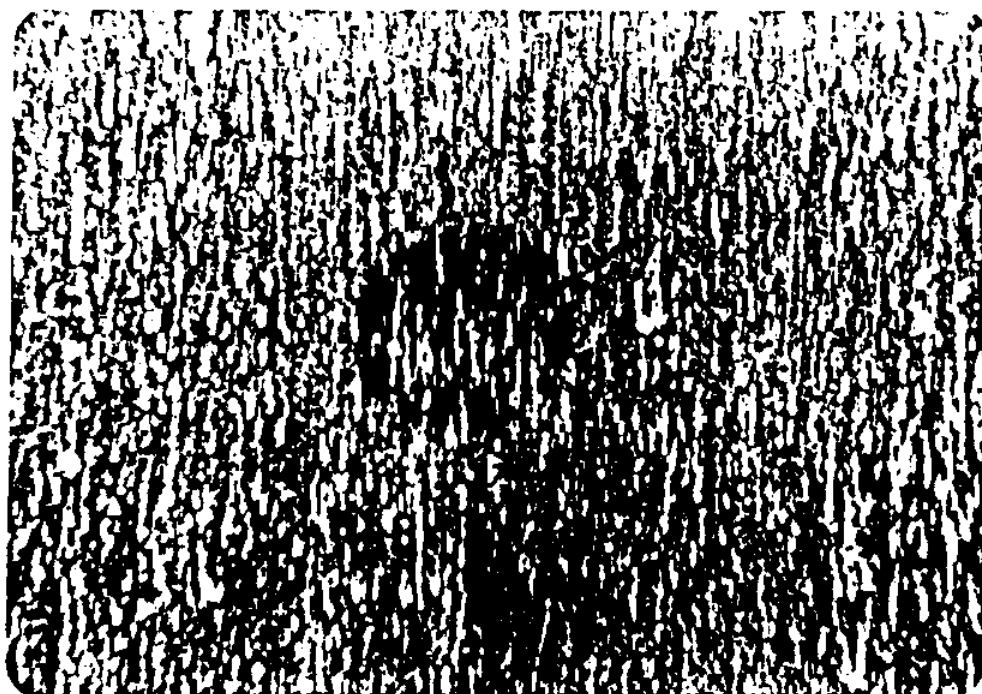
1cm

Fig. 53 Photograph of the thermographic image under "moderately
acceptable" testing conditions (R1=0.45, R2=0.3C,
ℓ=0.12 in., RK=0.40).

Fig. 54. Photograph of the thermographic image under "limiting" testing conditions (R1=0.25, R2=0.15, ℓ=0.12 in., RK≈0.40).
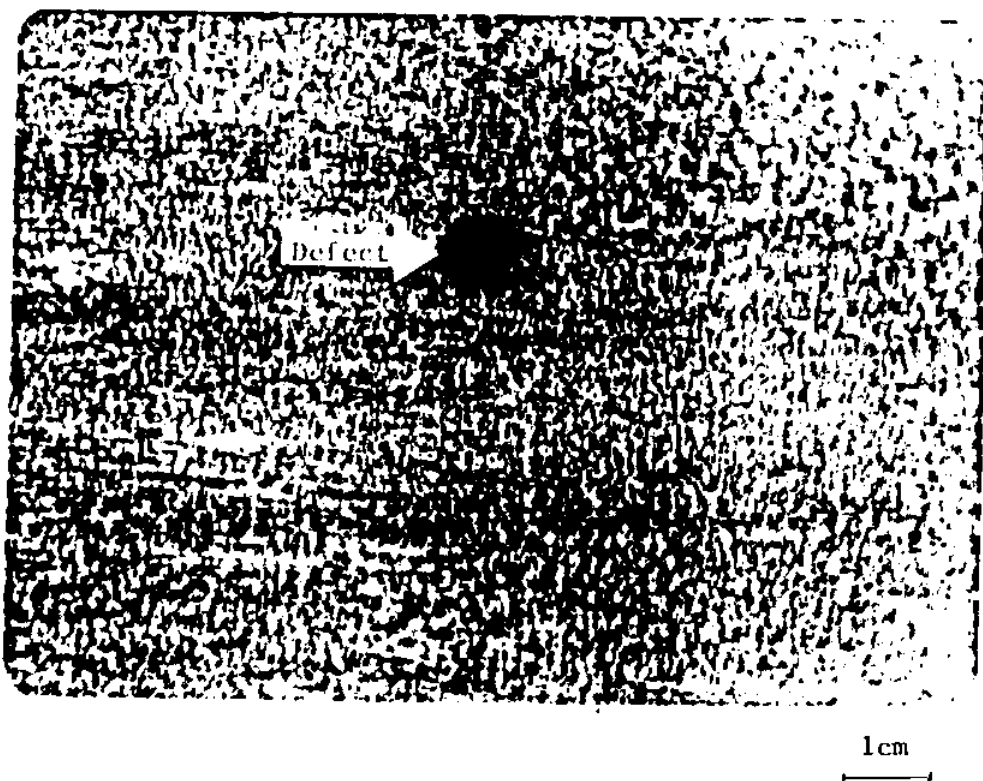
Fig. 55 Photograph of the thermographic image under "limiting" testing conditions (R1=0.60, R2=0.15, ℓ=0.12 in., RK≈0.40).

(A color xerox of this page is available for $1.00 from the MIT Sea Grant Office.)

54 and 55 were "limiting", and the detection of defects is not easy al-
though it is possible to electronically enhance the photographic data.

CHAPTER VIII

CONCLUSIONS

Cholesteric liquid crystals are compounds that pass through a transition phase in which they possess the flow characteristics of a liquid while retaining much of the molecular order of a crystalline solid. Because liquid crystals have the ability to indicate temperature by exhibiting brilliant changes in color over discrete, reproducible temperature ranges, they may be used to project a visual color image of minute thermal gradients which may be associated with material discontinuities.

The purpose of this investigation was (1) to examine the feasibility of using cholesteric liquid crystals for the detection of interlaminar defects in fiber reinforced laminates and (2) to establish the requirements for setting the testing conditions and for choosing a liquid crystal system to define the quantitative features of a delamination flaw in fiber reinforced laminates. A review and summary of the liquid crystal literature has been presented and the unique properties of cholesteric liquid crystals have been described.

Based upon this investigation, thermal testing with cholesteric liquid crystals provides a simple nondestructive evaluation technique for the detection of interlaminar flaws in fiberglass composite laminates. Virtually no training is required in order to recognize the presence of a flaw. Also, no complex electronic equipment is needed to record the data as any ordinary camera can be used to produce a permanent visual record

of the results.

A one-dimensional model of the heat conduction through a laminate, containing an interlaminar flaw, with natural convection on both faces has been devised. An analytical solution of the surface temperatures above the flawed and unflawed sections of the laminate has been developed. Non-dimensional groups have been identified which make it possible to define "optimal", "acceptable", "moderately acceptable", and "limiting" testing conditions in relation to the parameters of the delamination and the laminate being inspected. Comparisons between experiments and theory clearly show that interlaminar flaws can be distinctively seen under "optimal", "acceptable", or "moderately acceptable" testing conditions.

In general, the testing conditions may be chosen by satisfying the theoretical performance indices corresponding to either "optimal", "acceptable", or "moderately acceptable" conditions. In order to facilitate the conduct of future experiments, sets of data have been generated for most practical situations. The use of these data has been described in detail in section 6.6.

REFERENCES

1. R. E. Engelhardt and W. A. Hewgley, "Thermal and Infrared Testing", chapter 6 of Nondestructive Testing, A Survey, NASA SP-5113, Washington, D. C., 1973.

2. E. W. Kutzscher, K. H. Zimmerman, and J. L. Botkin, "Thermal and Infrared Methods for Nondestructive Testing of Adhesive-Bonded Structures", Materials Evaluation, July 1968, pp. 143-148.

3. W. E. Woodmansee, "Aerospace Thermal Mapping Applications of Liquid Crystals", Applied Optics, Vol. 7, No. 9, Sept. 1968, pp. 1721-1727.

4. W. E. Woodmansee, "Cholesteric Liquid Crystals and Their Application to Thermal Nondestructive Testing", Materials Evaluation, Oct. 1966, pp. 564-572.

5. Larry V. Best, "Use of Cholesteric Liquid Crystals for Locating Voids in Adhesively Bonded Helicopter Blades", Report No. USAMC-ITC-02-08-73-029, Army Material Command, Texarkana, Texas, March 1974.

6. LaMarr Sabourin, "Nondestructive Testing of Bonded Structures with Liquid Crystals", paper presented at the Structural Adhesive Bonding Conference, MSFC, March 15-16, 1966.

7. W. E. Woodmansee and H. L. Southworth, "Detection of Material Discontinuities with Liquid Crystals", Materials Evaluation, Aug. 1968, pp. 149-154.

8. S. E. Cohen, "The Application of Liquid Crystals for Thermographic Testing of Bonded Structures", NASA CR-88196, PD2-7, prepared under Contract No. NAS 8-20627 by the Proficiency Development Laboratory, Quality Engineering Department, Lockheed-Georgia Co., Marietta, Georgia, for Marshall Space Flight Center, NASA, Sept. 1967.

9. S. P. Brown, "Cholesteric Crystals for Nondestructive Testing", Materials Evaluation, Aug. 1968, pp. 163-166.

10. S. P. Brown, "Detection of Flaws in Metal-Honeycomb Structures by Means of Liquid Crystals", Report No. RS-TR-67-5, U. S. Army Missile Command, Redstone Arsenal, Alabama, June 1967.

11. H. L. Southworth and W. E. Woodmansee, "Thermal Nondestructive Testing with Cholesteric Liquid Crystals", Thermal Methods, Technical Session 3, Aug. 1969, pp. 81-87.

12. F. Reinitzér, Wiener Monatschr. Chem. 9, 421 (1888).

13. J. L. Fergason, "Liquid Crystals", Scientific American, Vol. 211, No. 2. Aug. 1964, pp. 77-85.

14. G. H. Brown, "Liquid Crystals and Some of Their Applications in Chemistry", Analytical Chemistry, Vol. 41, No. 13, Nov. 1969, pp. 26A-39A.

15. D. Maple Roger, "Utilization of Temperature Sensitive Liquid Crystals for Thermal Analysis and Application to Transducer Investigations", Naval Underwater Systems Center TR4235, May 30, 1972.

16. J. L. Fergason, "Liquid Crystals in Nondestructive Testing", Applied Optics, Vol. 7, No. 9, Sept. 1968, pp. 1729-1737.

17. C. W. Griffen and R. S. Porter, "Molecular Crystals 21(1973), p. 77.

18. T. E. Cooper, et al., "A Liquid Crystal Thermographic Study of a Heated Cylinder in Cross Flow", Naval Postgraduate School, Monterey, California, Nov. 1974.

19. L. C. Scala and G. D. Dixon, Molecular Crystals 7(1969), p. 44.

20. L. C. Scala and G. D. Dixon, Molecular Crystals 10(1970), p. 411.

21. G. D. Dixon, "Cholesteric Liquid Crystals in NDT", Materials Evaluation, June 1977, p. 51.

22. J. L. Fergason, N. N. Goldberg, and R. J. Nadalin, "Cholesteric Structure – II. Chemical Significance", Molecular Crystals, Vol. 1, 1966, pp. 309-323.

23. E. Sprow, "Liquid Crystals – A Film in Your Future?", Machine Design, Feb. 6, 1969, pp. 34-41.

24. Vedat S. Arpaci, "Conduction Heat Transfer", Addison-Wesley, 1966.

25. Francis B. Hildebrand, "Advanced Calculus for Applications", Second Edition, Prentice-Hall, Inc., 1976, Chapter 9.

26. Ibid., Chapter 5.

27. H. S. Carslaw and J. C. Jaeger, "Conduction of Heat in Solids", Clarendon Press, Oxford, 1959.

28. C. W. Tittle and V. L. Robinson, "Analytical Solution of Conduction Problems in Composite Media", ASME Paper No. 65-WA/HT-52.

29. C. W. Tittle, "Boundary Value Problems in Composite Media: Quasi-Orthogonal Functions", Journal of Applied Physics, Vol. 36, No. 4, April 1965, pp. 1486-1488.

30. Ruel V. Churchill, "Fourier Series and Boundary-Value Problems", McGraw-Hill Book Co., New York, 1963, p. 70.

31. M. N. Özisik, "Boundary Value Problems of Heat Conduction", International Textbook Co., Scranton, Pennsylvania, 1968, p. 275.

32. W. M. Rohsenow and H. Y. Choi, "Heat, Mass, and Momentum Transfer", Prentice-Hall, Inc., 1961, Chapter 17.

33. F. Kreith, "Principles of Heat Transfer", 3rd edition, Intext Educational Publishers, 1973, p. 12.

34. S. C. Peek, "Quartz-Iodine Lamps and Reflectors for Set Lighting", Journal of the SMPTE, Vol. 71, Sept. 1962, p. 667.

APPENDIX 1

LISTING OF COMPUTER PROGRAM

A.1 NOMENCLATURE OF MAIN PROGRAM

Symbol		Description	Unit
AK1	k_1	Thermal conductivity	Btu/hr ft F
AK2	k_2	Thermal conductivity	Btu/hr ft F
AK3	k_3	Thermal conductivity	Btu/hr ft F
ALFA1	α_1	Thermal diffusivity	ft^2/hr
ALFA2	α_2	Thermal diffusivity	ft^2/hr
ALFA3	α_3	Thermal diffusivity	ft^2/hr
H	h	Heat transfer coefficient	Btu/hr sq ft F
Q	q"	Net radiant heat flux	Btu/hr sq ft
X1	x_1	Geometrical variable (refer to Fig. 20)	ft
X2	x_2	Geometrical variable (refer to Fig. 20)	ft
X3	x_3	Geometrical variable (refer to Fig. 20)	ft
X4	x_4	Geometrical variable (refer to Fig. 20)	ft
NC		Number of data case	—
XINITA		Initial value for β_1	ft^{-1}
DELTA1		Initial step-size for β_1	ft^{-1}
DELTAT	Δt	where t is the maximum time and $\Delta t = t/80$	hr
X(1)	β_1	(refer to Fig. 24)	ft^{-1}
BETA(I)	β_{1i}	(refer to Fig. 24)	ft^{-1}
TTWO(NA,N)	$T^*_{IIs}(t)$	nondimensional temperature	—
TTWO(13,N)	Fo	nondimensional time corresponding to $T^*_{IIs}(t)$	—

```
C
C                      ***** MAIN PROGRAM *****
C
C
          *********          *********          *********
          COMMON X(3),BETA(250),DELTA(40),A(20),EIGEN(4),C(3),D(3),
        1 BI(3),TETA(4),AA(3),AB(3),W(3),BN(250),AN(250),DN(250),EIGFUN
        2 ,X1,X2,X3,AK2,AK3,SAF12,SAF13,ALFA2,ALFA3,I
          COMMON /TWO/    Q,H,DELTAO,TTWO(13,80),TONE(13,80),ABST12
        1 (13,80),DELTAT,AK1,ALFA1
          COMMON /XXX/ X4,NA
          INTEGER*2 XLAB(40)
C
C           ...........................................................
C           .READ DATA: MATERIALS PROPERTIES, GEOMETRICAL      .
C           .MAXIMUM TIME.                                      .
C           .VARIABLES, BOUNDARY AND INITIAL CONDITIONS,AND     .
C           ...........................................................
C
          READ(8,447)NC
   447    FORMAT(I5)
          NA=0
   777    READ(8,1000)AK1,AK2,ALFA1,ALFA2,H,Q,X2,X3,X4,DELTA1,
        1 XINITA,DELTAT
  1000    FORMAT(3E10.4)
          X1=0.0
          AK3=AK1
          ALFA3=ALFA1
          DELTAO=0.5
          NA=NA+1
          WRITE(5,1102) NA
          WRITE(6,1102)NA
  1102    FORMAT(' ',I5,'***************************************************')
          WRITE(6,1001)AK1,AK2,AK3,ALFA1,ALFA2,ALFA3,X1,X2,X3,X4
        1 ,XINITA,DELTAO,DELTA1,DELTAT,H,Q
          WRITE(5,1001)AK1,AK2,AK3,ALFA1,ALFA2,ALFA3,X1,X2,X3,X4
        1 ,XINITA,DELTAO,DELTA1,DELTAT,H,Q
  1001    FORMAT('      AK1=',1E11.5/'      AK2=',1E11.5/'      AK3=',
        1 1E11.5/'    ALFA1=',1E11.5/'    ALFA2=',1E11.5/'    ALFA3=',
        2 1E11.5/'       X1=',1E11.5/'       X2=',1E11.5/'       X3=',
        3 1E11.5/'       X4=',1E11.5/'   XINITA=',1E11.5/'   DELTAO=',
        4 1E11.5/'   DELTA1=',1E11.5/'   DELTAT=',1E11.5/'        H=',
        5 1E11.5/'        Q=',1E11.5/)
          X(1)=0.0
          SAF12=ALFA1/ALFA2
          SAF13=ALFA1/ALFA3
          ALFAR=1./SAF12
```

```
          AKR=AK2/AK1
          RL1=X2/X4
          RL2=(X3-X2)/X4
          BIL=H*X4/AK1
          WRITE(5,133)BIL,ALFAR,AKR,RL1 ,RL2
  133     FORMAT(*        ********************************************//
     1    *          BIL=*,1E11.5/*        ALFAR=*,1E11.5/
     2    *          AKR=*,1E11.5/*          RL1=*,1E11.5/
     3    *          RL2=*,1E11.5)

C
C
C         .................................................
C         .BY USING A STEPPING PROCEDURE IN WHICH A SIGN   .
C         .CHANGE DETECTS THE STEPPING INTERVAL WHTHIN WHICH.
C         .THE ROOT LIES, CALCULATE ANJ STORE THE ROOTS     .
C         .BETA(I) OF EQN.(90). CALL SUBROUTINE EIGF.       .
C         .................................................
C
          S=0.
          I=0
  110     I=I+1
          X(1)=XINITA+X(1)
          J=0
          DELTA(1)=DELTA1
  150     J=J+1
          DELTA(J+1)=DELTA(J)*DELTAO
            CALL  EIGF
  103     XA=EIGFUN
          X(1)=X(1)+DELTA(J)
            CALL  EIGF
          B=EIGFUN
          S=S+1.
          R=0.02
            IF(S*R-1.0)111,112,112
  112     S=0.
          WRITE(6,1101)X(1)
 1101     FORMAT(*  THE CURRENT VALUE OF X =          *,1E24.9)
  111       IF(XA*B)101,102,103
  102       IF(XA)104,105,104
  104     BETA(I)=X(1)
            GO TO 100
  105     BETA(I)=X(1)-DELTA(J)
            GO TO 100
  101       IF(DELTA(J)/X(1)-1.E-4)108,108,107
  108     BETA(I)=X(1)
            GO TO 100
  107     X(1)=X(1)-DELTA(J)
            GO TO 150
```

```
C
C
C              ...............................................
C              .CALL SUBROUTINE COEF. CALCULATE AND STORE THE  .
C              .COEFFICIENTS AN(I) WHICH CORRESPOND TO THE EIGEN-.
C              .VALUES BETA(I).                                 .
C              ...............................................
C
  100          CALL COEF
               BETAI=BETA(I)
               BXI=(BETA(I)*X4)/(3.141592654)
               ANI=AN(I)
               WRITE(6,2100)I,BETAI,ANI,BXI,J
 2100          FORMAT(' ',I4,3E18.9,I6)
               IF(15.0-ALFA1*(BETA(I)**2.0)/3600.0)120,120,110
C
C
C              ...............................................
C              .BY USING EQN. (105) , CALCULATE AND STORE      .
C              .TTWO(NA,N); ALSO CALCULATE AND STORE FOURIER NUM-.
C              .BER (TTWO(NA,13) AT THE SAME TIME.              .
C              ...............................................
C
  120          T=0.0
               DO 11 N=1,80
               T=T+DELTAT
               J=0
  155          J=J+1
               IF(15.0-ALFA1*(BETA(J)**2.0)*T)130,140,155
  130          K=J-1
               GO TO 160
  140          K=J
  160          Y=0.0
               DO 12 M=1,K
               AEX=-ALFA1*(BETA(M)**2.0)*T
               Y=Y+AN(M)*EXP(AEX)
   12          CONTINUE
               TTWO(NA,N)=(Y+(Q/(H*(2.0+BI(1)+BI(2)+BI(3))))*(1.0+BI(1)+
     1         BI(2)+BI(3)))*AK1/(Q*X4)
               TTWO(13,N)=ALFA1*T/(X4**2.0)
   11          CONTINUE
C
C
C              ...............................................
C              .CALL SUBROUTINE TWOTI.BY USING EQN.(35),CALCULATE.
C              .AND STORE TONE(NA,N). THEN,BY USING EQN.(1),AT    .
C              .THE SAME TIME CALCULATE  AND STORE ABST12(NA,N).  .
C              ...............................................
C
               CALL TWOTI
               IF(NA.LT.NC) GO TO 777
```

-126-

```
C
C
C       ..........................................................
C          .PLOT TONE(NA,N), TTWO(NA,N),AND ABST12(NA,N) VS.  .
C          .TONE(NA,13).                                      .
C       ..........................................................
C
        L=0
77      L=L+1
          IF(L.EQ.4) GO TO 95
        READ(8,44)XLAB
44      FORMAT(40A2)
          IF(L.EQ.1) GO TO 99
          IF(L.EQ.2) GO TO 98
          IF(L.EQ.3) GO TO 97
99   CALL QPICTR(ABST12,13,80 ,QY(1,2,3,4,5,6,7,8,9),QX(13)
  1    ,QLABEL(4),QXLAB(XLAB))
        GO TO 55
98      CALL QPICTR(TTWO,13,80 ,QY(1,2,3,4,5,6,7,8,9),QX(13)
  1    ,QLABEL(4),QXLAB(XLAB))
        GO TO 55
97      CALL QPICTR(TONE,13,80 ,JY(1,2,3,4,5,6,7,8,9),QX(13)
  1    ,QLABEL(4),QXLAB(XLAB))
55      GO TO 77
95      CALL EXIT
        END
```

A.3 NOMENCLATURE OF SUBROUTINE TWOTI

Symbol	Description	Unit
X	λ (refer to Fig. 22)	ft^{-1}
BETA(I)	λ_1 (refer to Fig. 22)	ft^{-1}
TONE(NA,N)	$T^*_{Is}(t)$ nondimensional temperature	--
ABST12(NA,N)	$\Delta T^*_{IIs}(t)$ nondimensional temperature difference	--
TONE(13,N)	Fo nondimensional time corresponding to $T^*_{Is}(t)$	--

```
C                      ***** SUBROUTINE TWOTI *****
C
C
C
       SUBROUTINE TWOTI
       DIMENSION       BN(250),DELTA(40),BETA(250)
       COMMON /TWO/     Q,H,DELTAO,TTWO(13,80),TONE(13,80),ABST12
     1 (13,80),DELTAT,AK1,ALFA1
       COMMON /XXX/ X4,NA
       EIGN(X,X4,BI)=((X*X4)**2.-BI**2.)*SIN(X*X4)-COS(X*X4)*(2.*BI*
     1 X*X4)
       COEF(X,X4,BI,Q,H)= ((2.0*Q)/(H*(2.0+BI)))*((BI/(X*X4))*COS(X*
     1 X4)-SIN(X*X4)-BI/(X*X4))/(X*X4+SIN(X*X4)*COS(X*X4))
       X=0.
       BI=H*X4/AK1
C
C             ........................................................
C             .BY USING A STEPPING PROCEDURE IN WHICH A SIGN       .
C             .CHANGE DETECTS THE STEPPING INTERVAL WITHIN         .
C             .WHICH THE ROOT LIES,CALCULATE AND STORE THE ROOTS.  .
C             .BETA(I) OF EQN.(29).                                .
C             ........................................................
C
       S=0.
       I=0
110    I=I+1
         IF(I.EQ.1) XINITA=1.010*BI/X4
         IF(I.GE.2) XINITA=1.57/X4
       X=X+XINITA
       J=0
       DELTA1=0.40/X4
       DELTA(1)=DELTA1
150    J=J+1
       DELTA(J+1)=DELTA(J)*DELTAO
103    XA=EIGN(X,X4,BI)
       X=X+DELTA(J)
       B=EIGN(X,X4,BI)
       S=S+1.
       R=0.02
         IF(S*R-1.0)111,112,112
112    S=0.
       WRITE(6,1101)X
1101   FORMAT(' THE CURRENT VALUE OF X =      ',1E24.9)
111      IF(XA*B)101,102,103
102      IF(XA)104,105,104
104    BETA(I)=X
         GO TO 100
105    BETA(I)=X-DELTA(J)
         GO TO 100
101      IF(DELTA(J)/X-1.E-4)108,108,107
108    BETA(I)=X
```

```
              GO TO 100
      107     X=X-DELTA(J)
              GO TO 150
C
C             ..........................................................
C             .BY USING EQN.(34), CALCULATE AND STORE EACH COEF-.
C             .FICIENT BN(I) WHICH CORRESPONDS TO THE EIGENVALUE.
C             .BETA(I).                                          .
C             ..........................................................
C
      100     BN(I)=COEF(X,X4,BI,Q,H)
              BNI=BN(I)
              BETAI=BETA(I)
              WRITE(6,1100)I,BETAI,BNI,J
     1100     FORMAT(' ',I10,2E16.5,I15)
                IF(15.0-ALFA1*(BETA(I)**2.0)/3600.0)120,120,110
C
C             ..........................................................
C             .BY USING EQN.(35),CALCULATE AND STORE TONE(NA,N)..
C             ..........................................................
C
      120     T=0.0
              DO 11 N=1,80
              T=T+DELTAT
              J=0
      155     J=J+1
                IF(15.0-ALFA1*(BETA(J)**2.0)*T)130,140,155
      130     K=J-1
                GO TO 160
      140     K=J
      160     Y=0.0
              DO 12 M=1,K
              AEX=-ALFA1*(BETA(M)**2.0)*T
              Y=Y+BN(M)*EXP(AEX)
       12     CONTINUE
            TONE(NA,N)=(Y+Q*(1.0+BI)/(H*(2.0+BI)))*AK1/(Q*X4)
              ABST12(NA,N)=ABS(TTWO(NA,N)-TONE(NA,N))
          ABST12(13,N)=TTWO(13,N)
              TONE(13,N)=ALFA1*T/(X4**2.0)
       11     CONTINUE
              RETURN
              END
```

```
                    ***** SUBROUTINE EIGF *****

C
C
C       ....................................................
C       .CALCULATE A THROUGH T USING EQNS. (83); THEN      .
C       .EVALUATE THE LEFT-HAND SIDE OF EQN.(90) FOR X(1)...
C       ....................................................
C       **********           **********           **********
C
        SUBROUTINE EIGF
        COMMON X(3),BETA(250),DELTA(40),A(20),EIGEN(4),C(3),D(3),
1       BI(3),TETA(4),AA(3),AB(3),W(3),BN(250),AN(250),DN(250),EIGFUN
2       ,X1,X2,X3,AK2,AK3,SAF12,SAF13,ALFA2,ALFA3,I
        COMMON /TWO/    Q,H,DELTAO,TTWO(13,80),TONE(13,80),ABST12
1       (13,80),DELTAT,AK1,ALFA1
        COMMON /XXX/ X4,NA
          AK1X1=AK1*X(1)
          AK12X1=(AK1/AK2)*X(1)
          X(2)=X(1)*SAF12
          AK23X2=(AK2/AK3)*X(2)
          X(3)=X(1)*SAF13
          AK3X3=AK3*X(3)
        X11=X(1)*X1
        X12=X(1)*X2
        X22=X(2)*X2
        X23=X(2)*X3
        X33=X(3)*X3
        X34=X(3)*X4
        SX11=SIN(X11)
        CX11=COS(X11)
        SX12=SIN(X12)
        CX12=COS(X12)
        SX22=SIN(X22)
        CX22=COS(X22)
        SX23=SIN(X23)
        CX23=COS(X23)
        SX33=SIN(X33)
        CX33=COS(X33)
        SX34=SIN(X34)
        CX34=COS(X34)
        A(1)=H*CX11+AK1X1*SX11
        A(2)=H*SX11-AK1X1*CX11
        A(3)=CX12
        A(4)=SX12
        A(5)=-CX22
        A(6)=-SX22
        A(7)=-AK12X1*SX12
        A(8)=AK12X1*CX12
        A(9)=X(2)*SX22
        A(10)=-X(2)*CX22
```

```
      A(11)=CX23
      A(12)=SX23
      A(13)=-CX33
      A(14)=-SX33
      A(15)=-AK23X2*SX23
      A(16)=AK23X2*CX23
      A(17)=X(3)*SX33
      A(18)=-X(3)*CX33
      A(19)=H*CX34-AK3X3*SX34
      A(20)=H*SX34+AK3X3*CX34
      EIGEN(1)=A(12)*A(17)*A(20)-A(12)*A(18)*A(19)-A(13)*A(16)*A(20)
     1 +A(14)*A(16)*A(19)
      EIGEN(2)=A(1)*A(4)*A(9)-A(1)*A(5)*A(8)-A(2)*A(3)*A(9)+A(2)*A(5
     1 )*A(7)
      EIGEN(3)=A(11)*A(17)*A(20)-A(11)*A(18)*A(19)-A(13)*A(15)*A(20)
     1 +A(14)*A(15)*A(19)
      EIGEN(4)=-A(1)*A(4)*A(10)+A(1)*A(6)*A(8)+A(2)*A(3)*A(10)-A(2)
     1 *A(6)*A(7)
      EIGFUN=EIGEN(1)*EIGEN(2)+EIGEN(3)*EIGEN(4)
      RETURN
      END
```

```
C
C
C
C                       ***** SUBROUTINE COEF *****
C
C
C
C             ..........................................................
C             .BY USING EQNS. (85) THROUGH (89),(98) THROUGH          .
C             .(100), AND(103), CALCULATE AND STORE THE COEF-         .
C             .FICIENTS AN(I).                                        .
C             .                                                       .
C             ..........................................................
C             **********          **********          **********
      SUBROUTINE COEF
      COMMON X(3),BETA(250),DELTA(40),A(20),EIGEN(4),C(3),D(3),
     1BI(3),TETA(4),AA(3),AB(3),W(3),BN(250),AN(250),DN(250),EIGFUN
     2,X1,X2,X3,AK2,AK3,SAF12,SAF13,ALFA2,ALFA3,I
      COMMON /TWO/    Q,H,DELTAO,TTWO(13,80),TONE(13,80),ABST12
     1(13,80),DELTAT,AK1,ALFA1
      COMMON /XXX/ X4,NA
      X(1)=BETA(I)
         CALL EIGF
      C(1)=1.
      D(1)=-(A(1)/A(2))*C(1)
         DEN1=A(2)*A(6)*A(9)-A(2)*A(5)*A(10)
      C(2)=(EIGEN(4)/DEN1)*C(1)
      D(2)=(EIGEN(2)/DEN1)*C(1)
         DEN2=DEN1*(A(17)*A(20)-A(19)*A(18))
      C(3)=(-EIGEN(4)*A(15)*A(20)-EIGEN(2)*A(16)*A(20))/DEN2
      D(3)=(EIGEN(4)*A(19)*A(15)+EIGEN(2)*A(19)*A(16))/DEN2
      BI(1)=(X2-X1)*H/AK1
      BI(2)=(X3-X2)*H/AK2
      BI(3)=(X4-X3)*H/AK3
         DNUM=Q/(H*(2.+BI(1)+BI(2)+BI(3)))
      TETA(1)=DNUM*(1.+BI(1)+BI(2)+BI(3))
      TETA(2)=DNUM*(1.+BI(2)+BI(3))
      TETA(3)=DNUM*(1.+BI(3))
      TETA(4)=DNUM
      AA(1)=-TETA(1)
      AA(2)=-TETA(2)-(X2+X1)*(TETA(2)-TETA(3))/(X3-X2)
      AA(3)=-TETA(3)-(X3+X1)*(TETA(3)-TETA(4))/(X4-X3)
      AB(1)=(TETA(1)-TETA(2))/(X2-X1)
      AB(2)=(TETA(2)-TETA(3))/(X3-X2)
      AB(3)=(TETA(3)-TETA(4))/(X4-X3)
      W(1)=SQRT(AK1/ALFA1)
      W(2)=SQRT(AK2/ALFA2)
      W(3)=SQRT(AK3/ALFA3)
      BN1=C(1)*D(1)*(COS(2.*X(1)*X1)-COS(2.*X(1)*X2))/(2.*X(1))
     1-(D(1)**2-C(1)**2)*(SIN(2.*X(1)*X2)-SIN(2.*X(1)*X1))/(4.*X(1))
     2+(C(1)**2+D(1)**2)*(X2-X1)/2.
      BN2=C(2)*D(2)*(COS(2.*X(2)*X2)-COS(2.*X(2)*X3))/(2.*X(2))
     1-(D(2)**2-C(2)**2)*(SIN(2.*X(2)*X3)-SIN(2.*X(2)*X2))/(4.*X(2))
```

```
2        +(C(2)**2+D(2)**2)*(X3-X2)/2.
         BN3=C(3)*D(3)*(COS(2.*X(3)*X3)-COS(2.*X(3)*X4))/(2.*X(3))
1        -(D(3)**2-C(3)**2)*(SIN(2.*X(3)*X4)-SIN(2.*X(3)*X3))/(4.*X(3))
2        +(C(3)**2+D(3)**2)*(X4-X3)/2.
         DBNN=(W(1)**2)*BN1+(W(2)**2)*BN2+(W(3)**2)*BN3
         AN11=AA(1)*(C(1)*(SIN(X(1)*X2)-SIN(X(1)*X1))/(X(1))
1        -D(1)*(COS(X(1)*X2)-COS(X(1)*X1))/(X(1)))
         AN12=AB(1)*(C(1)*((  X2*SIN(X(1)*X2)-X1*SIN(X(1)*X1))/(X(1))
1        +(COS(X(1)*X2)-COS(X(1)*X1))/(X(1)**2))+D(1)*((-X2*COS(X(1)*
2        X2)+X1*COS(X(1)*X1))/(X(1))+(SIN(X(1)*X2)-SIN(X(1)*X1))/(X(1)*
3        *2)))
         AN1=(AN11+AN12)*W(1)
         BN(1)=(AN1)/(DBNN)
         AN21=AA(2)*(C(2)*(SIN(X(2)*X3)-SIN(X(2)*X2))/(X(2))
1        -D(2)*(COS(X(2)*X3)-COS(X(2)*X2))/(X(2)))
         AN22=AB(2)*(C(2)*((+X3*SIN(X(2)*X3)-X2*SIN(X(2)*X2))/(X(2))
1        +(COS(X(2)*X3)-COS(X(2)*X2))/(X(2)**2))+D(2)*((-X3*COS(X(2)*
2        X3)+X2*COS(X(2)*X2))/(X(2))+(SIN(X(2)*X3)-SIN(X(2)*X2))/(X(2)*
3        *2)))
         AN2=(AN21+AN22)*W(2)
         BN(2)=(AN2)/(DBNN)
         AN31=AA(3)*(C(3)*(SIN(X(3)*X4)-SIN(X(3)*X3))/(X(3))
1        -D(3)*(COS(X(3)*X4)-COS(X(3)*X3))/(X(3)))
         AN32=AB(3)*(C(3)*((+X4*SIN(X(3)*X4)-X3*SIN(X(3)*X3))/(X(3))
1        +(COS(X(3)*X4)-COS(X(3)*X3))/(X(3)**2))+D(3)*((-X4*COS(X(3)*
2        X4)+X3*COS(X(3)*X3))/(X(3))+(SIN(X(3)*X4)-SIN(X(3)*X3))/(X(3)*
3        *2)))
         AN3=(AN31+AN32)*W(3)
         BN(3)=(AN3)/(DBNN)
         AN(I)=W(1)*BN(1)+W(2)*BN(2)+W(3)*BN(3)
         DN(I)=D(1)
         RETURN
         END
```

APPENDIX 2

DIMENSIONAL ANALYSIS

From Sections 4.2 and 4.3 it can be noted that T_{Is}, T_{IIs}, and ΔT depend upon the material and geometric properties of the laminate and the defect, and the thermal loading and environmental conditions. This may be expressed functionally as

$$T_{Is} = f_1(k_1,\alpha_1,\ell,h,q'',t,T_\infty) \qquad (2\text{-}1)$$

$$T_{IIs} = f_2(k_1,\alpha_1,k_2,\alpha_2,\ell,\ell_1,\ell_2,h,q'',t,T_\infty) \qquad (2\text{-}2)$$

$$\Delta T = |f_3(k_1,\alpha_1,k_2,\alpha_2,\ell,\ell_1,\ell_2,h,q'',t)| \qquad (2\text{-}3)$$

where $k_1 = k_3$ and $\alpha_1 = \alpha_3$ because the same material is above and below the flaw in the laminate. Because of the large number of parameters in eqns. (2-1), (2-2), and (2-3), it is very difficult to study the effect of each parameter on T_{Is}, T_{IIs}, and ΔT. Thus, the design of the "optimal" testing condition and the choice of the "best" liquid crystal system in relation to the parameters of the laminate, the flaw, and the environment are very complicated and, in fact, for many cases do not explicitly exist.

In order to address this difficulty, dimensional analysis is used to form a complete set of dimensionless groups all of which except one are independent. Fortunately in this case, the functional relation between the dependent dimensionless group and the independent groups is known. By putting the differential equations and the boundary conditions into a dimensionless form either by inspection or by a standard method [33],

a complete set of dimensionless groups can be obtained.

For the temperature response in Region I, a complete set of dimensionless groups is obtained by using eqns. (9) through (11) to give

$$Fo \equiv \alpha_1 t / \ell^2 \qquad (2\text{-}4)$$

$$Bi \equiv h\ell / k_1 \qquad (2\text{-}5)$$

$$\theta_{Is}^* \equiv k_1 (T_{Is} - T_\infty) / q''\ell \qquad (2\text{-}6)$$

where

$$\theta_{Is}^* = f_1 (Bi, Fo) \quad . \qquad (2\text{-}7)$$

The dimensionless group $\alpha_1 t / \ell^2$ is known as the Fourier number, Fo, and the group $h\ell / k_1$ is known as the Biot number, Bi.

For temperature response in Region II, a complete set of dimensionless groups is also obtained by using eqns. (45) through (49) as follows:

$$Fo \equiv \alpha_1 t / \ell^2 \qquad (2\text{-}8)$$

$$Bi \equiv h\ell / k_1 \qquad (2\text{-}9)$$

$$\theta_{IIs}^* \equiv k_1 (T_{IIs} - T_\infty) / q''\ell \qquad (2\text{-}10)$$

$$RK \equiv k_2 / k_1 \qquad (2\text{-}11)$$

$$RA \equiv \alpha_2 / \alpha_1 \qquad (2\text{-}12)$$

$$R1 \equiv \ell_1 / \ell \qquad (2\text{-}13)$$

$$R2 \equiv \ell_2 / \ell \qquad (2\text{-}14)$$

where

$$\theta_{IIs}^* = f_2 (Bi, Fo, RK, RA, R1, R2) \quad . \qquad (2\text{-}15)$$

The dependent dimensionless group is defined as

$$\Delta\theta^* = \left| \theta_{Is}^* - \theta_{IIs}^* \right| = \left| f_3'(Bi, Fo, RK, RA, R1, R2) \right| \qquad (2\text{-}16)$$

which reduces to

$$\Delta\theta^* = k_1 \Delta T / q'' \ell \quad . \qquad (2\text{-}17)$$

The dimensionless temperatures are θ_{Is}^*, θ_{IIs}^*, and $\Delta\theta^*$.

APPENDIX 3

DATA CURVES

In this appendix, various sets of data curves are presented. These curves should assist in the design of thermal testing conditions and in the choice of a liquid crystal system for most practical situations. Specific sets of data are plotted for all combinations of the following values for Bi and RK:

$$Bi = 0.03, 0.08, 0.2, 0.5$$

$$RK = 0.08, 0.2, 0.5$$

$$RA = 110$$

Figure showing T^*_{IIs} versus Fo for $B1 = .03$, $RK = .2$, with curves labeled by $(R1, R2)$: $(.05, .45)$, $(.15, .45)$, $(.25, .45)$, $(.05, .25)$, $(.15, .25)$, $(.25, .25)$, $(.05, .05)$, $(.15, .05)$, $(.25, .05)$.

B1 = .08
RK = .2
(R1,R2)

(.05,.05)
(.15,.05)
(.25,.05)

(.15,.25)

(.05,.25)
(.25,.25)

(.05,.45)
(.15,.45)
(.25,.45)

T^*_{IIs}

Fo

B1 = .08
RK = .5
(R1,R2)

(.05,.45)
(.15,.45)
(.25,.45)

(.05,.25)
(.15,.25)
(.25,.25)

(.05,.05)
(.15,.05)
(.25,.05)

ΔT*

Fo

B1 = .20
RK = .08
(R1,R2)

(.05,.45)

(.15,.45)

(.25,.45)

(.05,.25)
(.15,.25)
(.25,.25)

(.05,.05)
(.15,.05)
(.25,.05)

ΔT*

Fo

The graph shows curves with labels:

(.05,.45)
(.15,.45)
(.25,.45)

(.05,.25)
(.15,.25)
(.25,.25)

(.05,.05)
(.15,.05)
(.25,.05)

B1 = .20
RK = .08
(R1,R2)

Y-axis: T^*_{IIs} with values 0.0, 0.5, 1.0, 1.5, 2.0, 2.5, 3.0, 3.5

X-axis: Fo with values 0, 1, 2, 3, 4, 5, 6, 7, 8, 9, 10

B1 = .2
RK = .2
(R1,R2)

B1 = .2
RK = .5
(R1,R2)

(.05,.45)
(.15,.45)
(.25,.45)

(.05,.25)
(.15,.25)
(.25,.25)

(.05,.05)
(.15,.05)
(.25,.05)

ΔT*

F₀

B1 = .5
RK = .08
(R1,R2)

(.05,.45)
(.15,.45)
(.25,.45)

(.05,.25)
(.15,.25)
(.25,.25)

(.05,.05)
(.15,.05)
(.25,.05)

Fo

ΔT*

B1 = .5
RK = .08
(R1,R2)

Fo

T^*_{IIs}

(.05,.25)
(.15,.25)
(.25,.25)

(.05,.05)
(.15,.05)
(.25,.05)

(.05,.45)
(.15,.45)
(.25,.45)

B1 = .5
RK = .2
(R1,R2)

(.05,.45)
(.15,.45)
(.25,.45)

(.05,.25)
(.15,.25)
(.25,.25)

(.05,.05)
(.15,.05)
(.25,.05)

Fo

ΔT*

B1 = .5
RK = .2
(R1,R2)

(.05,.25)
(.15,.25)
(.25,.25)

(.05,.45)
(.15,.45)
(.25,.45)

(.05,.05)
(.15,.05)
(.25,.05)

T^*_{IIs}

Fo

Axis labels: Fo (horizontal axis), T^*_{IIs} (vertical axis)

Curve labels:
(.05,.45)
(.15,.45)
(.25,.45)

(.05,.25)
(.15,.25)
(.25,.25)

(.05,.05)
(.15,.05)
(.25,.05)

B1 = .5
RK = .5
(R1,R2)

PART II

THERMAL NONDESTRUCTIVE TESTING OF FIBERGLASS

LAMINATE CONTAINING SIMULATED FLAWS ORTHOGONAL

TO SURFACE USING LIQUID CRYSTALS

Samson S. Lee

James H. Williams, Jr.

ABSTRACT

Thermal nondestructive testing relies on the perturbation of heat flow
by the presence of flaws in a structure. The resultant surface tem-
perature anomaly may be revealed by a temperature-indicating cholesteric
liquid crystal coating applied to the surface of the structure.

A fiberglass laminate with simulated flaws orthogonal to the surface
was thermally tested using liquid crystals. Quartz-iodine lamps were
used as radiant heat sources. Thermographs were obtained from the test
and the flaws were detected at various degrees of "effectiveness".
The lateral heat flow above the flaw was found to be important for the
range of flaw sizes tested.

Various plots presenting the sensitivity and effectiveness of the
liquid crystal thermal nondestructive testing system are presented.

INTRODUCTION

Thermal nondestructive testing is a technique for detecting variations
in the thermal properties of a test structure and analyzing the resulting
thermal information to predict the presence and nature of defects in the
structure. If an external heat flux is suddenly imposed on a structure
containing a defect, the defect having different thermal properties com-
pared to those of the structure, will alter the heat flow pattern. If
the heat flow is altered sufficiently, a temperature distribution pro-
file anomaly will appear on the surface of the structure. In addition to
indicating the presence of the flaw, the details of such a temperature
anomaly may reveal some of the quantitative features of the flaw.

One inexpensive nondestructive evaluation technique is thermal test-
ing with cholesteric liquid crystals which are applied to the surface of
the test structure to reveal surface temperature distribution profiles.
Liquid crystals are grease-like chemical compounds that appear to change
color according to temperature [1].

Industrial investigations into the feasibility of using liquid
crystals in thermal testing can be dated back more than 15 years [2].
Major advantages of thermal nondestructive testing with liquid crystals
are its low cost and ease of application. The heat source can be a
simple photo lamp and the cost of liquid crystals has been estimated to
be approximately $1.00 per square meter [3]. Because an entire surface
can be tested and its surface temperature distribution observed in vivid
colors by the unaided eye in real time, the test is simple and requires

little personnel training to detect the presence of flaws.

Recent work by Mansouri et al. [4] established analytical bases for thermal nondestructive testing. If the lateral dimensions of an inclusion defect are much larger than the thickness of the test panel, a one-dimensional heat transfer analysis by Williams et al. [5] can predict the surface temperature distribution generated on the structure during thermal testing. Experimental results support this analysis [6]. The analysis is useful for planning thermal nondestructive tests and for the quantitative interpretation of the test results.

However, the heat transfer problem is more difficult if the lateral dimensions of the defect are not large compared to the thickness of the test structure. In this case, lateral heat flow cannot be ignored so the heat transfer solution requires numerical computations. This category of defects can be important and includes cracks orthogonal to the surface of the structure. This report presents the results of an experimental investigation of the effectiveness of liquid crystals in the thermal nondestructive testing of simulated cracks in fiberglass laminates.

EXPERIMENTS

A 23cm x 23cm panel of multiple-ply symmetric fiberglass composite was fabricated by laminating 50 prepreg sheets of unidirectional 3M Type 1002 fiberglass in an alternating fashion of 0°, ±45° and 90° to a total thickness of 1.27cm. The fiberglass panel was manufactured in a hot press according to 3M instructions. Cracks of various sizes were simulated by diamond-saw cuts of various widths and depths. A schematic of the test panel is shown in Fig. 1 and the detailed dimensions are shown in Fig. 2. As illustrated in Fig. 3, a typical flaw in the fiber-glass panel of thickness ℓ is a cut characterized by a width w and a depth d from the surface of the panel. The liquid crystals blend and the thermal testing procedure were similar to that used by Williams et al [6].

The liquid crystals blend was supplied in aerosol cans by Liquid Crystal Biosystem, Inc. The volume of the contents which was liquid crystals was 10%, the remainder of the fluid being a carrier. The blend reflected the entire color spectrum from red to violet with a color transition temperature of 32.7°C and a color-play range of 3.7°C. Fig. 4 shows the supplier-provided calibration curve for this liquid crystals blend [7]. The relative intensity of reflected light and the corre-sponding colors are plotted versus temperature for various wavelengths. Also, the ranges of temperatures which correspond to the various colors are listed.

The fiberglass test panel as produced was translucent. Thus, the thermographic images were enhanced by blackening the test surface prior

to the application of the liquid crystals. The surface of the laminate was cleaned and then painted with a can of Krylon ultra-flat black spray paint. The black paint was left to dry completely before applying the liquid crystals. Special care was taken to ensure the proper application of the liquid crystals as a nonuniform coating may generate an irregular color pattern even in the absence of a subsurface anomaly. The coating thickness was judged by eye and was found to be adequate if the entire surface of the panel appeared uniformly glossy when viewed obliquely. The best results were obtained when two or three coats of spray, having a total thickness of about 0.02mm, were applied uniformly over the entire surface. The surface was not allowed to dry between successive coats. Because of the degradation of the liquid crystals in the air, the laminate was always tested within a few hours of the application of the liquid crystals.

The test panel was mounted as shown in Fig. 5, which is a schematic of the entire test system. It was heated suddenly by a radiant heating unit consisting of photographic lights. Two 1,000watt quartz-iodine lamps with high-efficiency reflectors (Smith-Victor Model 750/1,000watt) were placed approximately 1m in front of the test panel. The units provided broad flat illumination capable of uniform heating of the entire panel surface. The lamps were geometrically arranged to irradiate the panel uniformly with the light beams incident on the panel at approximately 30°.

The photographic equipment was comprised of a 35mm single-lens reflex Nikon FM chrome camera body with a 135mm f/2.8 Auto Promaster

lens. The camera was located approximately 1.5m in front of the test panel, with the axis of the camera perpendicular to the face of the test panel. No optical filter was used for either lighting or photography. The same quartz-iodine lamps were employed for both heating and photography. Kodacolor II C-135 (ASA 100) color film was used.

After establishing uniform irradiation from the lamps and recording the room temperature, the test laminate was mounted on the test stand. The quartz-iodine lamps were turned on and a stopwatch was started. The panel was observed as the thermographic images developed as the surface temperature passed through the color-play range of the liquid crystals blend. At various intervals, photographs of the color images representing the surface temperature distribution of the laminate were taken, with the camera aperture and exposure time set according to the built-in light meter in the camera. The time on the stopwatch corresponding to each photograph was also recorded. Subsequent tests were conducted after the lamps were turned off and the panel cooled to the ambient temperature.

Above its transition temperature, the liquid crystals appeared wet, sometimes causing excessive glare. Most of this glare was eliminated by adjusting the position of the lamps without affecting the uniformity of the panel irradiation. While the remaining glare had negligible effect on the visual interpretation of the thermic patterns, this glare appears as whitish specks in the thermographs. (This should be kept in mind when viewing the thermographs in the next section.)

RESULTS AND DISCUSSIONS

The thermal testing of the fiberglass panel containing the flaws orthogonal to the surface was conducted at a room temperature T_∞ of 21.5°C. A typical sequence of thermographs of the surface temperature distributions is shown in Figs. 6 to 9 obtained at 2 min – 40 sec, 3 min – 35 sec, 5 min – 23 sec, and 7 min – 17 sec, from the initiation of the test, respectively. (The lower left-hand corner of the thermograph corresponds to the lower left-hand corner of the test panel as shown in Fig. 1.) All the flaws except those with a depth d of 0.76cm and 1.02cm can be detected to various degrees of "effectiveness" other than "unacceptable" as defined in [6].

Some useful nondimensional parameters were defined in [5] as follows:

$$T^*_{IS} = \frac{k(T_{IS} - T_\infty)}{q'' \ell} \tag{1}$$

$$T^*_{IIS} = \frac{k(T_{IIS} - T_\infty)}{q'' \ell} \tag{2}$$

$$Bi = \frac{h\ell}{k} \tag{3}$$

and

$$Fo = \frac{\alpha t}{\ell^2} \tag{4}$$

where Bi is the Biot number, Fo is the Fourier number, T_{IS}(°K) is the surface temperature over the unflawed region, T_{IIS}(°K) is the surface temperature over the flawed region, t(sec) is time, q" is the externally applied net uniform heat flux, h is the convection heat transfer coefficient and is taken to be 8.57 w/m^2 °K for natural convection, k is the thermal conductivity of fiberglass and is taken to be 0.338 w/m°K, and α is the thermal diffusivity of fiberglass and is taken to be 2.14 x 10^{-7} m^2/sec.

The surface temperature over the unflawed region of a uniform panel has been computed for various values of Bi [5]. According to eqn. (3), a fiberglass panel of 1.27cm thickness has a Bi of 0.32. The analytically predicted surface temperature over such an unflawed panel is represented by the line in Fig. 10. Considering regions far from any flaw as the unflawed regions of the test panel, the measured surface temperature should correspond to the curve in Fig. 10. By matching the measured nondimensional temperature T_{IS}^* with the analytically predicted curve, an estimate of the average value of the applied heat flux can be obtained. From three temperature data points, the value of q" is calculated to be about 940w/m^2. This average value of the heat flux places the three temperature data points close to the theoretical curve as shown in Fig. 10.

After establishing the magnitude of the externally applied net heat flux, the experimental data for surface temperatures above the flaws can be presented in the nondimensional form of T_{IIS}^*. Fig. 11 shows the nondimensional surface temperature for flaws of the same depth d but of

various widths w. Fig. 12 shows the nondimensional surface temperature

for flaws of the same width w but of various depths d. Also, shown in

Figs. 11 and 12 is the analytical curve for the surface temperature

T^*_{IS} over the unflawed region. The temperatures corresponding to flaws

with a narrower width and/or a deeper depth are generally closer to the

curve, thus indicating a smaller temperature difference $(T^*_{IIS} - T^*_{IS})$

and, therefore, less system effectiveness in the detection of these

flaws. Note that the flaws of depth 0.76cm and 1.02cm cannot be

detected with this test system configuration.

To observe the importance of lateral heat flow above the flaws,

the nondimensional surface temperature over the flaw is recomputed

based on a characteristic length of d in the parameters T^*_{IIS} and Fo.

The data are shown in Fig. 13 along with theoretical curves for tem-

peratures over unflawed regions of panels of thicknesses d (Bi = 0.064)

and ℓ(Bi = 0.32). If no lateral heat flow occurred, the material

above the flaw of depth d would behave like an unflawed uniform panel

of thickness d and the data points would stay close to the curve of

Bi = 0.064. As shown in Fig. 13, the data points instead stay close

to the curve of Bi = 0.32. Thus, lateral heat flow above the flaws

appears to be important.

An interesting observation is obtained by presenting the non-

dimensional data based on a characteristic length d as shown in

Figs. 14 and 15. (That is, the ℓ's in eqns. (2) and (4) are replaced

by d for Figs. 14 and 15.) The results from each flaw tend to

exhibit a linear behavior when the Fourier number is plotted on a

logarithmic scale. Whereas the data points tend to bunch together in Fig. 14, the data points in Fig. 15 clearly show this behavior.

The maximum number of color differences in the color spectrum of the liquid crystals over flawed and unflawed regions can be obtained directly from the individual thermographs. The significance of the maximum number of color differences is associated with the definitions of the degrees of effectiveness of liquid crystal thermal testing [6]. The "effectiveness" of a test with maximum numbers of color differences of 0 to 1, 1 to 2, 2 to 6, and above 6 is called "unacceptable", "limiting", "moderately acceptable", and "acceptable", respectively. Fig. 16 shows the maximum number of color differences for flaws of the same depth (d = 0.25cm) versus the width of the flaw plotted on a logarithmic scale. A straight line fits the data well. Similarly, Fig. 17 shows the maximum number of color differences for flaws of the same width (w = 0.25cm) versus the depth of the flaw plotted on a logarithmic scale. A straight line of negative slope fits these data well. Flaws with a width of 0.25cm and a depth greater than approximately 0.8cm fall on the vertical axis of the graph. In Fig. 18, the data from Figs. 16 and 17 are plotted together versus the width to depth ratios of the flaws on a logarithmic scale. A single straight line fits both sets of data. Figs. 16, 17 and 18 describe the sensitivity of the test system in detecting flaws orthogonal to the surface of the structure. The "effectiveness" classifications are indicated also.

Another way of presenting the sensitivity and "effectiveness"
classifications of the test system is to show the same data in a
contour plot as shown in Fig. 19. The vertical axis and the horizontal
axis represent the ratios of width and depth of the flaw to the thick-
ness of the test panel, respectively. The maximum number of color
differences is labelled inside the circles along the dotted-line con-
tours. These contours represent loci of constant maximum number of
color differences between flawed and unflawed regions. Thus, the
contours represent the sensitivity or effectiveness of the test
system.

CONCLUSIONS

Experimental investigations of thermal nondestructive testing using liquid crystals on a fiberglass panel containing simulated flaws orthogonal to the surface as shown in Figs. 1 and 2 have been performed. Some sequential thermographs are presented in Figs. 6 through 9. For a 32.7°C - 36.4°C liquid crystals color-play range and an external heat flux of 940w/m^2, various degrees of "effectiveness" of the thermal test in detecting the flaws as defined in [6] have been observed at a room temperature of 21.5°C. The heat flux was actually determined indirectly through back calculations by requiring regions far from the flaws to have a surface temperature corresponding to the temperature calculated in [5] for an unflawed panel of the same thickness.

As shown in Figs. 11 and 12, relatively narrow flaws and relatively deep flaws were found to result in a surface temperature close to that over the unflawed region making flaw detection more difficult. Further, it was concluded that lateral heat flow above a flaw of the size range considered can be important. The Fourier number and the nondimensional surface temperature in the flawed region, if both were computed on the basis of a characteristic length of d, were found to correlate as shown in Figs. 14 and 15.

The "effectiveness" of thermal nondestructive testing using liquid crystals depends on the maximum number of color differences between the flawed and unflawed regions. The maximum number of color differences was found to correlate with the width, the depth, and

the width to depth ratios of the flaws as shown in Figs. 16, 17 and 18, respectively. The effectiveness of the liquid crystal thermal non-destructive test system was further demonstrated in a contour plot of constant maximum number of color difference between the flawed and un-flawed regions as shown in Fig. 19. Figs. 16 to 19 give directly the sensitivity and effectiveness of this particular test system consisting of liquid crystals and the external heat flux in detecting flaws orthogonal to the surface of the fiberglass test panel. So, the fiber-glass panel can be considered as a simple "calibration block" that can be used to generate effectiveness plots for a range of liquid crystals thermal nondestructive testing systems.

REFERENCES

1. J.L. Fergason, "Liquid Crystals", Scientific American, Vol. 211, No. 2, August 1964, pp. 77-85.

2. W.E. Woodmansee, "Cholesteric Liquid Crystals and Their Application to Thermal Nondestructive Testing", Materials Evaluation, October 1966, pp. 564-572.

3. R.E. Engelhardt and W.A. Hewgley, "Thermal and Infrared Testing", Chapter 6 in Nondestructive Testing, A Survey, NASA SP-5113, Washington, D.C., 1973.

4. S.H. Mansouri, J.H. Williams, Jr., and S.S. Lee, "Nondestructive Detection of Delaminations and Inclusions in Fiberglass Laminates Using Liquid Crystals", M.I.T. Sea Grant Program (DOC-NOAA), July 1979. MITSG 81-16, Part I .

5. J.H. Williams, Jr., S.H. Mansouri and S.S. Lee, "One-dimensional Analysis of Thermal Nondestructive Detection of Delamination and Inclusion Flaws", British Journal of NDT, May 1980, pp. 113-118.

6. J.H. Williams, Jr., S.H. Mansouri and S.S. Lee, "Thermal Nondestructive Testing of Fiberglass Laminates Using Liquid Crystals", (accepted for publication by the British Journal of NDT).

7. LixKit Information Sheet, Liquid Crystal Biosystems, Inc., 26101 Miles Avenue, Cleveland, Ohio 44128.

ACKNOWLEDGMENTS

The M.I.T. Sea Grant Program (DOC-NOAA) is gratefully acknowledged for its support of this research.
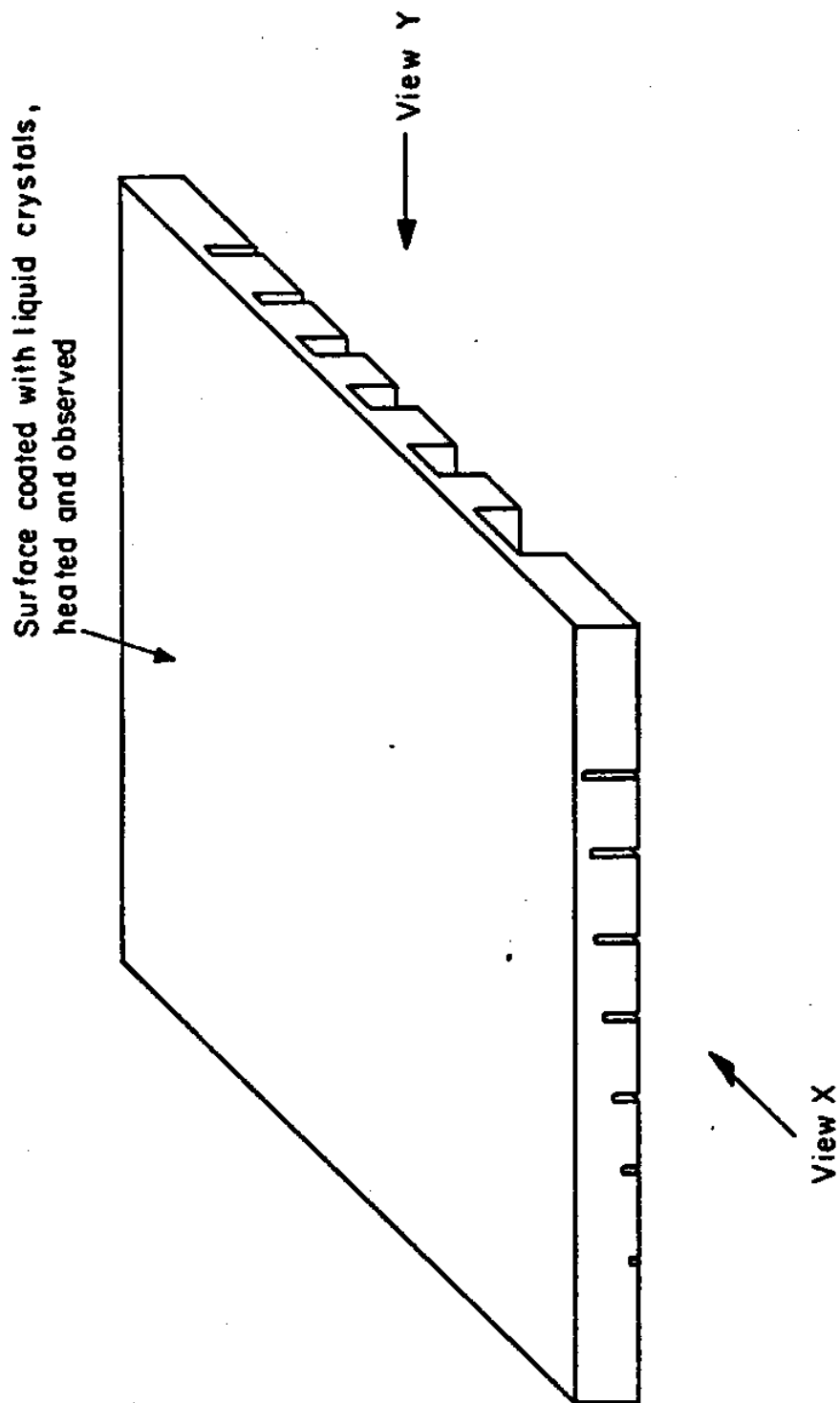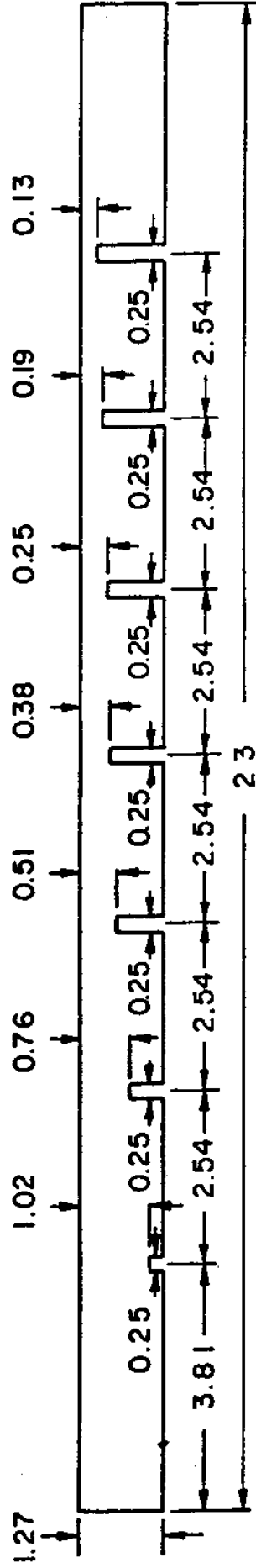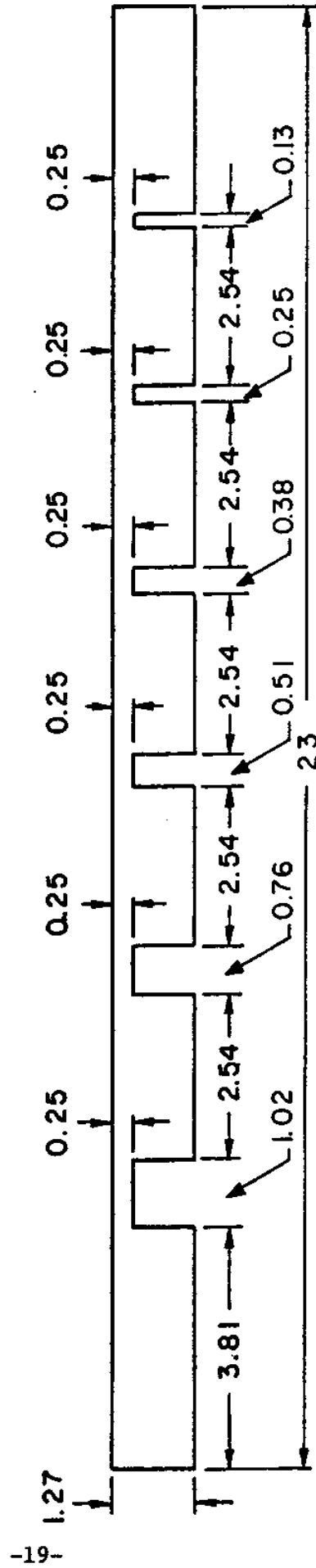
Fig. 1   Schematic of fiberglass test panel containing simulated flaws orthogonal to the surface. (Edgeviews X and Y are shown with dimensions in Fig. 2.)
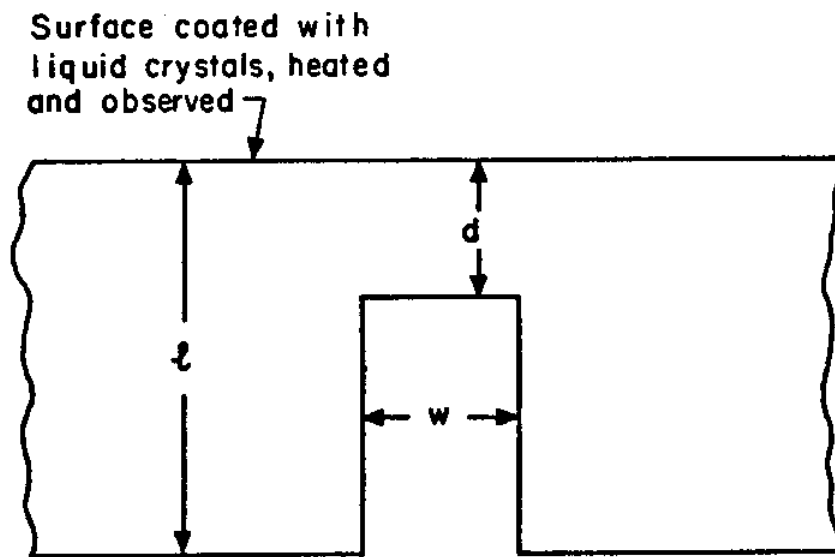
Fig. 2   Edgeviews of fiberglass test panel.

Fig. 3   Schematic of a typical flaw having a width w and a depth d in the fiberglass test panel of thickness ℓ.
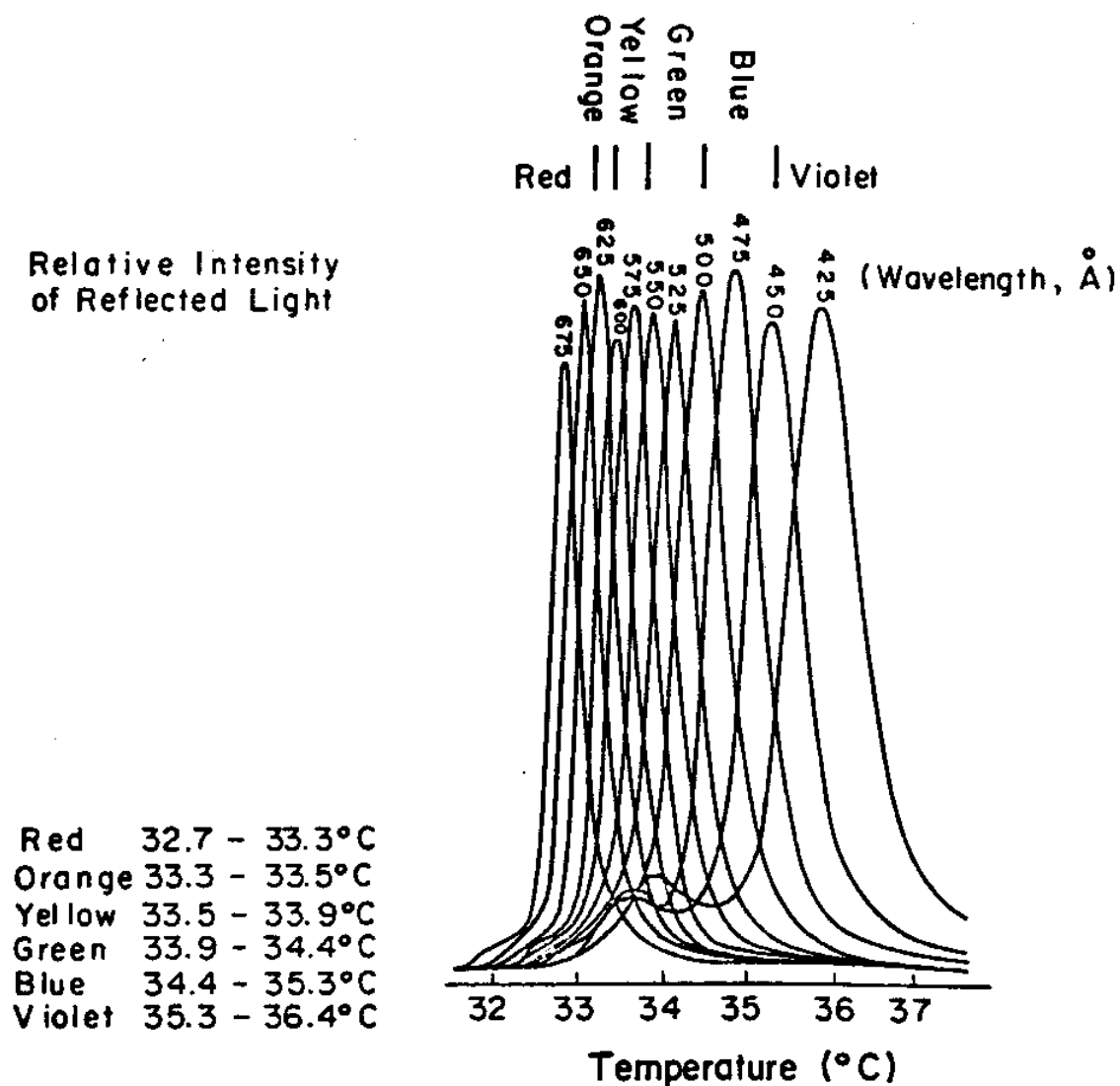
Fig. 4   Calibration of liquid crystals system with color-play range of 3.7°C from 32.7°C to 36.4°C.
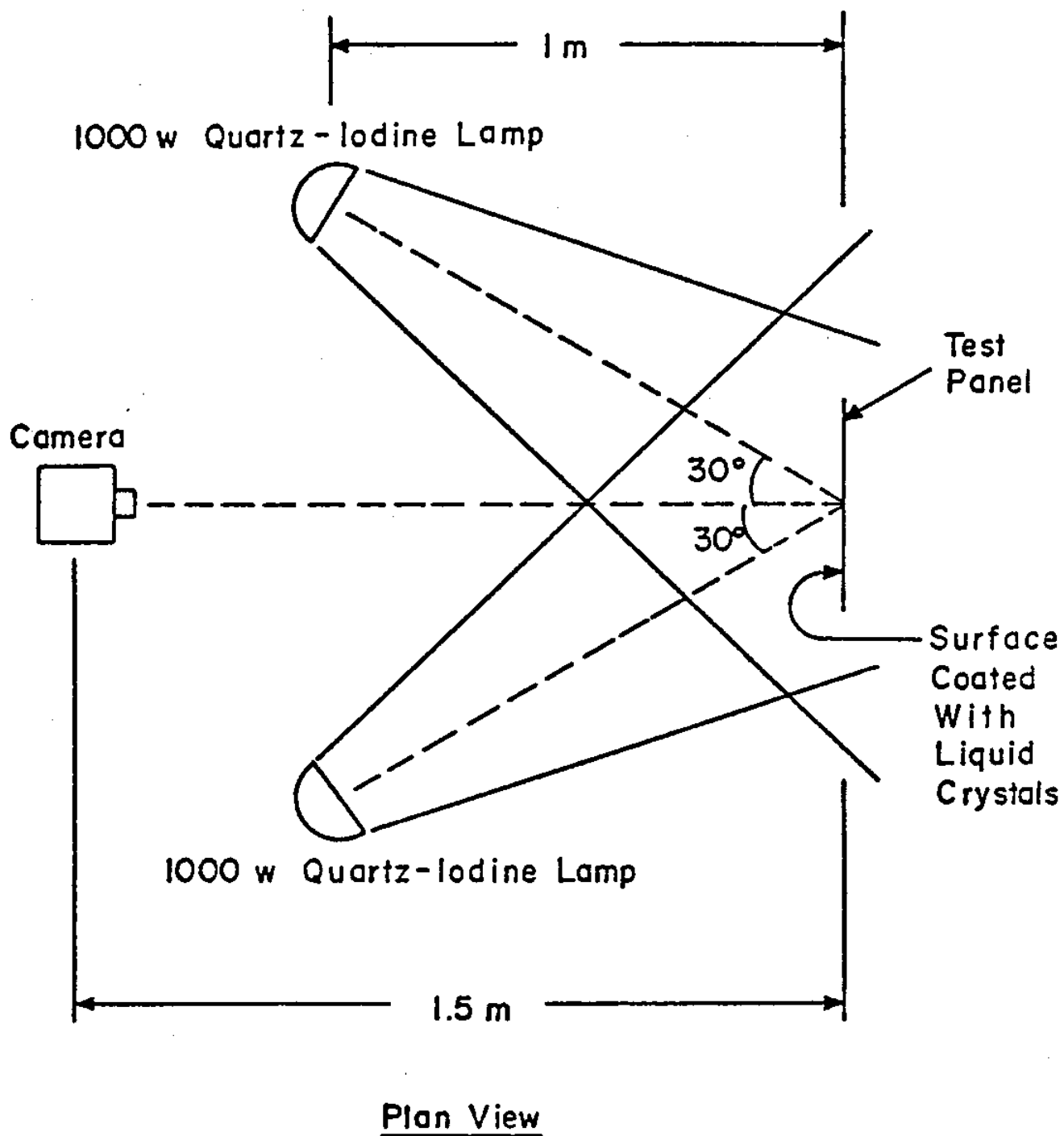
Fig. 5   Schematic of experimental system for thermal nondestructive testing of fiberglass panels using liquid crystals.
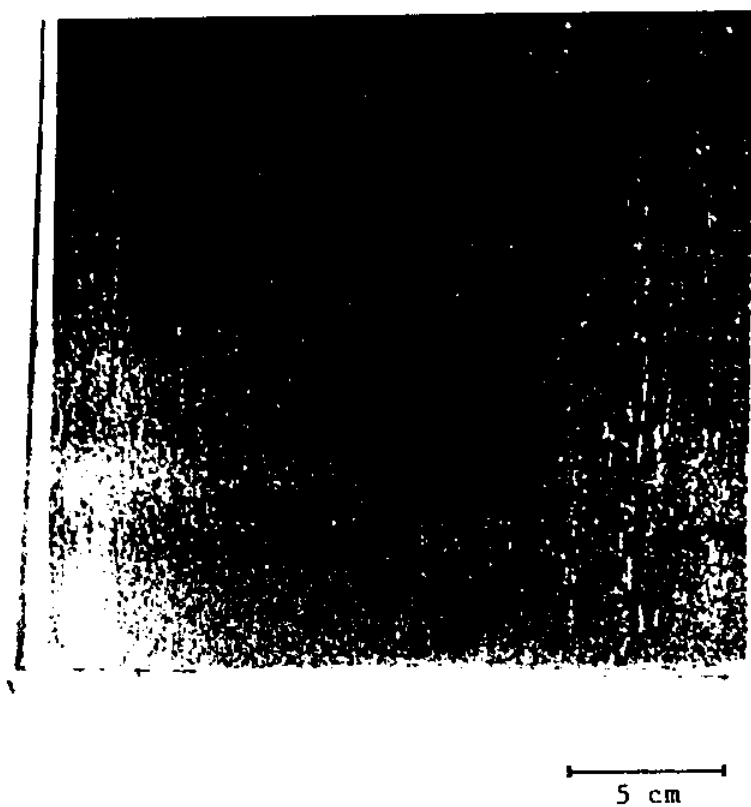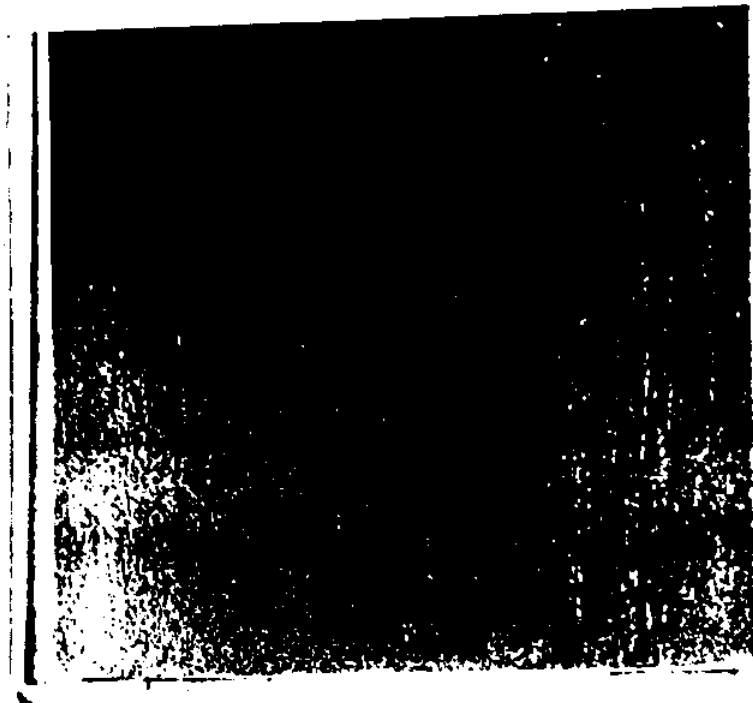
Fig. 6   Thermograph of fiberglass test panel obtained at 2 min - 40 sec from initiation of test.

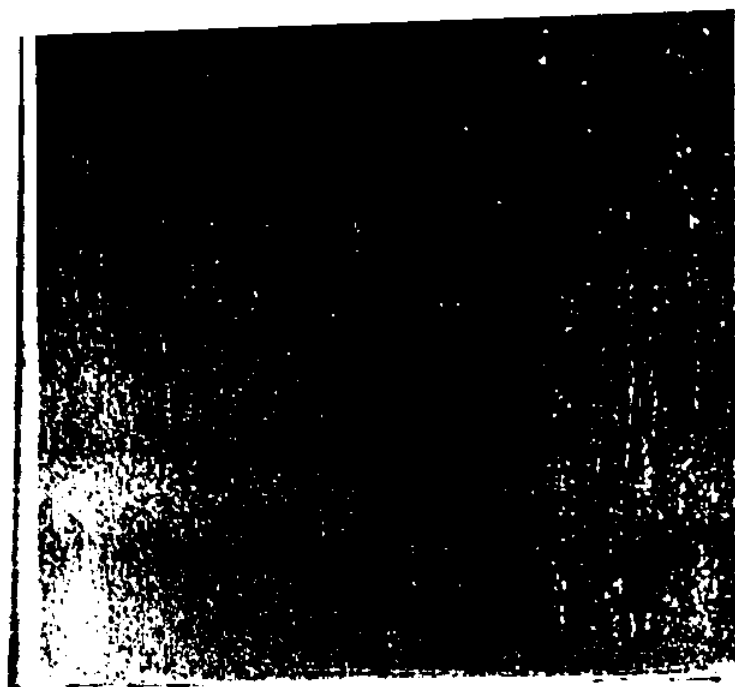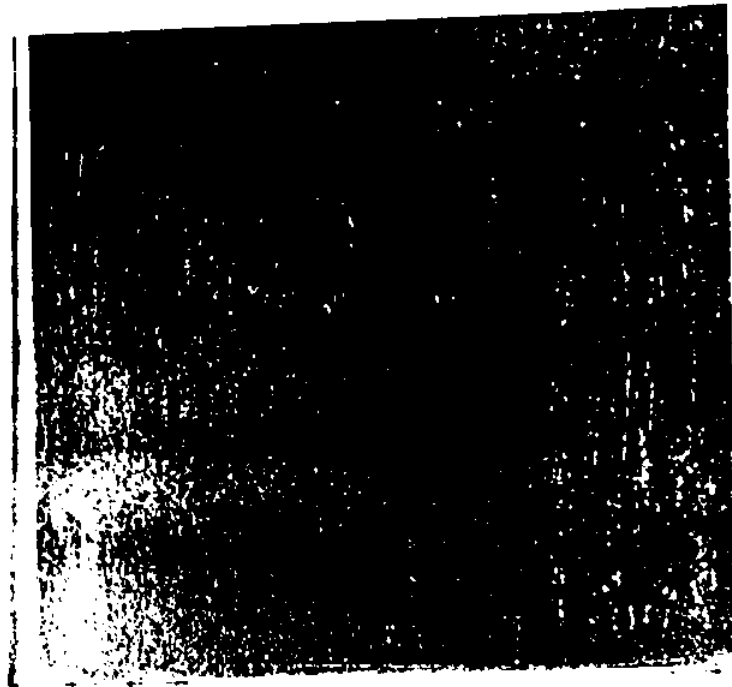Fig. 7   Thermograph of fiberglass test panel obtained at 3 min - 35 sec from initiation of test.

Fig. 8   Thermograph of fiberglass test panel obtained at 5 min - 23 sec from initiation of test.

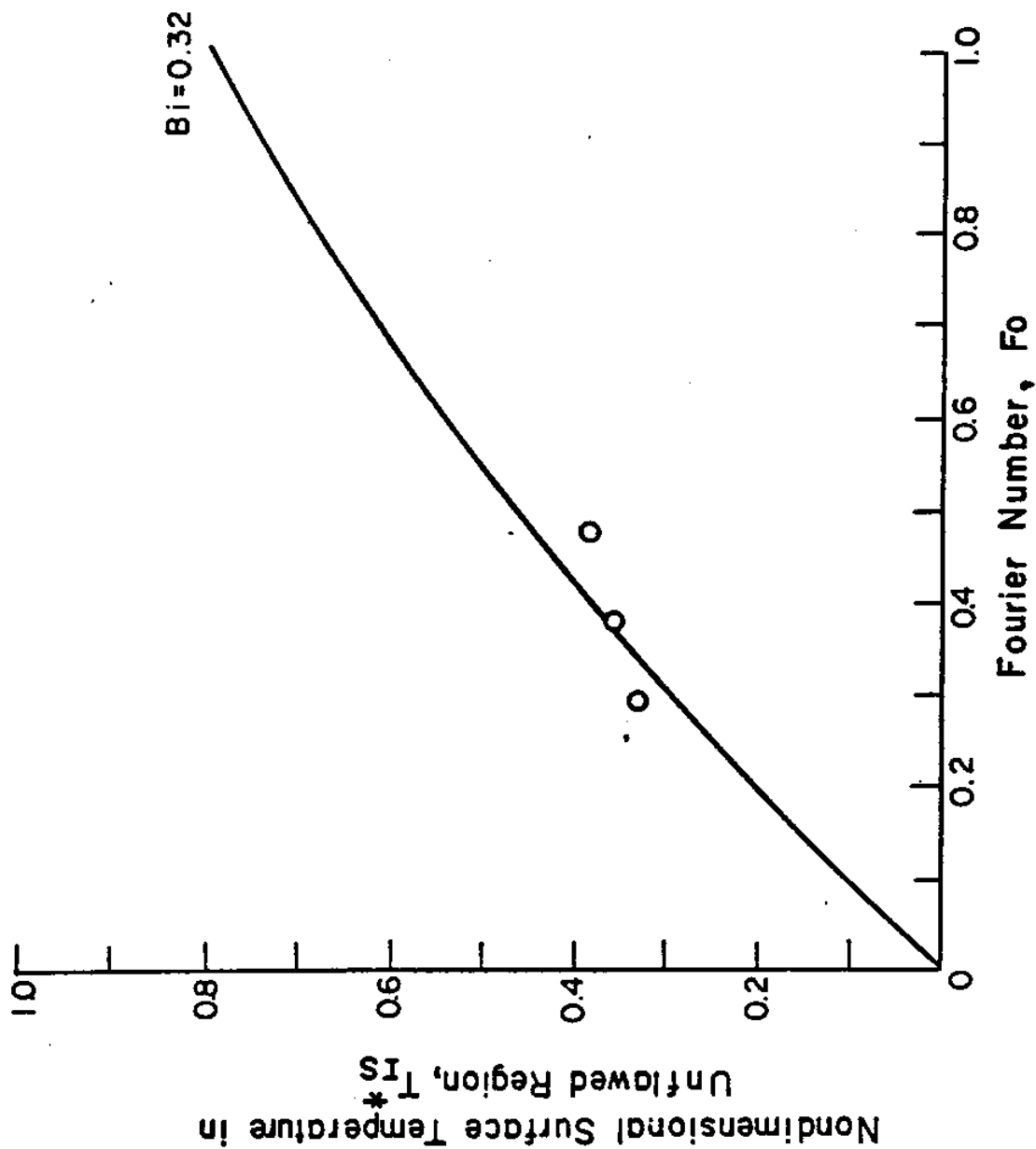Fig. 9   Thermograph of fiberglass test panel obtained at 7 min - 17 sec from initiation of test.

Fig. 10   Theoretical nondimensional surface temperature in unflawed region and three experimental data points which are based on $q'' = 940w/m^2$.

Fig. 11   Experimental nondimensional surface temperature T^*_{IIS} above flaws of same depth d. (Theoretical nondimensional surface temperature T^*_{IS} in the unflawed region is shown for comparison.)

Fig. 12   Experimental nondimensional surface temperature T^*_{IIS} above flaws of same width w. (Theoretical nondimensional surface temperature T^*_{IS} in the unflawed region is shown for comparison.)
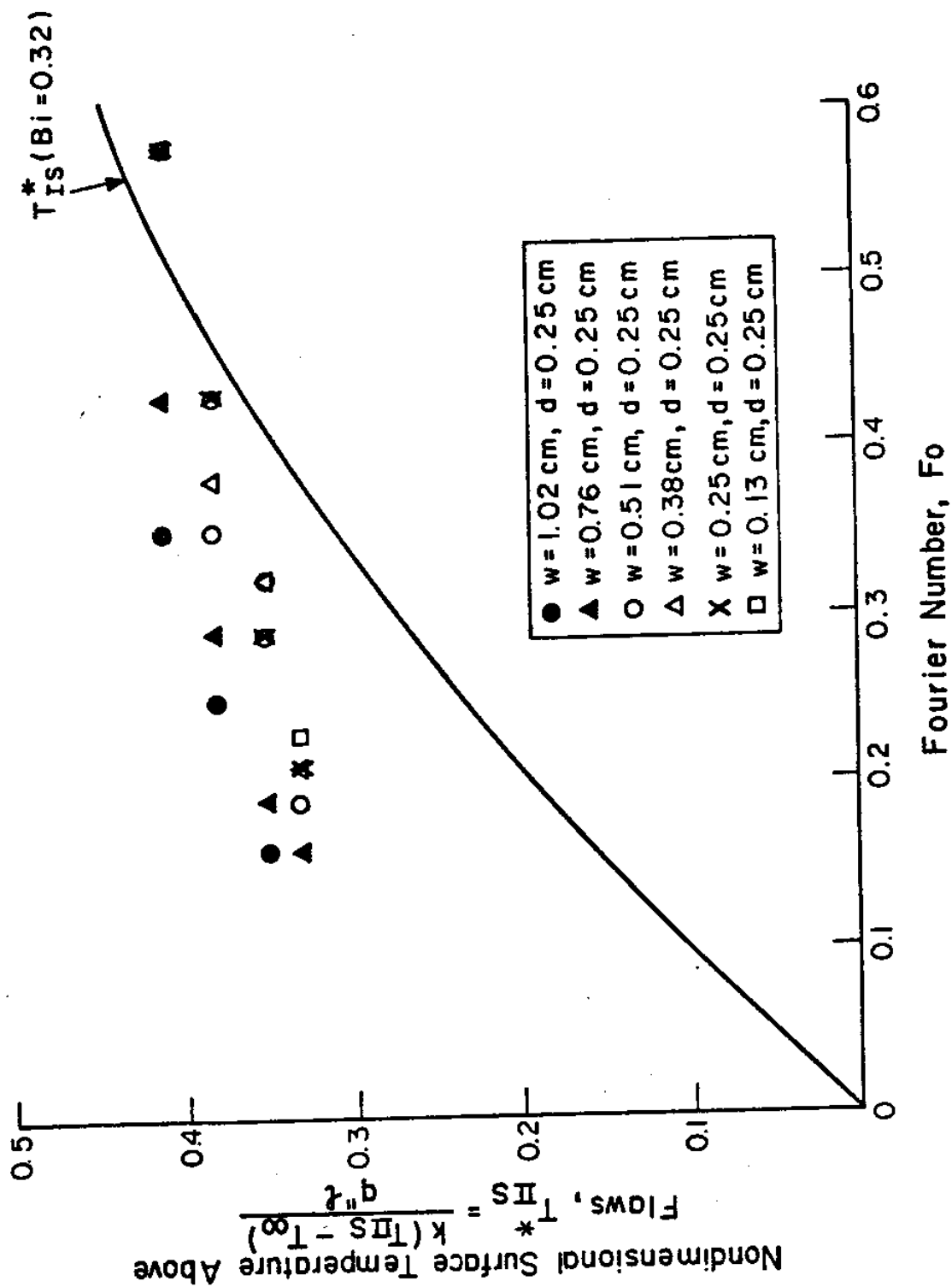
Fig. 13   Experimental nondimensional surface temperature T^*_{IIS} above flaws of same depth d. (Theoretical nondimensional surface temperature T^*_{IS} in the unflawed region for $\ell = 0.25cm$ (Bi = 0.064) and $\ell = 1.27cm$ (Bi = 0.32) are shown also.)

Surface coated with liquid crystals, heated and observed

View Y

View X

Fig. 1   Schematic of fiberglass test panel containing simulated flaws orthogonal to the surface. (Edgeviews X and Y are shown with dimensions in Fig. 2.)

View X

View Y

(All Dimensions in centimeters)

Fig. 2   Edgeviews of fiberglass test panel.

Surface coated with
liquid crystals, heated
and observed

Fig. 3   Schematic of a typical flaw having a width w and a depth d
in the fiberglass test panel of thickness ℓ.

Fig. 4   Calibration of liquid crystals system with color-play range
         of 3.7°C from 32.7°C to 36.4°C.

Fig. 5 Schematic of experimental system for thermal nondestructive testing of fiberglass panels using liquid crystals.

5 cm

Fig. 6   Thermograph of fiberglass test panel obtained at
2 min – 40 sec from initiation of test.

5 cm

Fig. 7   Thermograph of fiberglass test panel obtained at
3 min - 35 sec from initiation of test.

5 cm

Fig. 8   Thermograph of fiberglass test panel obtained at
5 min – 23 sec from initiation of test.

5 cm

Fig. 9   Thermograph of fiberglass test panel obtained at
7 min - 17 sec from initiation of test.

Fig. 10   Theoretical nondimensional surface temperature in unflawed region and three experimental data points which are based on q" = 940w/m².

Fig. 11 Experimental nondimensional surface temperature T^*_{IIS} above flaws of same depth d. (Theoretical nondimensional surface temperature T^*_{IS} in the unflawed region is shown for comparison.)

Fig. 12 Experimental nondimensional surface temperature T^*_{IIS} above flaws of same width w. (Theoretical nondimensional surface temperature T^*_{IS} in the unflawed region is shown for comparison.)

Fig. 13 Experimental nondimensional surface temperature T_{IIS}^* above flaws of same depth d. (Theoretical nondimensional surface temperature T_{IS}^* in the unflawed region for $\ell = 0.25$ cm ($Bi = 0.064$) and $\ell = 1.27$ cm ($Bi = 0.32$) are shown also.)

Fig. 14   Experimental nondimensional surface temperature T^*_{IIS} above flaws of the same depth d, where T^*_{IIS} and Fo are based on length d.
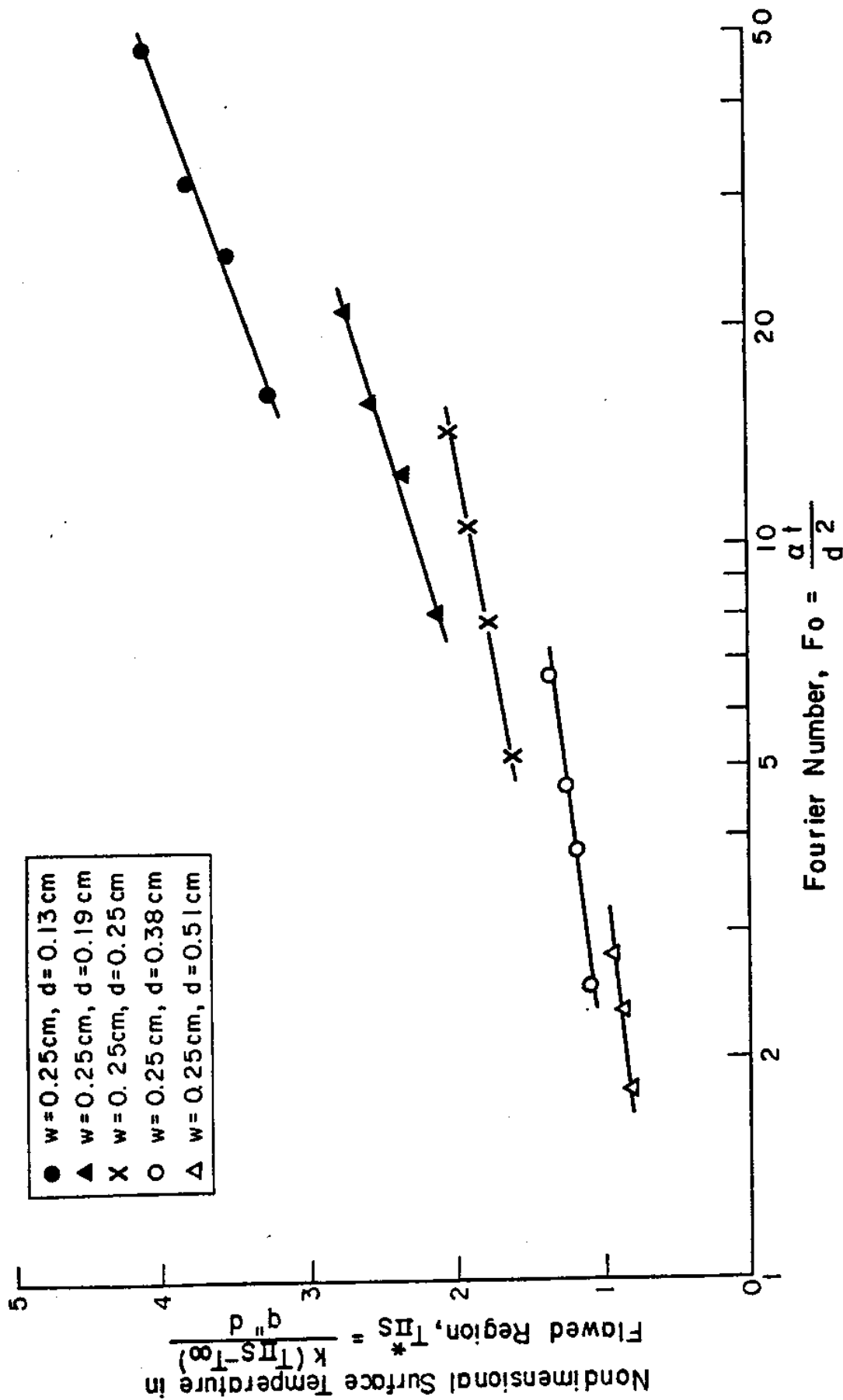
Fig. 15 Experimental nondimensional surface temperature T^*_{IIS} above flaws of same width w, where T^*_{IIS} and Fo are based on length d.
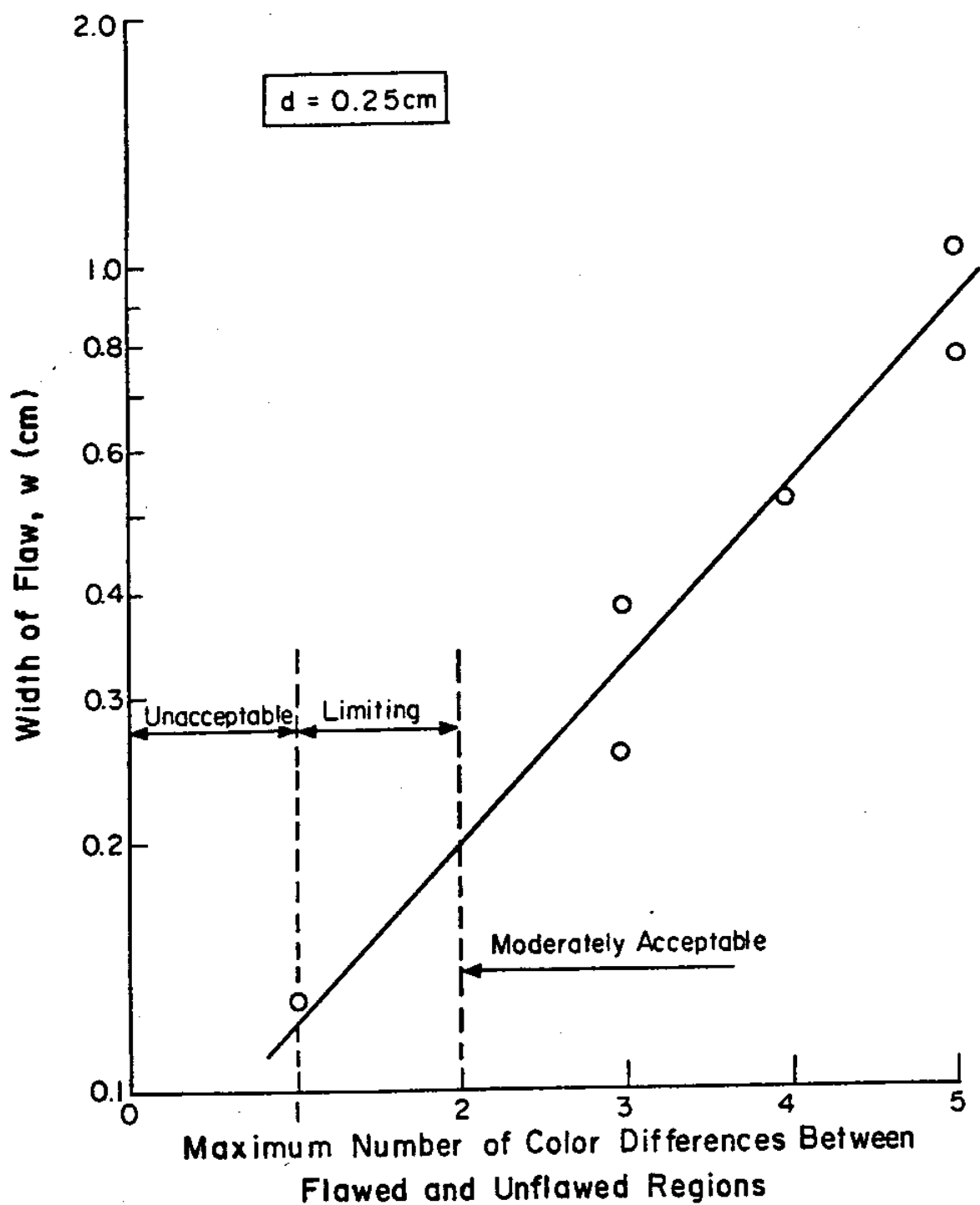
Fig. 16   Experimental maximum number of color differences between flawed and unflawed regions for flaws of same depth d.
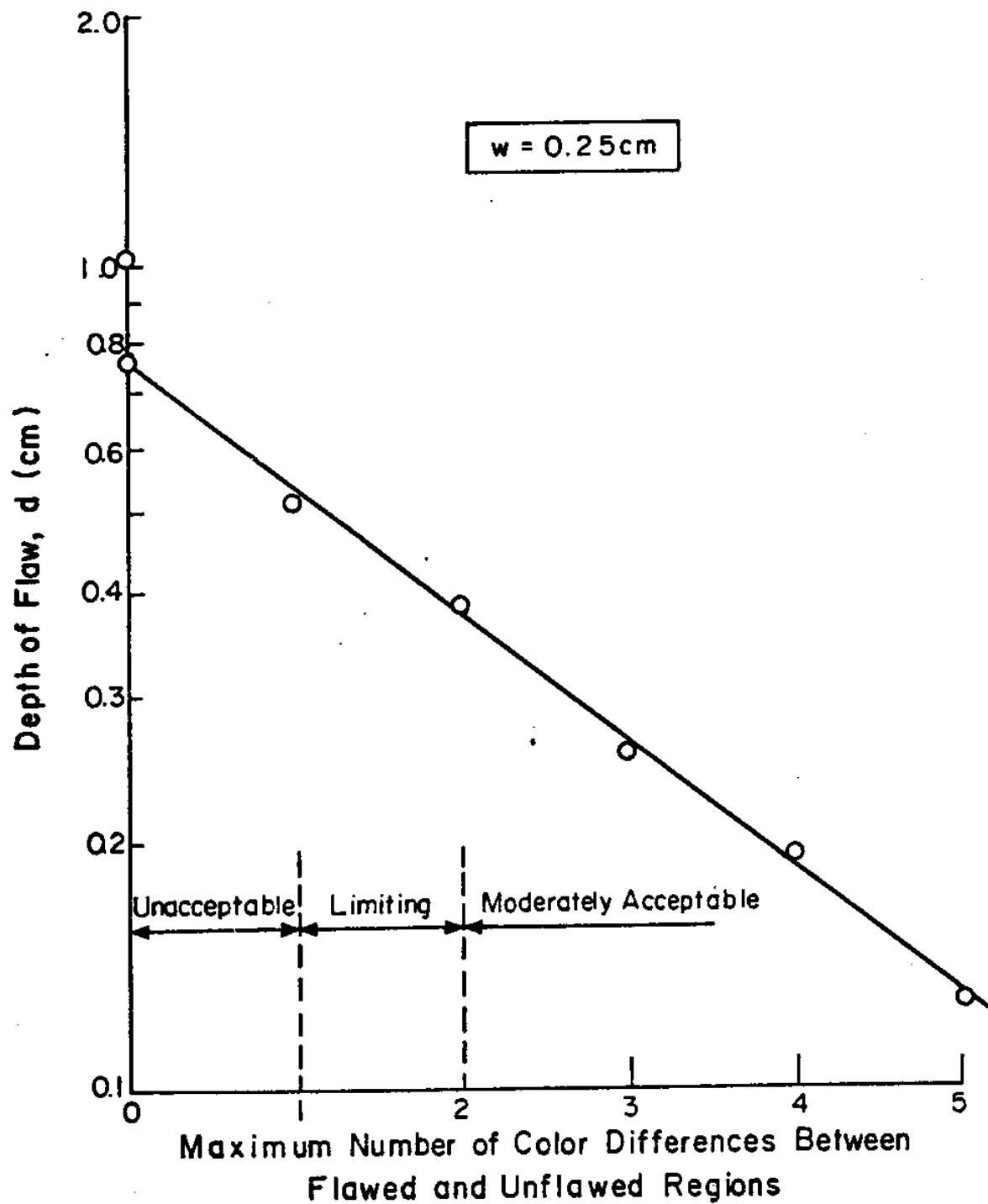
Fig. 17   Experimental maximum number of color differences between
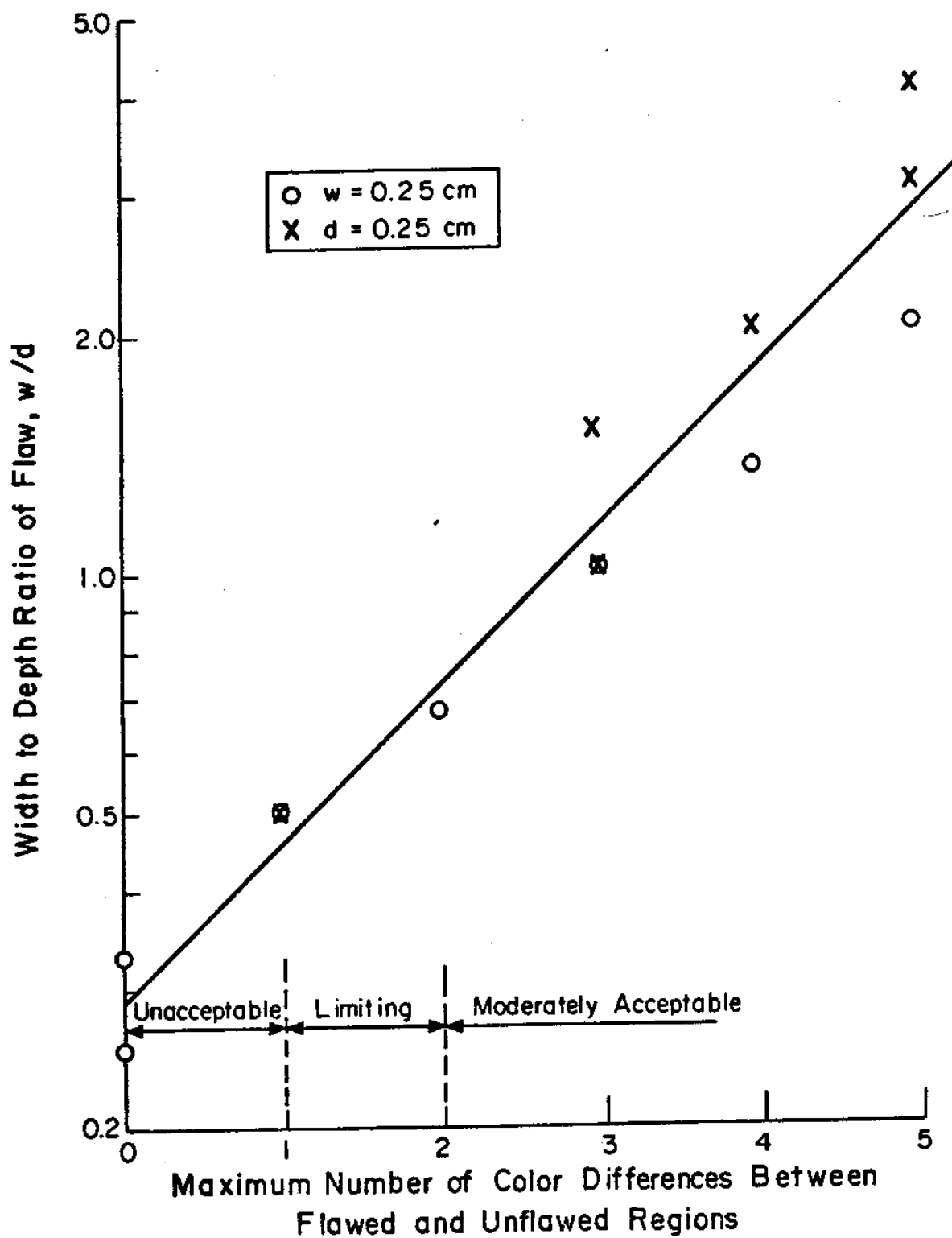flawed and unflawed regions for flaws of same width w.

Fig. 18   Experimental maximun number of color differences between flawed
and unflawed regions for flaws of various width to depth ratios.
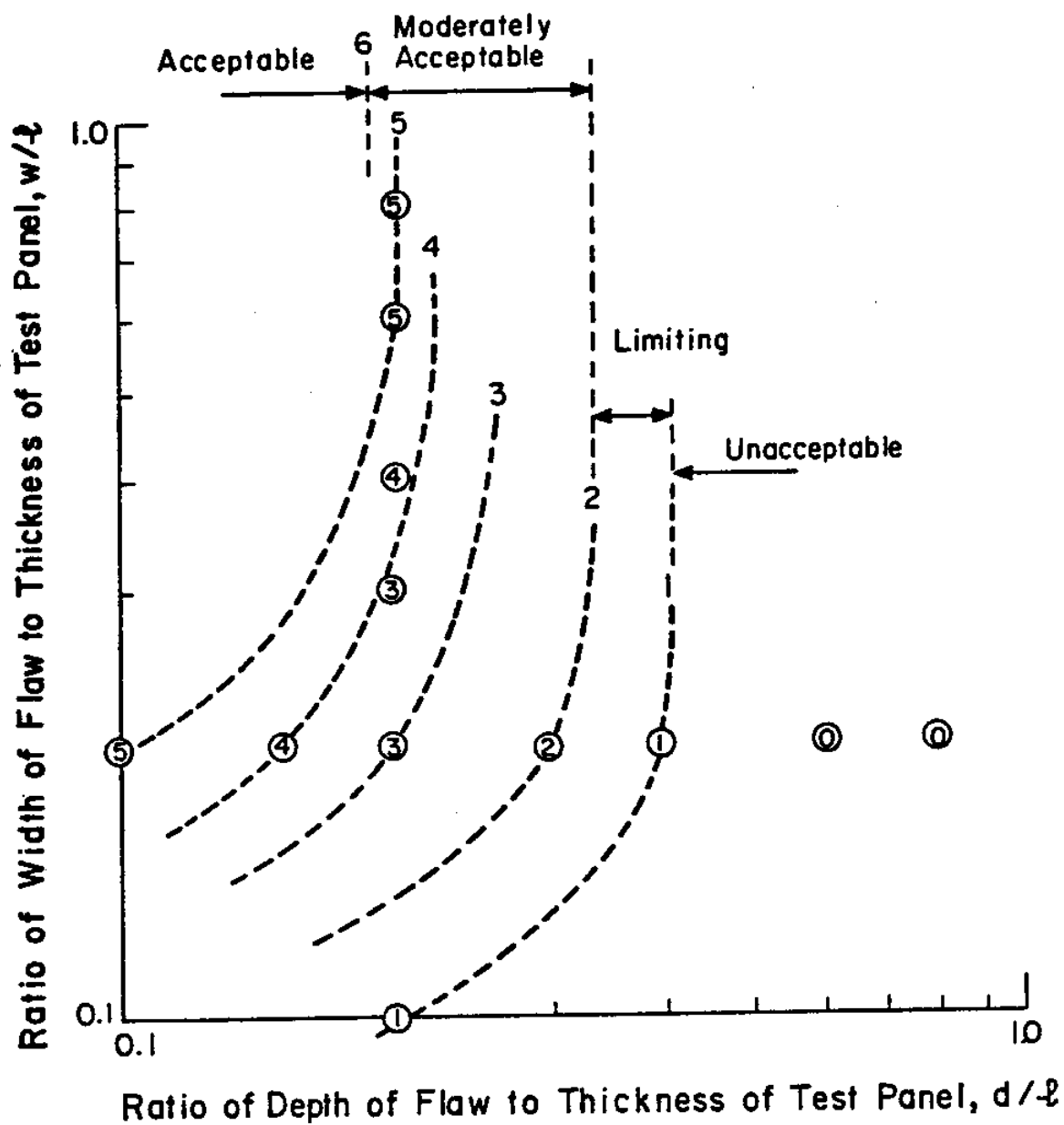
Fig. 19   Contours of constant maximum number of color differences
          between flawed and unflawed regions for the thermal testing
          system in detecting flaws orthogonal to surface of fiber-
          glass panel.